UNIVERSITY OF HAWAII
LIBRARY
JAN 8 '58

The PHILOSOPHICAL MAGAZINE

FIRST PUBLISHED IN 1798

. 2 **Eighth Series** **No. 24** **December 1957**

A Journal of Theoretical Experimental and Applied Physics

EDITOR
PROFESSOR N. F. MOTT, M.A., D.Sc., F.R.S.

EDITORIAL BOARD
SIR LAWRENCE BRAGG, O.B.E., M.C., M.A., D.Sc., F.R.S.
SIR GEORGE THOMSON, M.A., D.Sc., F.R.S.
PROFESSOR A. M. TYNDALL, C.B.E., D.Sc., F.R.S.

PRICE £1 5s. 0d. plus postage
Annual Subscription £13 10s. 0d. payable in advance

ALERE FLAMMAM.
Printed and Published by
TAYLOR & FRANCIS LTD.
RED LION COURT, FLEET STREET, LONDON, E.C.4

Announcing a new International Journal to appear in January 1958

Molecular Physics

Editor: H. C. LONGUET-HIGGINS
Assistant Editor: J. H. VAN DER WAALS

Editorial Board:

J. Bjerrum, *Copenhagen*; G. Careri, *Padua*; C. A. Coulson, *Oxford*; F. H. C. Crick, *Cambridge*; P. J. W. Debye, *Cornell*; D. Hadzi, *Ljubljana*; O. Hassel, *Oslo*; W. Heitler, *Zürich*; J. O. Hirschfelder, *Wisconsin*; D. F. Hornig, *Princeton*; J. A. A. Ketelaar, *Amsterdam*; J. G. Kirkwood, *Yale*; R. Kronig, *Delft*; J. W. Linnett, *Oxford*; A. Liquori, *Rome*; Dame Kathleen Lonsdale, *London*; P-O. Löwdin, *Uppsala*; M. Magat, *Paris*; W. Moffitt, *Harvard*; R. S. Mulliken, *Chicago*; A. Münster, *Frankfurt*; L. J. Oosterhoff, *Leiden*; L. E. Orgel, *Cambridge*; J. A. Pople, *Cambridge*; I. Prigogine, *Brussels*; R. E. Richards, *Oxford*; J. S. Rowlinson, *Manchester*; G. S. Rushbrooke, *Newcastle upon Tyne*; L. E. Sutton, *Oxford*; H. W. Thompson, *Oxford*; B. Vodar, *Bellevue, Paris.*

Physicists, chemists and their biological colleagues have a fundamental common interest in the properties of molecules and molecular assemblies and the need has been growing for a journal which would bring together experimental and theoretical contributions to this field.

The physical aspects of molecules will be dealt with, in particular:

1. The structure of molecules as determined by physical methods and interpreted by quantum mechanics;
2. The electromagnetic properties of molecules and the processes of molecular excitation, ionization and dissociation;
3. The interaction between molecules and the equilibrium and transport properties of molecular assemblies.

The following contributions have been received for the first volume:

1. Nuclear Magnetic Resonance and Rotational Isomerism in Substituted Ethanes. By J. A. Pople
2. Dielectric Properties of Iodine in Aromatic Solvents at 9000 Mc/sec. By G. W. Nederbragt and J. Pelle
3. On the Dipole Moments of Azines. By H. F. Hameka and A. M. Liquori
4. Electron–Electron Separation in Molecular Hydrogen. By M. P. Barnett, F. W. Birss and C. A. Coulson
5. On Irreversible Processes in Quantum Mechanics. By I. Prigogine and M. Toda
6. The Transport of Energy and Momentum in a Dense Fluid of Rough Spheres. By J. P. Valleau
7. Constant Pressure in Statistical Mechanics. By W. Byers Brown
8. One-dimensional Multicomponent Mixtures. By H. C. Longuet-Higgins

Price per part £1 5s. 0d. plus postage
Subscription per volume (4 issues) £4 15s. 0d. post free, payable in advance

Printed and Published by

TAYLOR & FRANCIS LTD
RED LION COURT, FLEET STREET, LONDON, E.C.4

Orders originating in U.S.A. and Canada should be sent to the
Academic Press Inc., 111 Fifth Avenue, New York, 3, N.Y., U.S.A.

Optical Absorption Lines of Hydrated Manganous Salts at Low Temperatures†

By R. PAPPALARDO
H. H. Wills Physics Laboratory, Bristol

[Received July 18, 1957]

ABSTRACT

The absorption spectra of four manganous hydrated salts (sulphate, chloride, fluosilicate and ammonium sulphate) have been investigated at 78°K and 20°K in the 15 000 cm^{-1} to 30 000 cm^{-1} range.

Several groups of lines are found, some of them showing subsplitting of the order of 10 cm^{-1}.

The results are satisfactorily interpreted by means of the ligand field theory ; a qualitative discussion of refinements of the cubic field scheme in relation to the observed spectra is also given.

§ 1. INTRODUCTION

THE absorption spectra of complex ions of elements of the iron group have been thoroughly investigated in recent years for the case of ions in solution (in particular, by Jørgensen 1956). Though the low temperature optical absorption has been studied in crystals of many salts of rare-earth elements, for the iron group (with the exception of Cr^{3+}) there is only the preliminary work of Gielessen (1935) and the recent work of Holmes and McClure (1957). The existence of a rather crude but successful theoretical scheme for interpreting optical absorption (Tanabe and Sugano 1954, Orgel 1952), and the achievements and limitations (Abragam and Pryce 1951 a, b) of the paramagnetic resonance methods, have both helped to stimulate considerable interest in the subject; it would be worth while making a systematic study of the optical absorption for the iron group of elements.

The theoretical scheme of interpretation—common to the cases of solutions and crystals—is based on the ligand field theory (Tanabe and Sugano 1954, Orgel 1952). The complex ion is considered as a system of four or six ligands bound to the central metallic ion by polarization forces ; this produces an electric field of determinate symmetry, with which the 3d electrons of the iron group element interact. Hence the spectroscopic terms of the free ion are altered, and the optical absorption is due to electron transitions between 3d orbitals, giving the crystal its characteristic coloration. These transitions, forbidden in the free-ion state, have a low probability in the complex ion.

---

† Communicated by Professor M. H. L. Pryce, F.R.S.

For the theoretical approach to the problem it is necessary to calculate the new set of levels of the ion ; for this purpose the ligand field model uses pure ionic functions which must possess the symmetry properties of the ligand field. The group theory treatment by Bethe (1929) gives readily the qualitative trend of the levels, in the cases of weak, intermediate, or strong fields with respect to the spin–orbit and spin–spin interactions. This calculation applies to crystals in general. Quantitative data for the resulting levels of the iron-group elements have been calculated by Tanabe and Sugano (1954) for the case of strong field, cubic symmetry (six octahedrally coordinated ligands), and neglecting spin–orbit interaction and non-cubic components of the ligand field. Orgel (1952) gave the analogous treatment for a weak field.

This formalism has been widely used to interpret the absorption bands of solutions ; the agreement between theory and experiment is quite satisfactory. A more exacting test of the ligand field theory would come from the study of crystals, since by working at low temperatures it is possible to resolve details of the absorption spectra, masked at room temperature by the broadening due to thermal vibrations. The study of the optical behaviour of crystals at low temperatures would give information on the departure of the ligand field from cubic symmetry and on the roles played by spin–orbit coupling, configuration interaction, and lattice vibrations. Information on the actual symmetry of the field acting on the 3d electrons in complex ions, and more accurate knowledge of their ground and excited states, would be useful for the interpretation of magnetochemical and paramagnetic resonance data (Abragam and Pryce 1951 a, b).

An experimental study of the absorption spectra of hydrated crystals containing iron-group elements has therefore been initiated. The present paper reports results on various manganous salts.

§ 2. Experimental

2.1. *The Cryostat*

The basic requirements of the cryostat were to cool the crystal and keep its temperature constant for a reasonable time, to avoid formation of frost along the path of light, and avoid the passage of light through the refrigerating liquid. All these requirements were met by the cryostat of fig. 1 ; the main disadvantage was that only one crystal could be investigated for each filling of hydrogen or nitrogen.

The cryostat was designed by Dr. H. D. Keith, and in its main features was similar to the one used by Johnson and Studer (1951). The transmission cell and the container for the refrigerating liquid were made from a single copper block so that if the crystalline sample was in good thermal contact with the body of the transmission cell it would reach the temperature of the liquid bath. To maintain constant temperature in the crystal for a reasonable time, the transmission cell and inner container

Fig. 1

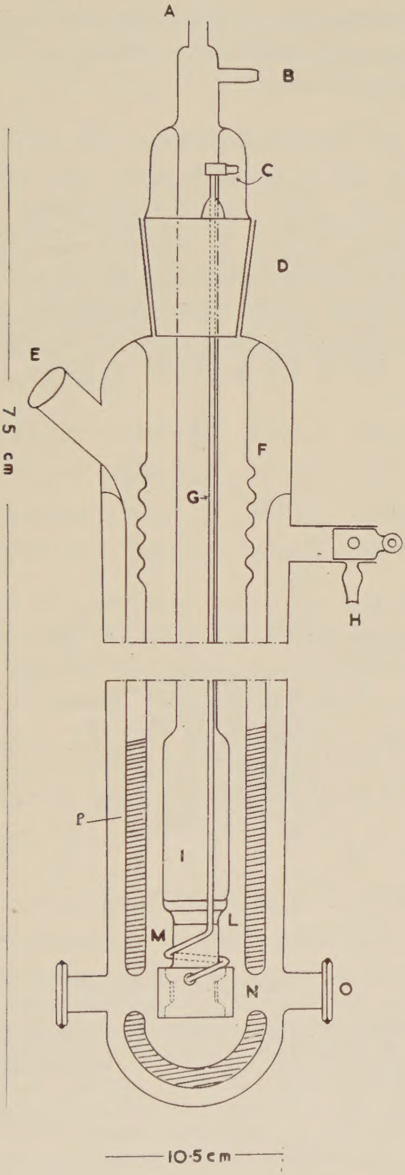

The cryostat.

A, inlet for refrigerating liquid ; B, hydrogen gas outlet ; C, exchange gas inlet ; D, greased joint ; E, liquid nitrogen inlet ; F, corrugations in glass jacket ; G, copper tubing for exchange gas ; H, main pumping tap for interspace vacuum ; I, glass portion of liquid hydrogen container ; L, Kovar seal ; M, main copper block ; N, transmission cell ; O, waxed windows ; P, liquid nitrogen.

were surrounded by a vacuum space and enclosed in a second dewar filled with liquid nitrogen. The nitrogen jacket was designed so as not to intercept the beam of light passing through the sample ; and this helped to maintain the outermost windows of the cryostat at room temperature free of condensation and frost.

2.2. *The Transmission Cell* (fig. 2)

This proved to be the most troublesome part of the system. It was originally designed for work with liquid helium ; since at this temperature good thermal contact is essential, the cavity containing the sample was filled with helium exchange gas at low pressure. To maintain the cavity gas-tight at low temperatures the following method was used. Transparent windows were mounted in thin copper diaphragms with Araldite and baked for an hour at 190°c (Roberts 1954) ; the diaphragms were then soldered to the main copper block with Hoyt metal No. 314. One of the windows was left assembled permanently, and the other could be removed and replaced when changing the sample. The heat required for soldering was liable to spoil the crystal ; on the other hand leaks would sometimes occur in the soldering during cooling, spoiling the interspace vacuum and causing rapid evaporation of the refrigerating liquid.

Fig. 2

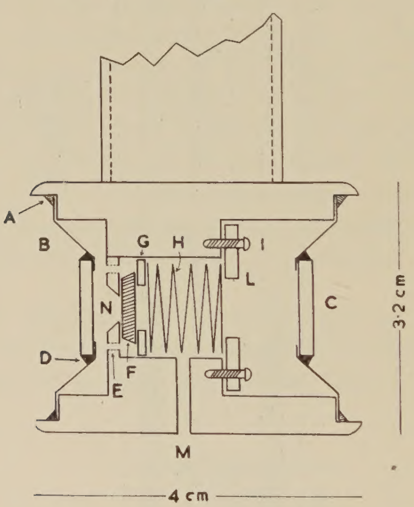

The transmission cell.

A, Hoyt metal soldering ; B, thin copper diaphragm ; C, transparent window ; D, Araldite ; E, small hole for gas exchange circulation ; F, crystalline sample ; G, copper ring ; H, light spring ; I, small screw to lock the copper ring L ; M, exchange gas inlet ; N, tapered hole for the light beam.

For the work with liquid hydrogen, the thermal contact obtained by clamping the crystal was quite satisfactory. The crystal was placed in the transmission cell in front of a tapered aperture, and pressed against the main copper block by a copper ring and a weak spring. It was locked in position by another copper ring, which was also in good thermal contact with the body of the cell.

2.3. *The Spectrograph*

For observing the narrow absorption lines, the more sensitive photographic method was preferred to spectrophotometric apparatus employing photocells and a monochronomator. A Hilger E.1, large quartz spectrograph, was used to investigate the range from 3300 Å to 6400 Å (30 300 cm^{-1} to 15 600 cm^{-1}). Typical values of the dispersion in various spectral regions were as follows :

7 Å/mm	(60 cm^{-1}/mm)	at	3400 Å	(29 400 cm^{-1}),
15 Å/mm	(70 cm^{-1}/mm)	at	4200 Å	(23 800 cm^{-1}),
25 Å/mm	(100 cm^{-1}/mm)	at	5000 Å	(20 000 cm^{-1}),
35 Å/mm	(100 cm^{-1}/mm)	at	6000 Å	(16 700 cm^{-1}).

The light source was a 50 watt lamp with a vertical filament. The light was first focused on the crystal sample and then concentrated on the slit of the spectrograph, using two quartz lenses. The spectrograms were taken on Ilford Rapid Process Panchromatic plates, and developed in a high contrast developer. On each plate some 12–14 spectrograms were taken, with exposure times increasing from 1 second to 10 minutes. The line spectrum of a mercury vapour lamp was recorded on each plate for calibration purposes.

2.4. *Wavelength and Intensity Determinations*

For wavelength measurements a precise plate calibration was derived using an iron arc spectrum. Reference points on this curve were given by the mercury lines recorded on every plate. All wavelength measurements were made by scanning the plates with a Hilger microdensitometer ; photographic enlargement was used as a check on the photometric tracing in any case of doubt.

Intensity determinations were restricted to absorption lines, since an accurate determination for bands is not possible with the photographic method. To evaluate the intensity of a line a photometric trace of the plate was taken, choosing a suitable exposure time. From this the general behaviour of the absorption near the line was deduced. To correlate quantitatively the value of the absorption peak of the line to its extrapolated background, it was necessary to know the sensitivity curve of the plate in that particular region, and for the amount of light passing through the given sample.

For this purpose galvanometer readings were taken, measuring the blackening of the plate corresponding to various exposure times for a given wavelength ; for good accuracy the setting was made at 1 or 2 mm from the line. A set of curves (galvanometer deflection against exposure time) was thus drawn ; on one or more of these curves, points were located corresponding to blackening at the maximum of the line and to the blackening of the extrapolated background in the absence of lines. Since far from cut-off the sensitivity of the plate did not vary appreciably over 1 or 2 mm, it was reasonable to assume that the deduced ratio of exposure times for the extrapolated background and the peak of the absorption line, was very nearly the value of the ratio at the actual site of the line. This ratio of exposure times was then correlated with the corresponding intensity ratio. To minimize errors, only the linear part of the calibration curves, far from saturation, was taken into consideration.

The values of the absorption deduced in this way did not require correction for reflection losses, were not sensitive to slight alterations in the geometry of the system, and did not require constant developing and fixing conditions from plate to plate. Naturally the procedure could not be applied to very strong absorption lines.

2.5. *The Crystalline Samples*

The crystals were grown from solutions of analytically pure chemicals. The samples were about 4×4 mm across and had thicknesses varying from 1 mm to 7 mm. They were lightly polished to reduce reflection losses and interference effects.

Samples of $MnSiF_6 . 6H_2O$ and $Mn(NH_4)_2(SO_4)_2 . 6H_2O$ were kindly supplied by Dr. L. C. Jackson.

2.6. *Operation*

The central part of the cryostat (liquid container—transmission cell) was demountable. After inserting the sample, this removable part was replaced and the cryostat sealed on top by a greased joint. The interspaces A and B and the transmission cell were evacuated. (Loss of transparency during this operation and the subsequent cooling sometimes spoilt the crystal samples.) The interspaces were then filled with dry oxygen gas at 0·5 atmospheric pressure, to provide an agent for heat exchange in the preliminary cooling of the system. The inner liquid container was also evacuated and flushed several times with hydrogen gas.

The outside jacket was slowly filled with liquid nitrogen. When the transmission cell reached the temperature of liquid nitrogen—usually after about 1½ hours—the interspaces were again exhausted, and liquid hydrogen (or nitrogen) was syphoned in.

Usually the 250–300 cm^3 of liquid hydrogen lasted for 5–6 hours ; in this time several spectrograms could be taken, once the temperature of the system had stabilized.

§ 3. EXPERIMENTAL RESULTS

Absorption spectra of each sample were taken at room temperature, at 78°K and 20°K. Only data for the measurements at 20°K are tabulated below; an outline of the results at the other temperatures is also given, as this is useful for the tentative interpretation that follows.

Fig. 8

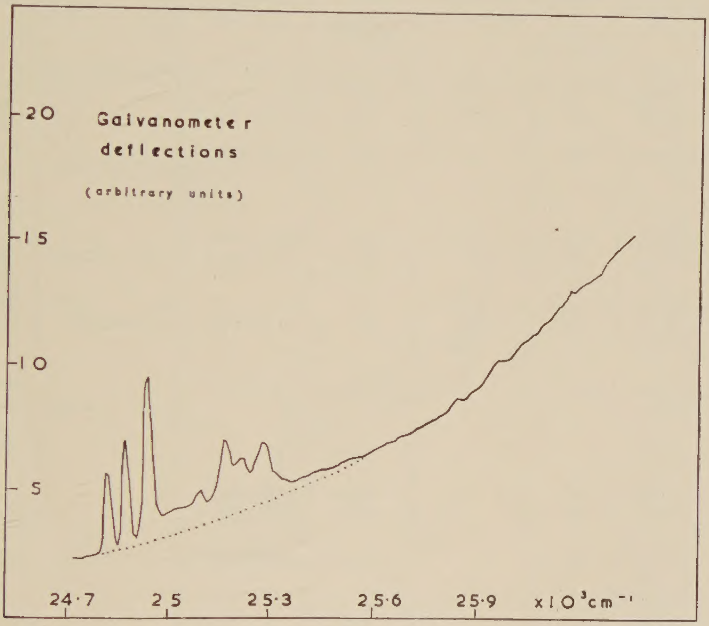

Microdensitometer curve for $MnSO_4 . 4H_2O$ at 20°K (25 000 cm^{-1} region).

The formula (3.1) of Tanabe and Sugano (1954) was used for the determination of oscillator strengths. The tabulated extinction coefficient for the maximum of a line is the coefficient α of the usual relation

$$I = I_0\ 10^{-\alpha x}.$$

The densities, molecular volumes and crystal structures of the salts were taken from Mellor, *Treatise on Inorganic and Theoretical Chemistry*. As regards the accuracy of the tabulated data, there may be occasional discrepancies of 80–100 cm^{-1} in the absolute wave-numbers: differences in wave-number of more than 100 cm^{-1} should be fairly accurate. The accuracy of the values of the absorption coefficient is not very good, and only the first figure is significant; this is reasonable considering the limitations of the photographic method. Values of relative intensity are only given for lines which have similar intensities and are not widely separated.

3.1. *Manganous Sulphate* $MnSO_4 . 4H_2O$

The crystal is monoclinic, with axial ratios $a : b : c :: 0{\cdot}8643 : 1 : 0{\cdot}587$, and $\beta = 90° 53'$. The sample investigated at 20°K (fig. 5, Pl. 56) had a thickness of 6·95 mm. In the spectral region investigated (3300 Å–6400 Å) there were several groups of lines (see table 1).

Table 1. Lines of $MnSO_4 . 4H_2O$ at 20°K

Group of lines	Wave-number at 20°K	Half-width in cm^{-1}	Relative intensity	Extinct. coeff. α_{max} (cm^{-1})	Oscillation strength	Sub-splitting Compnts.	Sub-splitting Sep. cm^{-1}	Remarks
	24838	30	0·5	0·3				Diffuse band at RT
A	24882	30	0·6	0·3	$1{\cdot}1\times10^{-8}$			
	24950*	30	1	0·4	$1{\cdot}5\times10^{-8}$*			Present at RT
	25025							weak
	25100	65	0·45	0·1	$0{\cdot}8\times10^{-8}$			
	25176	37	1·	0·3	$1{\cdot}1\times10^{-8}$	2	~15	rather broad
B	25221		0·65			2	~25	rather broad
	25278	68	0·8	0·2	$1{\cdot}5\times10^{-8}$	possibly		
	25311		0·35					
	25826	~30		~0·01	3×10^{-10}			weak
C	25880					2	~30	very weak but sharp
	25960			0·03				weak
D	27292	27		0·14	$0{\cdot}4\times10^{-8}$			
	27352	28		0·12	$0{\cdot}3\times10^{-8}$			
	27518	54		0·12	$0{\cdot}66\times10^{-8}$			
	27586							
	27640							
	27731			0·4				
	27778							
	27855							
	27910							
	27980			0·3				
	28050							
E	28090							
	28177							
	28248							
	28280							
	28296							
	28369							
	28425	48		0·02	$1{\cdot}3\times10^{-9}$			
	28465							
	28498							
	28670							
F	29700							very diffuse weak

* Oscillator strength $1{\cdot}4\times10^{-8}$ for the same line at room temperature.

A. A rather intense triplet centred on 24 900 cm⁻¹ (fig. 6, Pl. 56; fig. 8)
B. A complex pattern of lines at 25 200 cm⁻¹ (fig. 6, Pl. 56; fig. 8)
C. A faint quadruplet at 25 800 cm⁻¹ (fig. 6, Pl. 56; fig. 8)
D. An intense doublet at 27 300 cm⁻¹ (fig. 7, Pl. 56; fig. 9)
E. A broad band of complex structure centred on 27 800 cm⁻¹ (fig. 7, Pl. 56; fig. 9). The peaks of this band are shown in table 1.

3.2. *Temperature Effects*

At room temperature (fig. 3, Pl. 55) group A consists of a line at 24 934 cm^{-1} and a hazy band at 24 820 cm^{-1}: group B is a diffuse band from which two lines can be distinguished (at 25 120 cm^{-1} and 25 260 cm^{-1}). At nitrogen temperature (fig. 4, Pl. 55) both groups A and B are already assuming their final form—subsequent cooling to 20°K (figs. 5–7, Pl. 56) sharpens group A and reveals the subsplitting in the lines of group B. Group C only appears at 20°K. Groups D and E are absent at room temperature, and there is only a very faint, fairly broad band. Doublet D appears at liquid nitrogen temperature, together with a few weak lines of group E. At 20°K the doublet D is sharpened, and the complex pattern of E becomes very clear.

Fig. 9

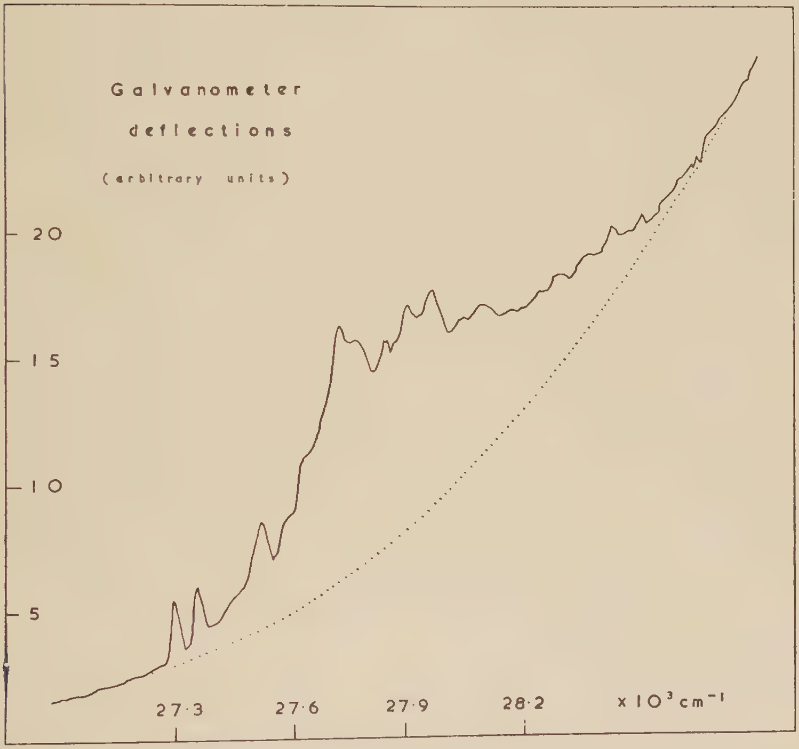

Microdensitometer curve for $MnSO_4 . 4H_2O$ at 20°K (27 000 cm^{-1} region).

3.3. *Manganous Chloride* $MnCl_2 . 4H_2O$

The crystal is monoclinic, with axial ratios $a : b : c :: 1{\cdot}15 : 1 : 0{\cdot}64$, and $\beta = 99° 25'$. The thickness of the sample investigated was 1·37 mm.

Table 2. Lines of $MnCl_2 . 4H_2O$

Group of lines	Wave-number at 20°K	Half-width in cm^{-1}	Relative intensity	Extinct. coeff. α_{max} (cm^{-1})	Oscillator strength	Subsplitting Compnts.	Sep.	Remarks
A	24318	26	0·7	0·3	10^{-8}	2	~ 9 cm^{-1}	sub-splitting very sharp
	24462	45	0·6	0·3	$1{\cdot}5 \times 10^{-8}$	2	~11 cm^{-1}	
	24500	42	0·35					
	24594	42	1	0·3	$1{\cdot}7 \times 10^{-8}$	2 possibly	~ 6 cm^{-1}	only line at room temp.
B	24690		0·3					very weak
	24802	45	0·7					
	24919	60	1		$1{\cdot}1 \times 10^{-8}$	2 possibly		
	25300							
C	27137	19	1	0·8	$1{\cdot}8 \times 10^{-8}$			sharp equi-distant lines
	27174	26	0·97					
	27207	28	0·96					
D	27300							
	27426							
	27525	77	1	0·5	$4{\cdot}5 \times 10^{-8}$	possibly		
	27570		1					
	27770							
E	29070	77	1	1	9×10^{-8}	3 possibly		diffuse
	29155	95	1			3 possibly		
	29330							

At 20°K the absorption spectrum is composed of (see table 2)

A. A main triplet with various subsplittings, at 24 500 cm^{-1} (fig. 12, Pl. 57; fig. 14).
B. Faint lines at 24 800 cm^{-1} (fig. 14).
C. A strong triplet of sharp lines at 27 150 cm^{-1} (fig. 13, Pl. 58; fig. 15).
D. A band extending up to 28 000 cm^{-1}, showing some structure. The peaks of this structure are shown in table 2 (fig. 13, Pl. 58; fig. 15).
E. Two broad lines at 29 100 cm^{-1}, showing some structure which is not very definite even at 20°K (fig. 13, Pl. 58; fig. 16).

3.4. *Temperature Effects*

At room temperature group A is very faint, but not diffuse, and the line at 24 600 cm^{-1} is the strongest of the group. The whole pattern becomes stronger at liquid nitrogen temperature (fig. 10, Pl. 57); finally at 20°K the subsplitting is enhanced, and the lines of group B too become more distinct (figs. 11–13, Pls. 57, 58). The other groups are absent at room temperature. They first appear at liquid nitrogen temperature, though rather blurred, becoming much sharper at 20°K.

Fig. 14

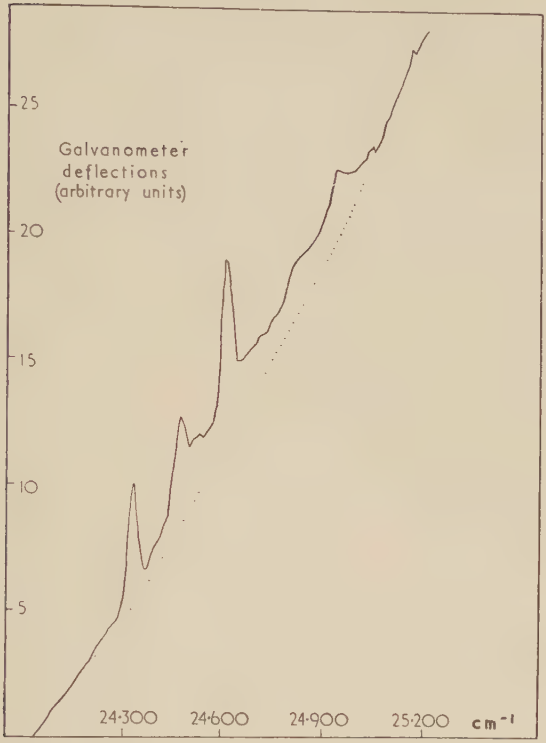

Fig. 15

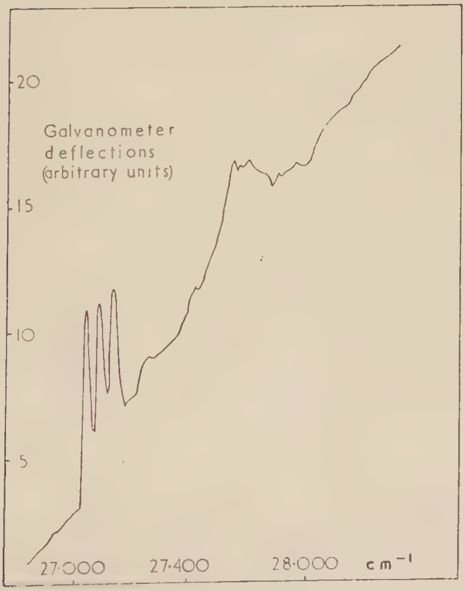

Microdensitometer curve for $MnCl_2 . 4H_2O$ (~27 000 cm^{-1}).

Fig. 16

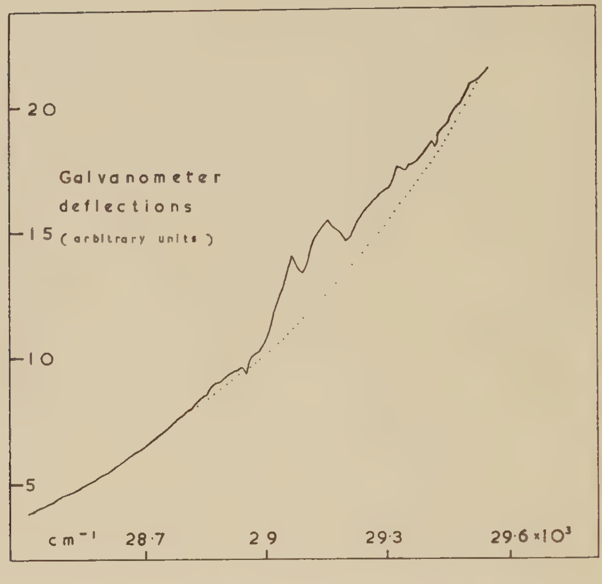

Microdensitometer curve for $MnCl_2 . 4H_2O$ at 20°K (29 000 cm^{-1} region).

Fig. 18

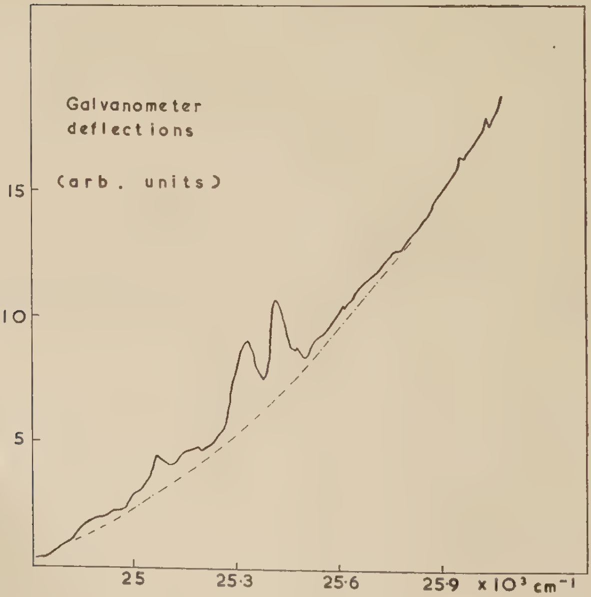

Microdensitometer curve for $MnSiF_6 . 6H_2O$ at 20°K.

3.5. *Manganous Fluosilicate* $MnSiF_6 . 6H_2O$

The crystals belong to the trigonal system, and have the axial ratio $a : c : : 1 : 0{\cdot}504$, and $\alpha = 112° 30'$. The thickness of the sample used was 3·87 mm.

Table 3. $MnSiF_6 . 6H_2O$

Group of lines	Wave-number at 20°K	Half-width in cm⁻¹	Relative intensity	Extinct. coeff. α_{max} (cm⁻¹)	Oscillator strength	Subsplitting Compnts.	Subsplitting Sep. cm⁻¹	Remarks
	24890							weak sharp doublet
A	24946							
	25002							
	25075	65		0·25	3×10^{-8}			Present, rather blurred at room temperature
	25170							
B	25330	85		0·45	7×10^{-8}	2	~14	
	25420	65		0·5	6×10^{-8}			
C	26413							?
	28900							?

At 20°K the spectrum consists of (see table 3 and fig. 17, Pl. 58)

A. One intense line, sided by a faint doublet at 24 980 cm⁻¹ and a broad line at about 25 170 cm⁻¹.

B. A fairly intense triplet, with two of the lines close together.

C. Very weak and narrow bands at about 26 410 cm⁻¹ and 28 900 cm⁻¹ though the evidence from the photometric tracing is not very conclusive.

3.6. *Temperature Effect*

As for the other salts, the cooling clarifies the relatively strong lines already existing at room temperature, and subsplitting becomes apparent at 20°K.

3.7. *Manganous Ammonium Sulphate* $Mn(NH_4)_2(SO_4)_2 . 6H_2O$

The crystals have axial ratios $a : b : c : : 0{\cdot}736 : 1 : 0{\cdot}497$, and $\beta = 107° 2'$. The sample used had a thickness of 1·98 mm. Only one line is detectable at 78°K, its wave-number being 25 220 cm⁻¹. Cooling to 20°K produces no appreciable change in position or intensity. At 20°K the line is preceded by a narrow band centred on 25 050 cm⁻¹ and by a very weak sharp doublet at 24 750 cm⁻¹ (fig. 19). Samples of $(Mn, Zn)SO_4$ with dilution ratios 1 : 1 and 1 : 5 were prepared to study the effect of diluting the paramagnetic ion. Unfortunately, both samples were spoilt during the cooling.

§ 4. INTERPRETATION OF THE EXPERIMENTAL RESULTS

4.1. *Cubic Field Model*

We shall now compare the theoretical predictions with the experimental data for the Mn^{2+} ion. Firstly it must be remembered that the calculations by Tanabe and Sugano were made with the hypothesis of a cubic ligand field, and that distortions from cubic symmetry and spin–orbit effects were ignored. Consequently, from this model we can expect to have an explanation of only the main features of the absorption.

Table 4. $Mn(NH_4)_2(SO_4)_2 . 6H_2O$

Group of lines	Wave-number at 20°K	Half width in cm^{-1}	Relative intensity	Extinct coeff. α_{max} (cm^{-1})	Oscillator strength	Sub-splitting	Remarks
	24728						weak sharp lines
	24795	~15			$1{\cdot}5\times10^{-9}$		
	25063		0·55				
	25144	66	1	0·2	3×10^{-8}		

The predicted levels for 3d systems were plotted by Tanabe and Sugano as a function of two adjustable parameters, Δ the ligand field strength, and B a combination of Slater–Condon parameters. For the Mn^{2+} ion the authors assume values of 1230 cm^{-1} for Δ, and 860 cm^{-1} for B, as for the free ion. However, the agreement with the absorption spectra of solutions is rather poor; Orgel (1955) suggested a value of 780 cm^{-1} for B, and then there is better agreement between the theoretical levels and the observed bands in solutions containing $[Mn(H_2O)_6]^{2+}$. It should be noted that this decrease in the value of B from the free ion to the complex ion state seems to be a common feature in other elements of the iron group, especially for trivalent ions; this is interpreted either as a spreading of the electronic cloud of the ion, or as evidence of partial covalent bonding. Assuming Orgel's value for B, we have the following sequence of quartet states beyond the $^6A_1(d\epsilon^3, d\gamma^2)$ ground state.

$^4T_1$ $(d\epsilon^4, d\gamma^1)$ at 15 200 cm^{-1}†
$^4T_2$ $(d\epsilon^4, d\gamma^1)$ at 19 500 cm^{-1}†
$^4A_1$ ^4E_a $(d\epsilon^3\ d\gamma^2)$ at 25 300 cm^{-1}
$^4T_2$ $(d\epsilon^3, d\gamma^2)$ at 26 950 cm^{-1} (extrapolated value)
^4E_b $(d\epsilon^3, d\gamma^2)$ at 30 400 cm^{-1}
$^4T_1$ $(d\epsilon^3, d\gamma^2)$ at 31 200 cm^{-1} (extrapolated value).

Levels having the same subshell configuration $(d\epsilon^{5-N}d\gamma^N)$ possess the same cubic field dependence, so that transitions between such states are expected to produce sharp lines instead of the more common bands. Transitions $^6A_1$ $(d\epsilon^3, d\gamma^2) \rightarrow {}^4T_1$, $^4T_2(d\epsilon^4, d\gamma)$ are expected to give only weak bands. Before applying these predictions to the crystals investigated, we must consider the evidence that justifies the assumption that the Mn^{2+} ion is surrounded by six water molecules, located approximately at the vertices of an octahedron. From x-ray analysis it is known that this is certainly the case for $MnSiF_6 . 6H_2O$. This has a distorted CsCl structure of octahedral radicals of $Mn(H_2O)_6$ and SiF_6, of similar shape and size, and lying parallel. There are no x-ray data for the other salts, but it seems likely from crystallographic evidence on all the salts of these transition elements that we can safely assume the octahedral model as a first approximation since the characteristics of the absorption are broadly similar for all the salts investigated.

---

† In aqueous solution Jørgensen (1956) finds these levels at 18 800 and 23 000 cm^{-1} respectively.

4.2. *Intersystem Combinations*

In the free ion state for Mn^{2+} there are no sextet states up to 50 000 cm $^{-1}$ apart from the ground state. Hence it is reasonable to consider the observed lines in the complex ion as due to intersystem combinations of $^6A_1$ (ground state) with upper quartet states. Transitions to levels of this kind are forbidden even in complex ions (see Hellwege 1948) if the spin S is a true quantum number. However, if there is a mixture of sextet with quartet states in the ground state, these transitions become possible even if their probability is small. Since the probability of the transitions is proportional to the square of the intermixing in the wave functions, assuming an oscillator strength f of 10^{-4} for intrasystem combinations and since the observed value of f is $\sim 10^{-8}$ for the lines of the manganous ion, the amount of contamination would be of the order 10^{-2}, which is reasonable. Intersystem combinations with $\Delta S=2$ seem very improbable because the spin-orbit coupling couples levels with $\Delta S=1$. Even if possible, they would only give very weak bands and not lines for

Fig. 19

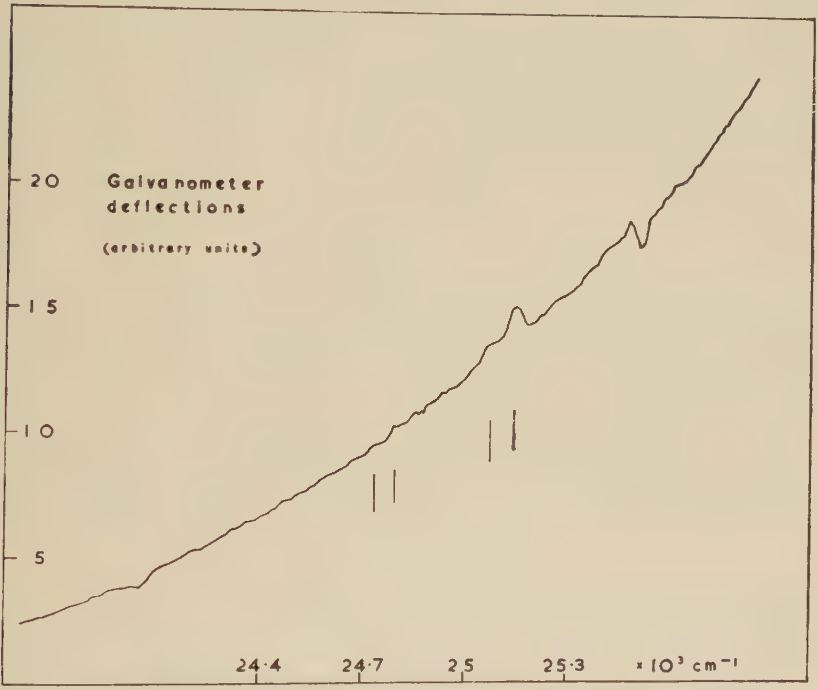

Microdensitometer curve of $Mn(NH_4)_2(SO_4)_2 \cdot 6H_2O$ at 20°K.

3d systems. If we consider the spectra of $MnCl_2 . 4H_2O$ and $MnSO_4 . 4H_2O$ we find that there are lines at $\sim$25 000 cm^{-1}, $\sim$27 000 cm^{-1} and $\sim$29 000 cm^{-1}, as expected if transitions occur from $^6A_1$ to $^4A_1$, ^4E_a; $^4T_2$ and ^4E_b respectively. Moreover, the wave-numbers of these lines are independent of temperature (even in the wide range from room temperature down to 20°K), as predicted. These are certainly remarkable achievements of the theory.

4.3. *Selection Rules*

Groups of lines appearing in some salts are missing in others; this could be explained in terms of selection rules that are dependent on the crystalline symmetry. Hellwege has calculated a set of selection rules valid for crystals of various symmetries, for electric and magnetic dipole, and electric quadrupole transitions. These selection rules cannot easily be applied in the present case since neither the symmetry and strength of the non-cubic part of the field, the order of magnitude of spin–orbit coupling, nor the nature of the transitions involved (electric or magnetic-dipole, or electric quadrupole) are known. Moreover Hellwege did not consider the effect of lattice vibrations.

4.4. *Excited Lattice Vibrations*

In a field of O_h symmetry electric dipole transitions are not possible because the overall parity cannot be conserved in the process. Hence in this case the parity requirements can only be satisfied by a combined process of electron transition and the excitation of lattice vibrations of suitable symmetry. However, this kind of process is not strictly necessary in the case of lower crystalline symmetry.

Some of the observed lines do seem to be coupled with lattice or complex ion vibrations, but others do not, although their oscillator strength is compatible with that of electric dipole transitions.

4.5. *Spin–Orbit Coupling*

For half-filled shells, as the d^5-configuration of Mn^{2+} and Fe^{3+} the Hund rule gives a spin–orbit coupling which is zero in a first order approximation. Second order effects in the free ion give splittings of about 50–100 cm^{-1}. We will assume that the spin–orbit coupling is present and effective to a similar extent in resolving the spin-degeneracy of orbital levels, even if we can only estimate the order of magnitude of its effect.

4.6. *Comparison of Spectra of Various Salts*

(*a*) In general for the four substances investigated the number of spectral lines increases from the fluosilicate and the Tutton salt to the chloride and the sulphate; this is in order of lowering of the internal symmetry, which is nearly trigonal in the first two cases (from magnetic susceptibility measurements) and rhombic in the latter two (as inferred from the macroscopic symmetry properties).

(*b*) Consider first the groups of lines A and B of the various salts. From densitometric readings a coupling with vibrations seems to be excluded—at least, in the sense that there is no excitation of a complex vibration pattern accompanying the electronic transitions. The influence of lattice vibrations seems to be limited to the production of fluctuations in the non-cubic part of the field, thus making the lines rather blurred at room temperature and at 78 K. Cooling reduces the thermal vibrations and thus stabilizes the non-cubic part of the field, the part responsible for the separation of the lines; the lines become sharper and small subsplittings of the order 10 cm^{-1} are observed. Now, if our assignment is correct—namely, that the lines at 25 000 cm^{-1} are due to the excitation $^6A_1 \rightarrow {}^4A_1, {}^4E_a$ even in a rhombic field there would be a maximum of three lines. Hence it is necessary to postulate that the spin–orbit coupling removes the spin degeneracy of the upper levels: the ground state, derived from a ^6S state, for present purposes is to be considered as not split, because eventual splittings due to spin–spin coupling are expected to be less than 1 cm^{-1} in magnitude. On the other hand, for the upper quartets the orbital levels are split into sublevels whose characters and numbers can be deduced from a group theory treatment (Bethe 1929, Opechowsky 1940) once the symmetry of the non-cubic part of the field is known. The maximum number of levels obtainable from the $^4A_1$, ^4E level due to spin–orbit coupling is six, since all levels remain doubly degenerate by Kramers' theorem.

We find a maximum of eleven lines in the 25 000 cm^{-1} region of the sulphate. Some of these presumably correspond to vibrational excitation. Since generally some of the lines found in this region are stronger than others, it is tempting to consider that the more intense lines are derived from the $^4A_1$ level, which for a field of cubic symmetry would be favoured in the contamination with the ground state $^6A_1$.

Concerning the nature of the lines, the oscillator strength of 10^{-8} observed for most of the lines could equally well correspond to the theoretical prediction (Tanabe and Sugano 1954) of 10^{-7} for electric dipole transitions, or to 4×10^{-9} for magnetic dipole transitions, since the predictions have an uncertainty of $\sim10^{-2}$. Only a study of optical anisotropy could resolve the choice.

(*c*) The lines of the quartet found for $MnSO_4 \cdot 4H_2O$ at 25 900 cm^{-1} are interesting. They are not a vibration replica of the first strong triplet at 24 900 cm^{-1}; they are quite sharp, but too weak to be connected with an electric dipole transition (oscillator strength being $\sim3\times10^{-10}$). The lines are probably due to a magnetic dipole or electric quadrupole process.

(*d*) Now consider the $^6A_1 \rightarrow {}^4F_2$ transition. From the densitometric analysis in the 27 000 cm^{-1} region it is clear that for the chloride and the sulphate the transition is coupled with excitation of vibration modes in the upper state. In agreement with this, these lines are more influenced by changes in temperature than the transitions at 25 000 cm^{-1} for which lattice vibrations simply produce fluctuations in the field. Moreover, the lines at 27 000 cm^{-1} are missing in the fluosilicate and the Tutton salt.

Now if the field symmetry is higher in these two salts, then correspondingly the number of allowed modes of vibrations is less. Hence the transition probability for these salts would be severely decreased.

(*e*) Finally, the lines observed at 29 000 cm^{-1} for $MnCl_2$ and the diffuse band at 29 700 cm^{-1} for $MnSO_4$ can be ascribed to the transition $^6A_1$ $(d\epsilon^3, d\gamma^2) \rightarrow {}^4E(d\epsilon^3, d\gamma^2)$ which is expected at 30 400 cm^{-1}. Since the lines of the chloride do not show a vibration structure, in the absence of spin–orbit coupling at most two lines are expected, even in a rhombic field. The spin–orbit effect increases the number of configurations for the E-orbital to a maximum of four.

§ 5. CONCLUSION

The ligand field theory applied to Mn^{2+} ions is in general agreement with the experimental data. The theory successfully predicts the approximate positions of the levels, the character of the lines corresponding to transitions to these levels from the ground state, and the fact that the wave-numbers of these lines are not affected by changes in temperature. However for a detailed investigation of the spectrum, this approach has to be refined to include the effects of non-cubic field, spin–orbit interaction and the lattice and complex ion vibrations. The analysis of the optical behaviour of complex ions does not appear to be a field for broad generalizations. The interaction of complex ions with the ligand and radiation fields could only be subjected to a more rigorous analysis by studying the optical anisotropy in crystals of high symmetry and the optical behaviour in a magnetic field.

ACKNOWLEDGMENTS

The author wishes to thank Professor M. H. L. Pryce for his constant interest in the research and for making available the facilities of the laboratory. He also wishes to express his gratitude to Dr. H. D. Keith who helped with the design of the apparatus, and Dr. L. C. Jackson and his staff for their help and advice in the low temperature aspects of the work. He is very grateful to the Collegio Borromeo in Pavia for providing the maintenance allowance.

REFERENCES

ABRAGAM, A., and PRYCE, M. H. L., 1951 a, *Proc. roy. Soc.* A, **205,** 135 ; 1951 b, *Ibid.*, **206,** 173.

BETHE, A., 1929, *Ann. Phys., Lpz.*, **3,** 133.

GIELESSEN, J., 1935, *Ann. Phys., Lpz.*, **22,** 537.

HELLWEGE, K. H., 1948, *Ann. Phys., Lpz.*, **6,** 98–150.

HOLMES, O. G., and MCCLURE, D. S., 1957, *J. chem. Phys.*, **26,** 1686.

JOHNSON, P. D., and STUDER, F. J., 1951, *Phys. Rev.*, **82,** 976.

JØRGENSEN, K. C., 1956, *Report to the Xth Solvay Council* ; 1954–56, *Acta chem. scand.*, Vol. 8–11.

OPECHOWSKY, W., 1940, *Physica*, **7,** 552.

ORGEL, L. E., 1952, *J. chem. Soc.*, **4,** 4756 ; 1955, *J. chem. Phys.*, **23,** 1824.

ROBERTS, V., 1954, *J. sci. Instrum.*, **31,** 251.

TANABE, Y., and SUGANO, S., 1954, *J. phys. Soc. Japan*, **9,** 753–66.

Specific Heat of Solids at High Temperatures†

By J. N. Eastabrook
Royal Aircraft Establishment, Farnborough, Hampshire

[Received August 6, 1957]

Summary

The temperature dependence of the specific heat of simple crystals at temperatures well above the Debye temperature is estimated by using, as a simple model, the two-atom anharmonic oscillator. It is found that the difference between C_V and the Dulong and Petit value is not much less than the difference between C_P and C_V. There is rough agreement with experiment.

§ 1. Introduction

THE specific heat of solids at constant volume (C_V), derived through a well-known thermodynamic formula from the measured value of the specific heat at constant pressure (C_P), is normally observed to increase steadily above the Dulong and Petit value as the temperature is raised. Born and Brody (1921) outlined a quantum theory relating this increase to the fact that the forces between atoms do not obey Hooke's law, and a simpler classical treatment was given by Schrödinger (1922). Neither treatment makes a quantitative comparison between theory and experiment. Nor do simplified accounts, using a two-atom model, given in books by Kittel (1953), Peierls (1955) and others.

The following treatment of the two-atom model connects the temperature coefficient of C_V with Grüneisen's γ and the coefficient of thermal expansion, and thus allows its magnitude to be estimated.

§ 2. Theory

The standard treatment of the two-atom model considers an atom to be executing its thermal motion along a straight line in an asymmetrical potential provided by a fixed atom. The total energy E is expressed in terms of the momentum p and the displacement x from the equilibrium inter-atomic distance (r) by the equation

$$E=\frac{p^2}{2m}+ax^2+bx^3+cx^4+dx^5+\ldots.$$

Here m is the mass of the atom and a, b, c, d, etc. are coefficients determined by the shape of the inter-atomic potential. It is important to note that if the equilibrium position is altered by imposing an external force on the atom, these coefficients are altered, because the expansion of the inter-atomic potential into a power series must then be made about a different point of the potential curve.

---

† Communicated by the Author.

The partition function (sum over states) is, in the form given by classical statistical mechanics,

$$Z=\iint \exp(-E/kT)\,dx\,dp$$

where T is the absolute temperature and k is Boltzmann's constant. It is assumed that the effect of the third and subsequent terms of the above expansion for E is small, and Z is obtained in the form of a power series in kT of which only the first two terms are retained :

$$Z=\frac{kT}{\nu}\left\{1+\left(\frac{15b^2}{16a^3}-\frac{3c}{4a^2}\right)kT\right\}.$$

Here ν is the frequency of vibrations of small amplitude and is given by

$$\nu=\frac{1}{\pi}\left(\frac{a}{2m}\right)^{1/2}. \qquad . \; . \; . \; . \; . \; . \; . \; . \quad (1)$$

The heat capacity per atom at constant volume is, to the first order in T,

$$C_{\mathrm{V}}=T\frac{\partial^2}{\partial T^2}(kT\ln Z)=k(1+2BkT) \qquad . \; . \; . \; . \; . \; . \quad (2)$$

where

$$B=\frac{15b^2}{16a^3}-\frac{3c}{4a^2}. \qquad . \; . \; . \; . \; . \; . \; . \; . \quad (3)$$

This is the usual result. The purpose of the following analysis is to relate B to measured quantities.

The mean value of x is (Kittel 1953)

$$\langle x\rangle=Z^{-1}\int x\exp(-E/kT)\,dx\,dp=-\frac{3b}{4a^2}kT \qquad . \; . \; . \quad (4)$$

to a first approximation. It is evident that if $|b|$ is large both the thermal expansion and the increase of C_{V} will be large. This correlation, noted by Born and Brody, suggests that B should be evaluated by relating it to the thermal expansion, and this may be done by introducing also the change of vibration frequency with volume.

A change of volume, in terms of this model, implies that the position of equilibrium has been shifted by an impressed force. As previously noted, the coefficients a, b, c, etc. are functions of the equilibrium inter-atomic distance r. If the distance from the new position of equilibrium is x, and the impressed force A has moved the position of equilibrium a distance dr, the distance from the old position of equilibrium is $x+dr$.

The actual potential energy is the same, whether expressed as a power series with the old coefficients about the old position of equilibrium, or with new coefficients about the new position of equilibrium. Hence

$$-Ax+a(x+dr)^2+b(x+dr)^3+c(x+dr)^4+\dots$$
$$=(a+da)x^2+(b+db)x^3+(c+dc)x^4+\dots.$$

Since this is true for all values of x, we may equate coefficients of powers of x and obtain the equations

$$\frac{da}{dr}=3b, \quad \frac{db}{dr}=4c, \text{ etc.} \quad \dots\dots\dots \quad (5)$$

From eqns. (1) and (5),

$$\frac{1}{\nu}\frac{d\nu}{dr}=\frac{3}{2}\frac{b}{a}.$$

This, with eqn. (4), gives

$$-\frac{r}{\nu}\frac{d\nu}{dr}\frac{1}{r}\frac{\partial\langle x\rangle}{\partial T}=\frac{9b^2}{8a^3}k.$$

If the distances between nearest neighbours in a crystal behave in the same way as the inter-atomic distance in this model, then

$$-\frac{d\ln\nu}{d\ln V}\alpha=\frac{9b^2}{8a^3}k, \quad \dots\dots\dots \quad (6)$$

where α is the volume coefficient of expansion and V is the volume of the crystal.

Now
$$-\frac{d\ln\nu}{d\ln V}=\gamma \quad \dots\dots\dots \quad (7)$$

where γ is the quantity used by Grüneisen (1926) in his discussion of thermal expansion. It may be obtained experimentally from the relation

$$\alpha=\frac{\gamma C_V}{VK_T} \quad \dots\dots\dots \quad (8)$$

where K_T is the isothermal bulk modulus. If γ is defined by eqn. (8), then eqn. (7) is not exact, but the approximation is reasonable in the present context.

Equations (3), (6) and (7) now give

$$Bk=\frac{5}{6}\gamma\alpha\left(1-\frac{4ca}{5b^2}\right). \quad \dots\dots\dots \quad (9)$$

The dimensionless parameter ca/b^2 depends on the shape of the inter-atomic potential curve, but is not affected by stretching the curve uniformly parallel to either axis. It may be evaluated for any assumed type of inter-atomic force law. (Measurements of volume at high pressures give a and b, but are not in general accurate enough to give c.)

According to Slater (1939), a potential suitable for metals is that due to Morse:

$$v=L\exp\{-2a_1(r-r_0)\}-2L\exp\{-a_1(r-r_0)\},$$

where L and a_1 are constants, r is the distance between atoms and r_0 is the equilibrium distance under zero external force. In this case ca/b^2 is 7/12, and

$$2Bk=\frac{8}{9}\gamma\alpha.$$

A form of potential used by Mie (1903) and others is

$$v=-\frac{M}{r^m}+\frac{N}{r^n},$$

where M, N, m and n are positive constants and n is greater than m. In this case eqn. (9) gives

$$2Bk=\left(\frac{2}{3}+\frac{mn-2}{(m+n+3)^2}\right)\gamma\alpha.$$

Table 1 shows that the value of the quantity $q=2Bk/\gamma\alpha$ is rather insensitive to n and m. Referring to eqn. (2), we therefore have finally, to the first order in T,

$$C_V=k(1+q\gamma\alpha T) \quad . \quad . \quad . \quad . \quad . \quad . \quad . \quad . \quad (10)$$

where q is expected to be not much less than unity.

Table 1

n m	9 1	5 1	5 3	9 3	9 6	Morse potential
q	0·71	0·70	0·77	0·78	0·83	0·89

Both γ and α are slow functions of temperature, but here they have been regarded as independent of T, and the treatment has been to the first order in T. Higher terms undoubtedly exist, and are likely to be of some importance near the melting point, but the limited purpose of the present treatment is to obtain an approximation for the linear term and compare it with the general trend of experimental results.

§ 3. DISCUSSION

The thermodynamic relation between C_P and C_V, combined with eqn. (8), gives

$$C_P=C_V(1+\gamma\alpha T). \quad . \quad . \quad . \quad . \quad . \quad . \quad . \quad . \quad (11)$$

Equations (10) and (11) show that the increase of C_V above the Dulong and Petit value is only a little less than the difference between C_p and C_V. The exact relation is of course dependent on the nature of the interatomic force law. To the first order in T, eqns. (10) and (11) combine to give

$$\frac{1}{C_p}\left(\frac{\partial C_p}{\partial T}\right)_p=(1+q)\gamma\alpha. \qquad (12)$$

In table 2, experimental values of the left-hand side for a few simple substances are compared with values of $\gamma\alpha$ evaluated at twice the Debye temperature.

The effect of using twice the Debye temperature rather than, say, room temperature is small but appreciable. The rather arbitrary choice could be avoided only by use of a higher order of approximation for C_V than that given by eqn. (10). For the metals listed, the electrons make a small contribution C_e to the specific heat, and the second column of table 2 shows $(\partial C_e/\partial T)_p/C_p$ calculated for one free electron per atom.

Table 2. Units are 10^{-5} °C^{-1}

	$\frac{1}{C_p}\left(\frac{\partial C_e}{\partial T}\right)$	$\frac{1}{C_p}\left(\frac{\partial C_p}{\partial T}\right)_p$	$\gamma\alpha$ at 2θ	Ratio $(1+q)$	Reference
Pb	4	34	19	1·8	Douglas and Dever (1954)
Cu	2	23	12	1·9	Landolt-Bornstein (1912–36)
Na	4	85	35	2·4	Dauphinee *et al.* (1955)
NaCl	—	43	24	1·8	Popov and Gal'chenko (1951)
KCl	—	39	21	1·9	Skuratov and Lapushkin (1951)
KBr	—	38	22	1·7	Cooper (1953), Skuratov and Lapushkin (1951)

This has been subtracted from the observed $(\partial C_p/\partial T)_p/C_p$ to give the lattice contribution shown in the third column. The ratio in the fifth column is an experimental measure of $1+q$, which according to table 1 is expected to lie between 1·7 and 1·9.

For sodium $(\partial C_p/\partial T)_p/C_p$ is rather larger than suggested by this crude theory. Furthermore, it increases markedly near the melting point. The present discussion, having been taken only as far as terms linear in T, cannot indicate how much of this increase is to be expected in a perfect lattice and how much has to be assigned to other causes such as the thermal generation of crystal defects (Carpenter 1953).

In recent discussions of the 'linear chain', Dugdale and MacDonald (1954) and MacDonald and Roy (1955) conclude that C_V should decrease with increasing temperature. They suggest that the difference between this behaviour and that of simple solids is a real difference between a linear chain and a solid body. This seems unlikely in view of the agreement obtained above with an even simpler model. The relevant error in the general discussion of MacDonald and Roy is that they regard their λ_i (equivalent to the a, b, c, etc. of the present discussion) as independent of volume, and therefore obtain too low a value for C_P.

§ 4. CONCLUSION

A crude theory predicts that above the Debye temperature C_V exceeds the Debye value by almost as much as C_P exceeds C_V, which roughly agrees with experimental results for several simple solids.

ACKNOWLEDGMENTS

I wish to thank Mr. L. G. Carpenter and Dr. D. L. Martin for valuable discussions, and Mr. W. N. Mair for improving the presentation.

REFERENCES

BORN, M., and BRODY, E., 1921, *Z. Phys.*, **6,** 132.
CARPENTER, L. G., 1953, *J. chem. Phys.*, **21,** 2244.
COOPER, C. B., 1953, *J. chem. Phys.*, **21,** 777.
DAUPHINEE, T. M., MARTIN, D. L., and PRESTON-THOMAS, H., 1955, *Proc. roy. Soc.* A, **233,** 214.
DOUGLAS, T. B., and DEVER, J. L., 1954, *J. Amer. chem. Soc.*, **76,** 4824.
DUGDALE, J. S., and MACDONALD, D. K. C., 1954, *Phys. Rev.*, **96,** 57.
GRÜNEISEN, E., 1926, *Handbuch der Physik*, **10,** 1.
KITTEL, C., 1953, *Introduction to Solid State Physics* (London : Chapman and Hall), pp. 78, 87.
LANDOLT-BORNSTEIN, 1912–1936, *Physikalisch-Chemische Tabellen* (Berlin : Springer).
MACDONALD, D. K. C., and ROY, S. K., 1955, *Phys. Rev.*, **97,** 673.
MIE, G., 1903, *Ann. Phys. Lpz.*, **11,** 657.
PEIERLS, R. E., 1955, *Quantum Theory of Solids* (Oxford : Clarendon Press).
POPOV, M. M., and GAL'CHENKO, G. L., 1951, *Zh. Obshch. Khim.*, **21,** 2220.
SCHRÖDINGER, E., 1922, *Z. Phys.*, **11,** 170.
SKURATOV, S. M., and LAPUSHKIN, S. A., 1951, *Zh. Obshch. Khim.*, **21,** 2217.
SLATER, J. C., 1939, *Introduction to Chemical Physics* (New York : McGraw-Hill), p. 453.

Thermal Expansion of Solids at High Temperatures†

By J. N. Eastabrook
Royal Aircraft Establishment, Farnborough, Hampshire

[Received August 6, 1957]

Summary

In a theory of thermal expansion above the Debye temperature, the increases of specific heat and Grüneisen's γ with temperature are taken into account. The increase of expansion coefficient with temperature observed in several simple substances is shown to be about that expected for a perfect crystal. It is not evidence for the thermal generation of defects in the crystal.

§ 1. Introduction

The volume coefficient of thermal expansion (α) is normally observed to increase with increasing temperature, even well above the Debye temperature. This increase has been thought by some investigators (Lawson 1950, Uno 1951, Gertsriken 1954) to be a measure of the rate of increase of vacancy concentration with temperature.

However, Grüneisen's theory of thermal expansion predicts an increase of α with increasing temperature for a perfect crystal, and has been used by Grüneisen (1926), Nix and MacNair (1942) and Fischmeister (1956) to explain the increase observed for many simple substances. All these authors regard the two constants of Grüneisen's equation (Q_0 and $(m+n+3)$ in Grüneisen's notation) as independent constants to be determined empirically. They are in fact both related to the nature of the inter-atomic forces and hence to each other. When this relationship is taken into account it is found that Grüneisen's equation predicts only part of the observed increase of α at high temperatures.

This discrepancy, noted by Fischmeister, was made clear by Fletcher (1957), who used the basic Grüneisen hypotheses to obtain an explicit relation between α and temperature. The increase of α at high temperature thus calculated for potassium chloride is about half the experimental value.

In Grüneisen's theory, thermal expansion is related to the failure of Hooke's law by noticing that the frequencies of atomic vibrations are dependent on volume. The failure of Hooke's law is not, however, taken into account in dealing with the energy of the thermal vibrations, for which the Debye expression is used. This procedure is justified in obtaining a value for α at low temperatures, but it will be shown that a better approximation is needed to obtain the variation of α above the Debye temperature.

---

† Communicated by the Author.

In the following treatment Grüneisen's law is obtained in a form which allows the theory of the variation of specific heat at high temperatures developed by Born and Brody (1921) and Schrödinger (1922) to be applied. An expression is thus derived for the variation of Grüneisen's γ with temperature. The increase of thermal expansion with temperature is found to be about twice that given by Grüneisen's theory, and the result is compared with experiment for some simple crystals.

§2. GRÜNEISEN'S LAW IN EXACT FORM

Let p, V, T and S be the pressure, volume, temperature and entropy of a fixed mass of a crystalline substance. Following Varley (1956) and Wilson (1941), we start with Maxwell's relation

$$\left(\frac{\partial p}{\partial T}\right)_V=\left(\frac{\partial s}{\partial V}\right)_T$$

which may be written

$$-\left(\frac{\partial p}{\partial V}\right)_T\left(\frac{\partial V}{\partial T}\right)_p=-\left(\frac{\partial S}{\partial T}\right)_V\left(\frac{\partial T}{\partial V}\right)_S$$

or

$$K_T\alpha=-\frac{C_V}{T}\left(\frac{\partial T}{\partial V}\right)_S, \qquad (1)$$

where α is the volume coefficient of expansion, K_T is the isothermal bulk modulus and C_V is the heat capacity at constant volume. With γ defined by

$$\gamma=-\frac{V}{T}\left(\frac{\partial T}{\partial V}\right)_S=-\left(\frac{\partial \ln T}{\partial \ln V}\right)_S, \qquad (2)$$

eqn. (1) may be written

$$\alpha=\frac{\gamma C_V}{VK_T} \qquad (3)$$

or, using a well-known thermodynamic relation,

$$\alpha=\frac{\gamma C_p}{VK_S} \qquad (4)$$

where K_S is the adiabatic bulk modulus. Equations (3) and (4) are exact. To make them useful some information about γ must be obtained from statistical mechanics.

§3. THE VALUE OF γ

3.1. *γ in the Debye Approximation*

In the Debye approximation the entropy is of the form

$$S=f(\theta/T)$$

where θ is a function of volume only. Hence, for constant S, T is proportional to θ, so that eqn. (2) becomes

$$\gamma = -\frac{d \ln \theta}{d \ln V} . \qquad (5)$$

Thus γ is independent of temperature in the Debye approximation.

Since V and K_S are slow functions of temperature, eqn. (4) shows that α is approximately proportional to C_p. This is the original version of Grüneisen's law.

When Grüneisen's formula for the temperature variation of K_T is put into eqn. (3), together with γ from eqn. (5), the resulting expression for α becomes identical, to the first order in T, with the equation used by Grüneisen, Nix and Fischmeister mentioned in § 1.

3.2. *The Failure of Grüneisen's Equation*

The question is, whether the failure of this equation at high temperatures is caused by imperfections in the crystal or by a fault in the theory.

It is not due to errors in the expression for K_T: according to eqn. (3), with γ and C_V constant, α is inversely proportional to VK_T, but table 1 shows that for several simple substances α actually increases appreciably faster than $1/VK_T$.

Table 1

	$\frac{1}{\alpha}\left(\frac{\partial\alpha}{\partial T}\right)_p$	$-\frac{1}{K_T}\left(\frac{\partial K_T}{\partial T}\right)_p - \alpha$	$\frac{1}{C_V}\left(\frac{\partial C_V}{\partial T}\right)_p$	$\frac{\epsilon}{\gamma_0}$
Pb	84 (Stokes and Wilson 1941)	47 (Bridgman 1923)	15	2·5
Cu	47 (Nix and McNair 1941)	23 (Overton and Gaffney 1955)	11	2·2
Na	220 (Hagen 1883)	78 (Quimby and Siegel 1938)	50	2·8
NaCl	95 (Fischmeister 1956)	56 (Slater 1924)	19	2·0
Kcl	97 (Glover 1954)	38 (Slater 1924)	18	3·3

Units are 10^{-5} °C^{-1} Values of $(\partial C_V/\partial T)_p/C_V$ are computed at twice the Debye temperature.

The cause of the failure must therefore be the prediction that γC_V is constant at high temperatures. This prediction is not a result of the approximations peculiar to Debye's theory, for, as may easily be shown, any theory which resolves the heat motion into that of a number of independent harmonic oscillators gives an expression for the entropy which leads to a constant value for γ at temperatures high enough to excite all the oscillators fully.

Hence the discrepancy between the experimental results and the predictions of Grüneisen's equation must be due either to imperfections in the crystal or to the use of the harmonic approximation. In the next section the latter possibility is investigated.

3.3. *First Approximation for the Temperature Dependence of* γC_V

If the harmonic approximation were valid, $(\partial C_V/\partial T)/C_V$ would, after subtraction of the electronic contribution, be small at high temperatures, but it is actually quite comparable with $(\partial K_T/\partial T)/K_T$. Since it is only in the harmonic approximation that γ has been shown to be constant, we now try to assess the variation of γ with temperature, using, in eqn. (2), an expression for the entropy which takes account of the anharmonic nature of the thermal motion. Born and Brody (1921) have shown that the Helmholtz free energy at high temperatures is, to a second approximation,

$$F=3RT\{\ln(\nu/kT)-BkT\}.$$

Here ν is the geometric mean of the frequencies of the normal modes at small amplitudes, and B is a quantity independent of T which expresses the effect of departures from Hooke's law.

Since $S=-(\partial F/\partial T)_V$, it is easy to obtain

$$C_V=T(\partial S/\partial T)_V=3R(1+2BkT) \quad . \quad . \quad . \quad . \quad (6)$$

and

$$\gamma C_V=V(\partial S/\partial V)_T=3R\gamma_0(1+2BkT\epsilon/\gamma_0) \quad . \quad . \quad . \quad . \quad (7)$$

where

$$\gamma_0=-\frac{d\ln\nu}{d\ln V} \quad . \quad . \quad . \quad . \quad . \quad . \quad . \quad . \quad (8)$$

and

$$\epsilon=\frac{d\ln B}{d\ln V}. \quad . \quad . \quad . \quad . \quad . \quad . \quad . \quad . \quad (9)$$

Thus γC_V increases ϵ/γ_0 times faster than C_V itself. Since B has not been calculated accurately, only a crude value of ϵ is obtainable. Although ϵ depends on the nature of the inter-atomic forces, which vary from substance to substance, it is possible to make some rough general estimates.

In the theory of Born and Brody and Schrödinger, the energy is stated in terms of the normal momentum and position coordinates, p_i and q_i of the crystal in the form

$$E=\tfrac{1}{2}\sum_l(p_l^2+\omega_l^2q_l^2)+f_3(q_i)+f_4(q_i).$$

The ω_l are the angular frequencies of oscillation of the normal modes at infinitesimally small amplitudes. The quantity f_3 is the sum over all values of i, j, k, of terms $b_{ijk}\,q_i\,q_j\,q_k$ where the b_{ijk} are unknown coefficients which depend on the nature of the inter-atomic forces. Similarly f_4 is the sum over i, j, k, l, of $c_{ijkl}q_iq_jq_kq_l$. It may be shown that the value of B is then

$$B=\sum\frac{b_{ijk}b_{lmn}}{\omega_i\omega_j\omega_k\omega_l\omega_m\omega_n}-\sum\frac{c_{ijkl}}{\omega_i\omega_j\omega_k\omega_l},$$

where the first summation includes only those terms for which the denominator can be expressed in the form $\omega_a^2\omega_b^2\omega_c^2$ and the second summation includes only those terms for which the denominator has the form $\omega_a^2\omega_b^2$.

If we assume that all the coefficients of the second-, third-, and fourth-order terms in the expression for the potential energy depend on volume in the same way, then

$$\frac{d\ln B}{d\ln V}=-\frac{d\ln\omega^2}{d\ln V}=-2\frac{d\ln\nu}{d\ln V}.$$

Hence, from eqns. (8) and (9),

$$\epsilon\ \gamma_0=2. \qquad \text{. . . . . (10)}$$

The derivation of this equation takes account of the coupling between atomic vibrations, but makes the crude assumption that all the ω_i^2, b_{ijk} and c_{ijkl} alter in proportion when the volume is altered. Another approach is to ignore the coupling and treat a two-atom model, using an empirical form of inter-atomic potential to determine the volume dependence of the coefficients. It has been shown in a previous paper (Eastabrook 1957) that the two-atom model allows a reasonable estimate of the quantity B. From eqns. (1), (3) and (5) of that paper one easily obtains, the same notation,

$$\frac{\epsilon}{\gamma_0}=6\left(\frac{15}{16}-\frac{4ca}{3b^2}+\frac{5da^2}{12\,b^3}\right)\Big/\left(\frac{15}{16}-\frac{3ca}{4b^2}\right).$$

Table 2 shows values of ϵ/γ_0 obtained with a Morse potential, and with a Mie potential using various values of the exponents m and n. It will be noted that ϵ/γ_0 is not very sensitive to m and n. Thus, from both table 2 and eqn. (10) we expect ϵ/γ_0 to be about two or three; that is, γC_V should increase two or three times faster than C_V. A comparison (table 1) of the rates of increase of $(VK_T)^{-1}$ and C_V shows that according to eqn. (3), about half the increase of α should be related to the increase of γC_V and the rest to the decrease of VK_T.

Table 2

n m	5 1	9 1	5 3	9 3	9 6	Morse potential
ϵ/γ_0	2·48	2·44	2·86	2·86	3·16	3·17

From eqn. (3),

$$\frac{1}{\gamma C_V}\left(\frac{\partial(\gamma C_V)}{\partial T}\right)_p=\frac{1}{\alpha}\left(\frac{\partial\alpha}{\partial T}\right)_p+\frac{1}{K_T}\left(\frac{\partial K_T}{\partial T}\right)_p+\alpha. \qquad \text{. . . (11)}$$

Thus an experimental measure of ϵ/γ_0 is obtained by comparing the quantity on the right with $(\partial C_V/\partial T)_p/C_V$ after allowing, where necessary, for the small electronic contribution. Independent measurements of the quantities needed in eqn. (11) are rarely concordant, and the figures for ϵ/γ_0 in table 1 should be regarded merely as evidence of a general trend. They are, as predicted above, about two or three.

§4. Conclusion

The variation of γ and C_V with temperature must be taken into account when applying Grüneisen's law to the increase of thermal expansion at high temperatures. A rough calculation of the variation of γC_V shows that the increase of α observed in each of several simple substances is such as would be expected for a perfect crystal. Thus the increase of thermal expansion at high temperatures cannot be regarded as evidence for the thermal generation of defects in the crystal.

Acknowledgments

I wish to thank Mr. L. G. Carpenter and Dr. G. C. Fletcher for valuable discussions, and Mr. W. N. Mair for useful criticism.

References

Born, M., and Brody, E., 1921, *Z. Phys.*, **6,** 132.
Bridgman, P. W., 1923, *Proc. Amer. Acad. Arts. Sci.*, **58,** 166.
Eastabrook, J. N., 1957, *Phil. Mag.*, **2,** 1415.
Fischmeister, H. F., 1956, *Acta cryst.*, **9,** 416.
Fletcher, G. C., 1957, *Phil. Mag.*, **2,** 639.
Gertsriken, S. A., 1954, *Doklady Acad. Nauk.*, **98** (2), 211.
Glover, R. E., 1954, *Z. Phys.*, **138,** 222.
Grüneisen, E., 1926, *Handbuch der Physik*, **10,** 1 (Berlin : Springer).
Hagen, E., 1883, *Ann. Phys. Lpz.*, **19,** 436.
Lawson, A. W., 1950, *Phys. Rev.*, **78,** 185.
Nix, F. C., and MacNair, D., 1941. *Phys. Rev.*, **60,** 597 ; 1942, *Ibid.*, **61,** 74.
Overton, W. C., and Gaffney, J., 1955, *Phys. Rev.*, **98,** 969.
Quimby, S. L., and Siegel, S., 1938, *Phys. Rev.*, **54,** 293.
Schrödinger, E., 1922, *Z. Phys.*, **11,** 170.
Slater, J. C., 1924, *Phys. Rev.*, **23,** 488.
Stokes, A. R., and Wilson, A. J. C., 1941, *Proc. phys. Soc. Lond.*, **53,** 658.
Uno, R., 1951, *Busseiron Kenkyu*, **36,** 32.
Varley, J. H. O., 1956, *Proc. roy Soc.* A, **237,** 413.
Wilson, A. J. C., 1941, *Proc. phys. Soc. Lond.*, **53,** 235.

The Internal Friction of Cold-Worked Copper at Low Temperatures†

By D. H. Niblett and J. Wilks
Clarendon Laboratory, Oxford

[Received July 19, 1957]

Summary

The internal friction of cold-worked polycrystalline copper has been measured in the temperature range 20° to 300°K, and a study made of the maximum in the curve of internal friction *versus* temperature first observed by Bordoni. The measurements indicate how the internal friction varies as a function of the amount of cold work, and also the effect of impurities in the metal and of neutron irradiation. The results are discussed with particular reference to recent theoretical treatments by Seeger.

---

§ 1. Introduction

The internal friction of several cold-worked metals in the temperature range from 4° to 300°K has been measured by Bordoni (1949, 1954), who showed the existence of a peak in the curve of damping against temperature. Bordoni's principal results, obtained at frequencies between 10 and 40 kc/s, are shown in fig. 1, the internal friction being expressed in terms of the quantity $1/Q$ (the logarithmic decrement δ divided by π). The largest peak occurs for copper at a temperature of about 90°K. For aluminium, lead and silver the damping is smaller; the peaks are less pronounced, and occur at somewhat different temperatures. The existence of such peaks has subsequently been confirmed by the present authors (1955) in the case of copper, and by Bömmel (1955) and Hutchison and Filmer (1956) who made measurements at frequencies in the megacycle range on single crystals of lead and on polycrystalline aluminium respectively.

As no completely satisfactory explanation of these peaks was available, the present work was undertaken in order to obtain more systematic information; in particular to investigate the internal friction as a function of cold work more closely than had been done previously. All the present experiments have been made on copper, as this metal appeared to show the largest effect. Measurements have also been made to investigate the effects of neutron irradiation and of the introduction of impurity atoms. Two short notes giving a brief account of some of our results have already been published (Niblett and Wilks 1955, 1956).

---

† Communicated by the Authors.

Fig. 1

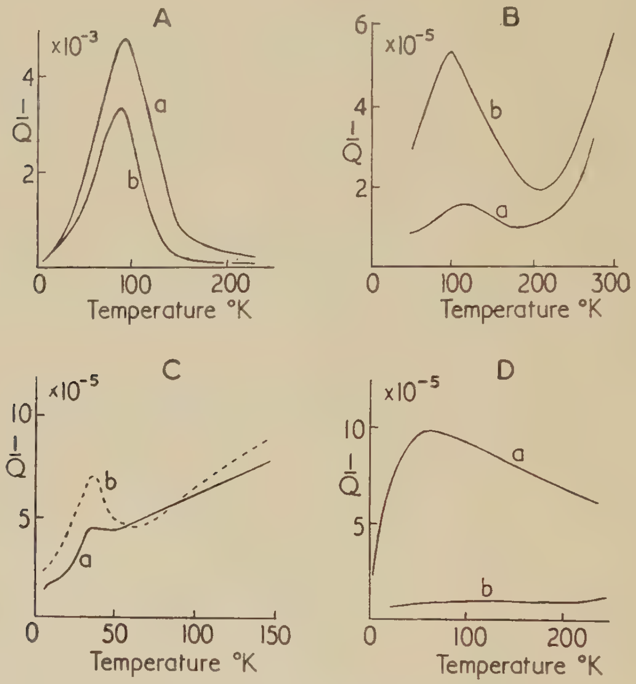

Internal friction in metals (Bordoni 1954).

A. Chemically pure polycrystalline copper. (*a*) machined; (*b*) after 10 hours annealing at 150°C.
B. 99·9% pure aluminium. (*a*) after 1 hour anneal at 140°C; (*b*) after 2% permanent strain.
C. Lead. (*a*) chemically pure; (*b*) commercial.
D. Silver. (*a*) machined; (*b*) after $1\frac{1}{2}$ hours anneal at 200°C.

§ 2. Apparatus

The principal features of our experimental arrangement are illustrated in fig. 2. The specimen, a rectangular bar 8 cm long, 1 cm wide and about 1·8 mm thick, is supported on the edges of two razor blades, which are positioned at the nodes of fundamental flexural vibrations. The bar is driven at its resonant frequency by applying an alternating voltage to an electrode placed beneath its centre, the separation of the electrode from the specimen being about 0·3 mm. To detect the resulting motion of the bar, two electrodes are placed one at each end of the specimen, thus forming small parallel-plate condensers, each with a capacity of about 3 μμF. The movement of the specimen produces changes in the capacity of these condensers, whose magnitude is proportional to the amplitude of the vibrations. These variations in capacity are measured by a circuit in which the condensers are connected in parallel with the tank circuit of a quartz oscillator; motion of the specimen produces a modulation of the output of the oscillator, and this is displayed on a cathode-ray oscilloscope. A measurement is made by observing the free decay of the oscillations on switching off the drive voltage, either by photographing the oscilloscope trace or with a level recorder. (A level recorder with a suitable logarithmic potentiometer converts an exponentially-decaying signal into a linear pattern on a moving strip of paper, and the internal friction is given immediately from the slope of the trace.)

Fig. 2

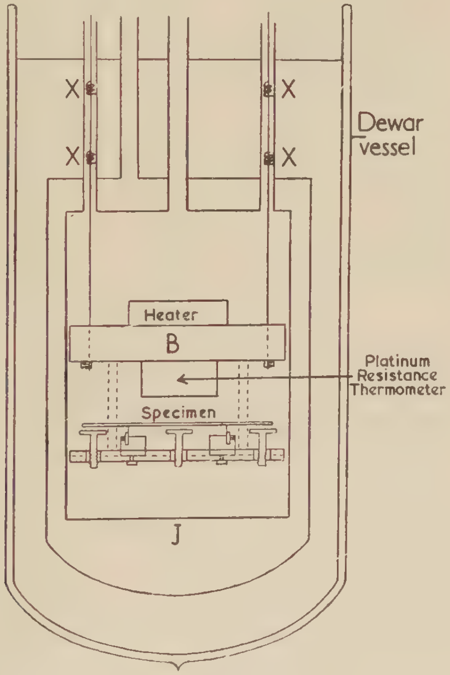

Apparatus for measuring internal friction at low temperatures.

The absolute value of the strain amplitude may in principle be calculated from the driving voltage and the separation of the plates, but this is rather difficult as the gap is small and not always quite uniform. Also as the strain varies throughout the specimen, the experiments measure the internal friction for a range of strain amplitude; we therefore indicate the amplitude of the vibrations by giving an estimate of the mean strain. In spite of considerable uncertainty in the absolute value of the strain, it is of course possible to obtain accurate values of the relative amplitudes on a given specimen *in situ*.

The razor blades which support the specimen are clamped rigidly in small brass blocks, which are screwed into a groove in a brass base-plate; this is attached by four pillars to a further brass block B, weighing about a kilogram, suspended by three wires from the top of the cryostat. (The fine copper leads soldered to the wires at X ensure that any heat coming down the wires is taken up by the liquid in the dewar.) The cryostat itself is in turn mounted on a massive iron framework embedded in a block of concrete, the whole assembly being designed to reduce the effect of external vibrations to a minimum. The specimen and brass block, B, are enclosed by a vacuum jacket, J, which in turn is surrounded by a second vacuum jacket immersed in liquid hydrogen or oxygen. Heating coils are attached to the brass block, B, and to the outside of the jacket, J, in order that measurements can be made over the whole temperature range from 20°K to 300°K. Helium exchange gas at a pressure of about 2 mm of mercury is introduced into the inner vacuum space to establish thermal equilibrium within the jacket J; this space is, however, evacuated before a measurement is made, in order to eliminate damping due to the gas. Temperatures are measured by means of a platinum resistance thermometer, wound on a brass former attached to the underside of the brass block.

§ 3. Results

3.1. *Preliminary*

We have subtracted from all our results the damping due to the thermo-elastic effect, using an expression due to Zener (1937) which has been verified experimentally by Bennewitz and Rötger (1938) for german silver reeds, by Zener *et al.* (1938) for copper, and by Berry (1955) for α-brass. In all cases the correction is a small fraction of the total damping, being less than 2% in the region of the peaks. Unless otherwise stated the measurements were made on high purity oxygen-free polycrystalline copper (99·999%) supplied by the British Non-Ferrous Metals Research Association. All the specimens were first annealed in argon for one hour at 600°C, and then plastically deformed at room temperature by longitudinal extension in a Hounsfield tensometer. The ends of the specimen, which had been gripped in the jaws of the tensometer, were cut off before the internal friction was measured. In a preliminary experiment a specimen was strained 4% and its internal friction subsequently measured at room temperature as a function of time. A large fraction of the increase in damping produced by the deformation disappeared within a few hours; this is the so-called Köster effect first observed in brass and steel (Forster and Köster 1937, Köster and Rosenthal 1938). All the specimens in the present experiments were therefore left at room temperature for several days after deformation before measurements were made, so that any further changes in the damping, associated with the Köster effect, would be negligible.

3.2. *The Effect of Cold Work*

The temperature dependence of the damping of one annealed specimen prior to deformation is shown in fig. 3. The two curves were obtained during separate experiments on the same specimen at strain amplitudes in the ratio of 2 to 5, the value of the strain amplitude being of the order of 10^{-8}. At higher values of the strain amplitude the damping increases rapidly with increasing amplitude at all temperatures ; hysteresis effects are observed and it becomes difficult to obtain reproducible readings (Niblett 1956).

Fig. 3

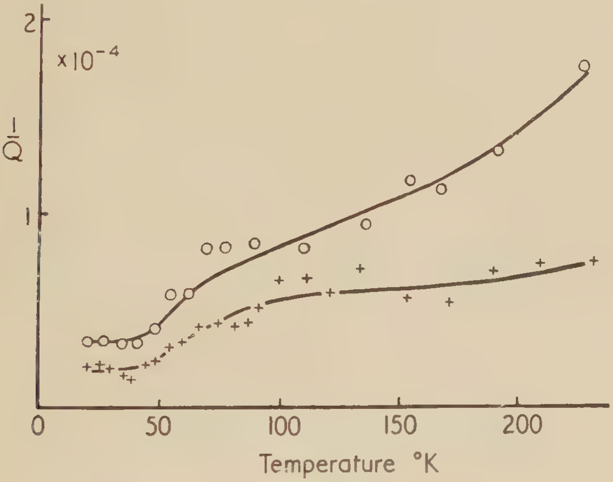

The internal friction of annealed copper. Strain amplitudes in arbitrary units : + 2, ○ 5.

The effect of varying amounts of cold work up to 8·4% extension is shown in fig. 4 : all the measurements were made at a strain amplitude of the order of 10^{-7}, and at a frequency of approximately 1100 cycles per second. The most obvious feature of the curves is the existence of two peaks in the internal friction at temperatures of about 32°K and 75°K which become more pronounced in the more strongly cold-worked specimens. For amounts of cold work greater than 2% the peak at the higher temperature is similar in shape to that observed by Bordoni (1949, 1954) for copper, although his measurements do not seem to have been sufficiently detailed to resolve the second peak. (However, Bordoni's results do show some irregularity in the region where this peak might be expected.) The shape of the curve for copper strained 0·5% is similar to that obtained by Bordoni for silver, while that for copper strained

Fig. 4

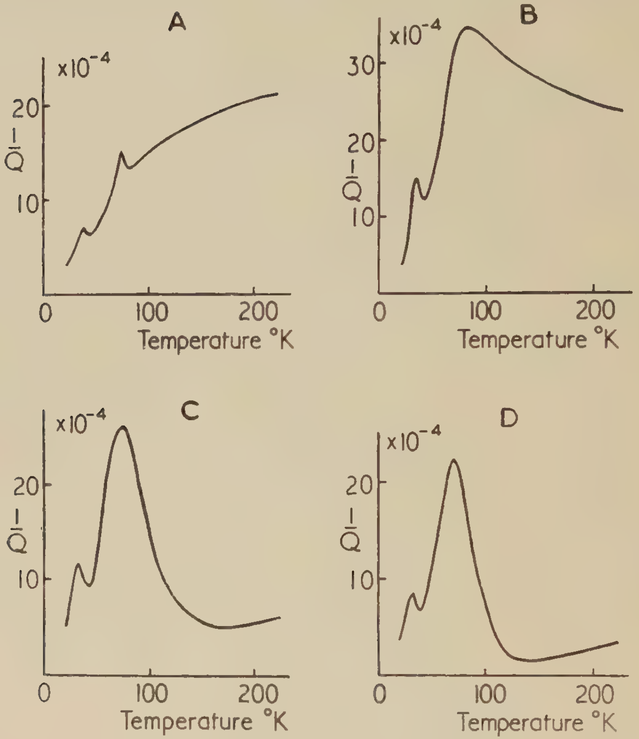

The internal friction of copper.

A. Strained 0·1%. B. Strained 0·5%.
C. Strained 2·2%. D. Strained 8·4%.

Fig. 5

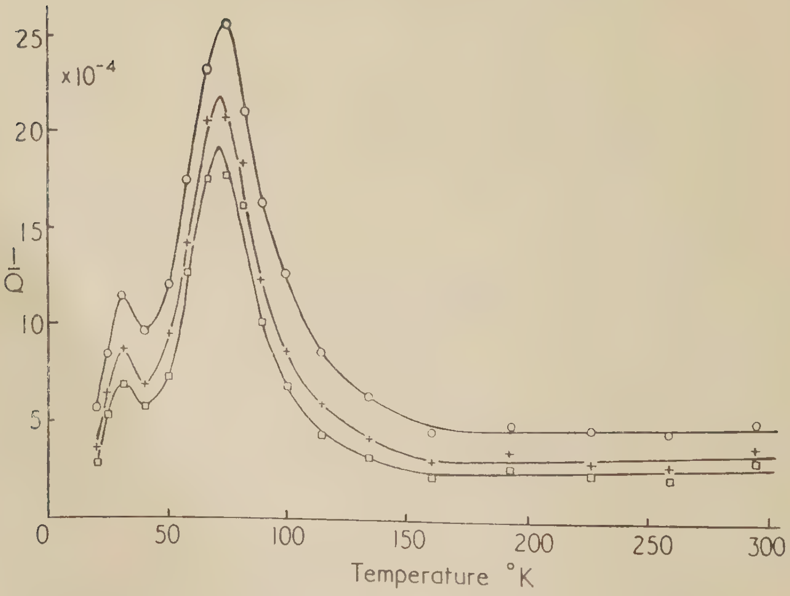

Amplitude dependence of the internal friction of copper, strained 2·2%. Strain amplitudes in arbitrary units : □ 1, + 10, ○ 100.

0·1% bears some resemblance to Bordoni's curve for lead. Hence the marked variation in the shape of Bordoni's curves may arise not so much from the difference in materials but rather from the metals being subjected to different amounts of cold work.

In the more strongly cold-worked specimens the damping is to a first approximation independent of the strain amplitude; this is illustrated in fig. 5, which shows the internal friction of a specimen strained 2·2% measured at three strain amplitudes in the ratio 1 : 10 : 100 (the absolute values being in the range 10^{-9}–10^{-6}). This absence of strong amplitude dependence, together with the fact that the stresses applied during a measurement have virtually no effect on the state of strongly cold-worked specimens, results in these measurements being much more reproducible than those on annealed copper.

At first, both peaks increase in amplitude (at a similar rate) with increasing deformation, and appear to be superposed on a background of friction arising from some different mechanism, presumably that responsible for the damping in the annealed state. Ultimately at extensions of more than about 2%, the amplitude of the peaks becomes approximately independent of the amount of pre-strain. It is to be noted that the peaks occur at approximately the same temperatures for each specimen. It seems that the friction of specimens which have suffered only small pre-strains may be resolved into two components consisting of peak and background, and in this case also the shape and position of the peaks appear similar to that at the higher deformations. Therefore we propose to treat the mechanism responsible for this peak as a separate process, apart from that responsible for the background, and it is with this mechanism that the present paper is principally concerned. The question of the background friction is considerably more complex and is still not understood in detail even at room temperature.

3.3. *Effect of Frequency*

All the measurements so far described were made at a frequency of about 1100 cycles per second. Although it is of interest to obtain measurements at different frequencies, it is difficult to vary the frequency over a wide range with the present apparatus because this involves changing the thickness of the specimen. At higher frequencies the specimen rapidly becomes too thick and stiff to drive; at lower frequencies it becomes too thin to handle. Measurements have, however, been made on a thinner bar with a resonant frequency of 380 cycles per second, which had been strained 9·1%. The friction was similar to that for similarly strained thicker specimens, except that the internal friction peaks now occurred at about 67 K and 30 K (Bordoni's measurements at 30 kc/s show a peak at about 90°K.)

Thus in the more heavily cold-worked specimens, the damping is approximately independent of strain amplitude, the maximum damping is substantially independent of frequency, and the temperature T where the peak occurs varies with frequency. This suggests that the internal friction may arise from a relaxation mechanism, and one might expect to find a relation of the form

$$f = A \exp(-W/kT) \quad \ldots \ldots \quad (1)$$

where f is the frequency of measurement, A a constant, and W the activation energy for the process (see for example, Zener 1948). Hence, a plot of the logarithm of the frequency against the inverse of the temperature at which the peak occurs should give a straight line whose slope is the activation energy. The available information consists of our results at about 1100 c/s and 380 c/s, and Bordoni's measurements at about 30 kc/s. These do not lie very closely on one line, possibly because the peak cannot be attributed to one single activation energy, as is also suggested by the facts that the peaks are broader than might be expected. However, taking the best line possible one obtains a value for the activation energy of about 0·1 ev.

A further criterion for relaxation processes is that there is a change in the elastic modulus, E, on passing through the region of the peak, such that $\Delta E/E = 1/Q_m$ where Q_m is the value of Q at the peak. There is some uncertainty in obtaining exact values of the modulus change associated with the peaks because of the presence of the background friction, but a corresponding modulus change of this order is observed in the more heavily cold-worked specimens.

3.4. *Effect of Annealing*

The effect of annealing at various temperatures was observed using specimens which had been strained 0·1% and 8·4%, and therefore exhibited damping typical of the background and the peaks respectively. All the annealing was carried out in an atmosphere of argon. An anneal for one hour at 200°c had practically no effect on the internal friction of the specimen strained 0·1%, but a subsequent anneal for one hour at 250°c reduced the damping over the whole temperature range to a value as low as that for an unstrained specimen. In the case of the specimen strained 8·4%, an anneal for one hour at 180°c reduced the heights of the peaks by about 40% without changing the general shape of the curve (fig. 6); this result is similar to that obtained by Bordoni after an anneal at 150°c for 10 hours (fig. 1 (*a*)). A subsequent anneal for one hour at 250°c had little additional effect on the damping. After a further anneal for one hour at 350°c, the peaks had disappeared and the curve of damping against temperature was similar to that for a fully annealed or slightly strained specimen. It is also to be noted that the measurements shown in fig. 5 were obtained with the same specimen as that used for fig. 4 (*c*) after a lapse of several months; thus no appreciable annealing occurs at room temperature. Hence it appears that the peaks are not to be associated with the motion of free defects created by the deformation. This suggests that the relaxation mechanism responsible for the internal friction may be the motion of segments of dislocation line, with a comparatively low activation energy, of the order of 0·1 ev.

3.5. *Effect of Impurities and Neutron Irradiation*

Measurements have been made on copper containing 0·0026% bismuth and 0·032% phosphorus, and the results for specimens strained 0·17% and 5·5% are shown in fig. 7. The curves are rather similar in shape to those for correspondingly strained pure copper, but in each case the damping at all temperatures is reduced by a factor of about ten. A

Fig. 6

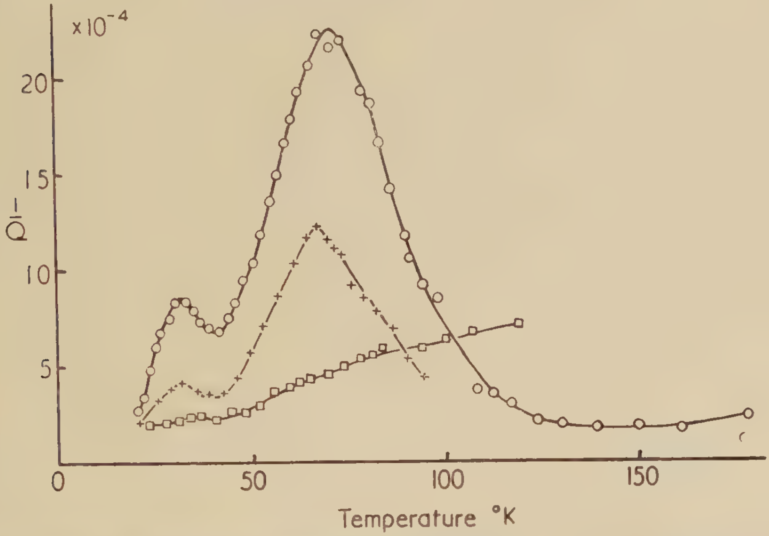

Effect of annealing on the internal friction of copper. ○ After straining 8·4%. + After 1 hour anneal at 180°c. ☐ After 1 hour anneal at 350°c.

Fig. 7

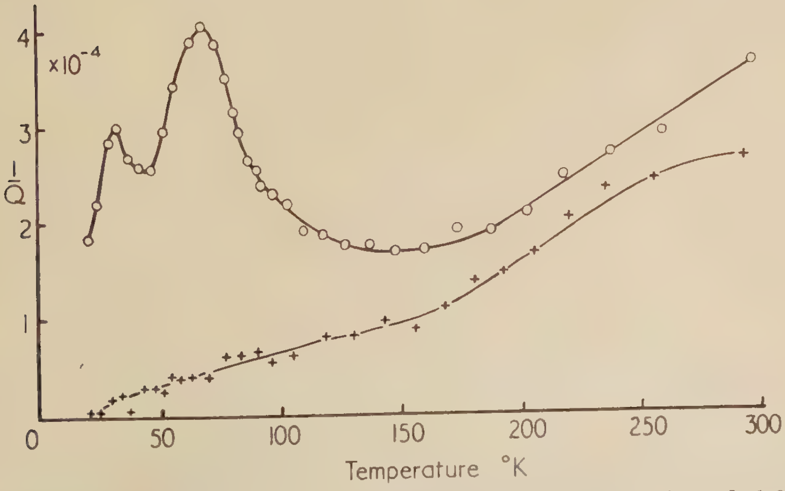

The internal friction of copper, containing 0·0026% bismuth and 0·032% phosphorus. + Strained 0·17%. ○ Strained 5·5%.

similar reduction in the friction has been observed after neutron irradiation as is shown in fig. 8 for a specimen which was first strained 6·6% and then irradiated to a flux of 5×10^{18} n.v.t. in the pile at the Atomic Energy Research Establishment, Harwell. There appears to be a slight shift of the temperature of the peak in these experiments, of about 5° to lower temperatures, but to a first approximation the position and shape remain unchanged. Thus even though the motion of the dislocation lines is considerably reduced the activation energy for the process remains substantially unchanged; and this suggests that it does not depend markedly on the distance between pinning points. Also the effect of cold work is to produce a more complex dislocation net with shorter lengths of free lines, yet the activation energy remains unchanged. Thus the length of dislocation lines responsible for the internal friction peak cannot be specified either by the distance between the nodes of a dislocation net or between pinning points associated with impurity atoms or points defects. (This conclusion is at variance with an explanation of these peaks offered by Mason 1955.) Clearly some form of unit displacement of the dislocation line is involved; and there appear to be two possibilities. Either a bulge is formed by thermal activation as discussed in § 4, or the line becomes pinned and unpinned from some point defects. In the latter case the magnitude of the friction would depend critically on the amount of impurity present. Nearly all our work was done with 99·999% high purity copper in which one might have supposed that the impurity content was quite low. Another experiment was performed on copper from a different source with a significantly better specification: the specimen was annealed *in vacuo*, strained 5·3%, and had a resonant frequency of about 750 c/s. Apart from the presence of a third peak at about 200°K which we refer to later, the friction is similar to that observed before, although the height of the peak is greater

Fig. 8

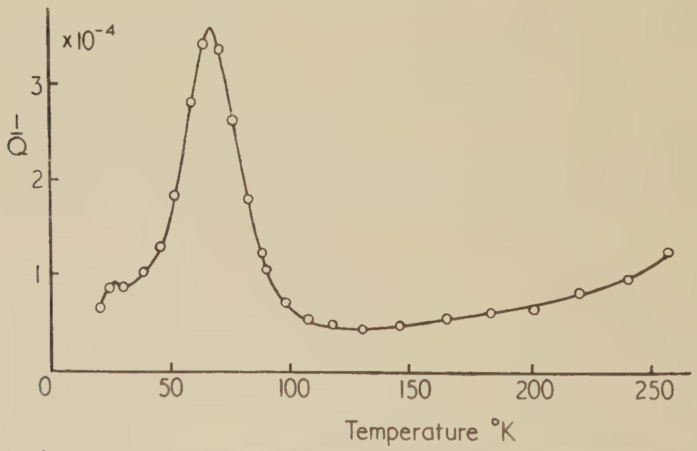

The internal friction of copper, strained 6·6% and subsequently neutron irradiated (5×10^{18} n.v.t.).

(fig. 9). Bordoni's results at 30 kc/s also give the same magnitude of peak for nominally pure copper from some quite different source. If unpinning from impurities were responsible for the friction, it is rather remarkable that all these experiments give such similar results. On the other hand, such a situation is to be expected on a theory due to Seeger which is described below.

Fig. 9

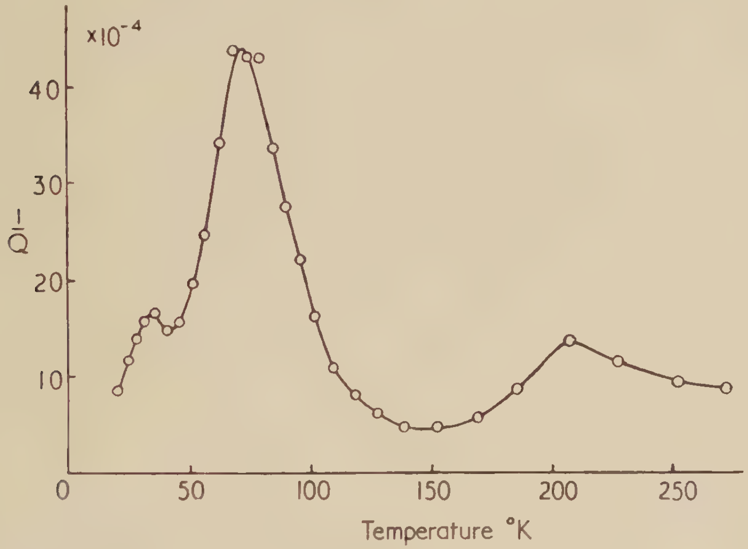

The internal friction of the high purity copper, strained 5·3%.

§ 4. DISCUSSION

4.1. *Seeger's Treatment*

According to Seeger (1955 a), internal friction will arise from the motion of dislocation lines lying parallel to lattice directions. Consider a length of dislocation (AB in fig. 10 (*a*)) lying in a position of minimum energy

Fig. 10

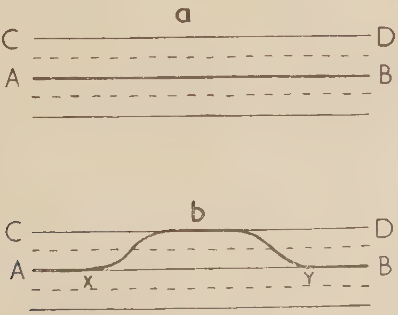

Seeger's dislocation mechanism.

(*a*) Dislocation in position of minimum energy.

(*b*) Bulge in dislocation. (Full straight lines represent positions of minimum energy, broken lines represent positions of maximum energy.)

along a close-packed direction in a lattice, and suppose that an applied stress is tending to move it forward in a direction parallel to itself. If the dislocation acts as a rigid rod, a stress equal to the Peierls' force will be required to move it over the potential barrier to the next equilibrium position CD, but if the line is flexible it may be able to move forward much more easily. Thus, if a small bulge (XY in fig. 10 (*b*)) is formed as the result of thermal fluctuation, a quite small stress will cause it to spread out sideways, as the potential barriers opposing motion in directions parallel to AB and CD are very small. The length of a bulge formed by thermal activation will be determined by the fact that its energy of formation is a minimum ; a longer bulge would require more energy to surmount the Peierls' barrier, while a shorter one would involve a greater increase in line length and energy. A bulge of this type may be regarded as a pair of kinks of the kind which arise when a dislocation passes from one lattice row to the next. In the absence of any stress the two kinks will attract and annihilate each other, but an applied stress will tend to move them apart and increase the slipped area. For a given applied force there will be a certain critical separation of the kinks d_{crit} above which they will separate further, and below which they will come together. Internal friction arises under the influence of an applied stress because of the formation of these bulges : the motion of the two constituent kinks is approximately reversible for small displacements, but as soon as the critical distance d_{crit} is exceeded they will move apart rapidly and irreversibly. The internal friction will be of the general form associated with relaxation processes, as for example is the internal friction arising from the motion of solute atoms in solid solutions subjected to stress induced ordering.

The activation energy for the relaxation process responsible for the internal friction will be W the energy of formation of a bulge. In his initial treatment Seeger (1955 a) took W to be $2w$ where w is the additional energy associated with a single kink in a dislocation which is otherwise parallel to a lattice direction. The value of w is determined by specifying the form of the dislocation by the differential equation

$$E\frac{d^2y}{dx^2}=\mathbf{b}\sigma_{\mathrm{p}}\left(1-\cos\frac{2\pi y}{a}\right)$$

where E is the energy of unit length of line, a the lattice spacing, $\mathbf{b}$ the Burgers' vector, and σ_{p} the Peierls' stress ; hence Seeger (1956) obtains the value

$$w=\frac{2a}{\pi}\sqrt{\left(\frac{2E_0ab\sigma_{\mathrm{p}}}{\pi}\right)}\dagger.$$

However, this treatment is admittedly only an approximation as it ignores the precise form of the energy barrier which must be surmounted

---

† This expression which appears to be the correct one differs by a factor 2 from that previously given by Read (1953).

during the formation of a bulge. A rather more extensive but still approximate treatment (Seeger 1956) leads to the expression

$$W=w[1+\tfrac{1}{4}\log(16\sigma_{\rm p}/\pi\sigma)]$$

where σ is the applied stress: this implies that a factor of 100 on the magnitude of the amplitude changes W by about 20% and so shifts the position of the peak by about 15°. As no such shift is observed (fig. 5), it appears that the approximation is not a very good one. However Seeger *et al.* (1957) have recently reported the results of a much more complete treatment in which the relaxation time is derived from the theory of stochastic processes. This treatment, which has not yet been published in detail, is rather involved so that the expressions for the activation energy and frequency term in eqn (1) cannot be given in an explicit form: reference must therefore be made to the aforesaid paper. In the next paragraph we compare this treatment with our experimental results.

The most satisfying aspect of Seeger's treatment is that his mechanism accounts for a relaxation process with a quite closely defined activation energy, and in the latest treatment this depends only very slightly on the strain amplitude for strains of the order used in the experiments. The treatment also accounts for the presence of two distinct peaks in the internal friction temperature curves. Only dislocations lying parallel to the principal lattice directions will move in the manner discussed; dislocations lying in other directions may move easily under the action of much smaller stresses (Mott and Nabarro 1948) and the relaxation mechanism will not arise. As dislocations lying parallel to lattice directions in a close-packed f.c.c. lattice may have Burgers' vectors corresponding to either a screw or mixed screw-edge orientation, we may expect two activation energies, one for each orientation.

The initial increase of the internal friction with cold work is to be associated with the increase in the number of dislocations, and there are at least two possibilities as to why the friction does not continue to increase for pre-strains greater than 2%. Possibly the density of dislocations continues to increase, but the effect of their interactions becomes so pronounced that they are less liable to lie along lattice directions (Seeger 1956). Alternatively, the number of dislocations may increase much more slowly at the higher stresses, the increased strain arising primarily to the motion of dislocations already present surmounting barriers at which they were previously held up. In either case the behaviour of the internal friction should be reflected in the stress–strain curve, and Feltham and Meakin (1957) have observed a change from linear to parabolic hardening in polycrystalline copper for a strain of about $1\frac{1}{2}$%. (This result being substantially independent of grain size.)

In order to calculate the value of the activation energy from this theory, it is necessary to assume expressions for the energy (E_0) and the inertial mass (m) of unit length of dislocation, and for the Peierls' stress $\sigma_{\rm p}$. As the value of this last parameter is still rather uncertain compared with the other two, Seeger *et al.* assume that $E_0=\frac{1}{2}G\mathbf{b}^2$ and $m=E_0/v_t^2$ (v_t is the velocity of shear waves in the metal), and use the experimental value of the activation energy to calculate a value for σ_p. For the strain amplitudes used in the present experiments, the results of such a calculation are substantially independent of the amplitude, and give $\sigma_\mathrm{p}\simeq 2{\cdot}5\times 10^{-4}G$. If we wish to throw the experimental results into the form of eqn. (1), then Seeger's treatment shows that the term A is weakly temperature dependent but that to a reasonable approximation is about 10^{10}. This is considerably lower than the value obtained in previous treatments which regarded the dislocation as a rigid rod oscillating in the potential trough, but is still appreciably higher than the experimentally determined value of about 10^9. The magnitude of the maximum friction depends on the total length of dislocation in the crystal, on the fraction which is lying parallel to lattice directions and on the length of individual runs of dislocations. Although it is hardly possible to make an exact estimate, it seems that if the total length of line in cold-worked material is taken to be 10^{10} cm^{-2}, then only about 0·1% of the dislocations would contribute to the damping. This would appear to be a reasonable figure in view of the small size of the Peierls' force compared with the other forces acting on the dislocations. It may be noted that electron micrographs (Hirsch *et al.* 1956) do not show much evidence of dislocations lying parallel to lattice directions but it must be remembered that the scale of the mechanism proposed by Seeger is quite small. Thus the critical length of a bulge is estimated to be about 60 atoms, so that even if the mechanism only occurs when runs considerably longer than this are parallel to lattice directions, lengths of a few hundred Å would be sufficient to produce the effect. These could well be present and not show up clearly in the existing photographs.

4.2. *The Effect of Impurities and Neutron Irradiation*

The internal friction is much reduced at all temperatures in copper containing quite small quantities of bismuth and phosphorus. Such an effect is well established at room temperatures (e.g. Marx and Koehler 1950), and must arise from pinning of the dislocations by the impurities. Although a similar explanation will still be valid at lower temperatures in the region of the peaks, two points call for comment. If, as seems probable, the friction at room temperature arises from the motion of dislocation segments about 1 μ long, then an impurity concentration of 1 in 10^4 may have a considerable effect on their mobility. At first sight, such a concentration appears hardly adequate to reduce friction arising from the motion of segments only 60 atoms long. However, during the cold work the dislocations move through the specimen and will interact with any impurity atoms they encounter; thus the concentration of impurities along a dislocation will be greater than the average throughout the specimen. Secondly, if we accept the above explanation of the two peaks, the results imply that pure screws as well as mixed dislocations may be pinned by impurity atoms. This may arise either through their splitting into partials, or due to electronic interaction (Stehle and Seeger 1956). The higher damping observed in the nominally purest copper specimen (fig. 9) may of course be explained by a reduction in the number of pinning points.

The effect of neutron irradiation on a specimen is to reduce the friction of deformed specimens to values rather similar to those observed in impure copper, and it appears that the dislocations are now pinned by interactions with point defects created by the irradiation. Measurements of the change in electrical resistance produced by irradiation (e.g. Marx *et al.* 1952) together with an estimate of the resistivity associated with one vacancy or interstitial suggests that the number of point defects introduced will be roughly of the same order as the concentration of impurity atoms in the specimens previously discussed. The pinning is presumably due to jogs which result from interactions between dislocations and point defects and which restrict the motion of the dislocations (Seeger 1955 b). Irradiation prior to deformation does not reduce friction, but this is hardly to be expected because most of the dislocations responsible for the friction are only introduced by the cold work. In fact the friction has a value somewhat higher than that of the unirradiated copper (fig. 11), and it may be that this is a secondary effect of the increased hardness brought about by irradiation (Billington and Siegel 1950). This is accompanied by a much coarser mode of slip (Jamison and Blewitt 1952), and it may be that for a given amount of slip there is less interaction between the dislocations

Fig. 11

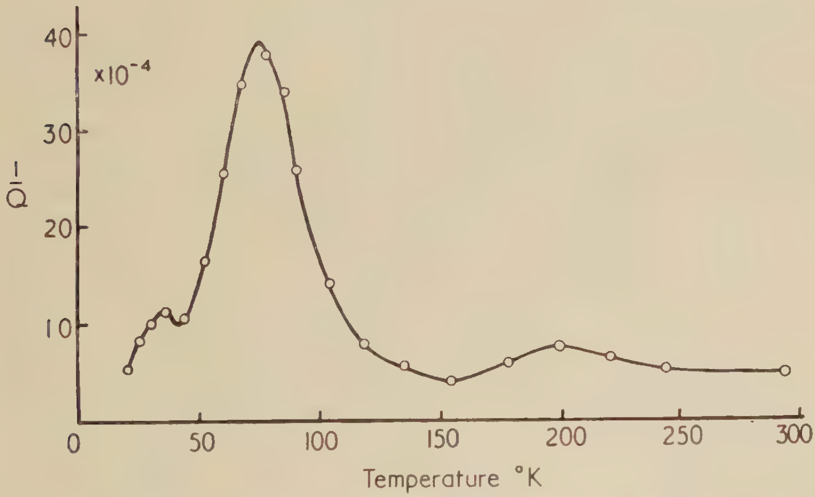

The internal friction of copper, neutron irradiated (5×10^{18} n.v.t.) and subsequently strained 5·1%.

themselves. It is also to be noted that the specimen deformed after irradiation shows a small broad peak in the region of 200°K; this peak which appears common to all specimens so treated is similar to that observed in the nominally purer copper.

4.3. *The Peierls' Stress*

It would appear from the above discussion that Seeger's mechanism gives a good qualitative account of the experimental results, but quantitatively does not lead to the correct magnitude for either the activation energy or the frequency factor. It is true that the value for the Peierls' force is similar to ones calculated theoretically (Dietze 1952, Seeger 1955 a) but as is well known this latter figure depends very critically on the width of the dislocation (e.g. Foreman *et al.* 1951). The latest and most complete treatment (Seeger *et al.* 1957) leads to a value for the Peierls' stress considerably lower than those obtained previously but which is still considerably higher than the yield stress of single crystals (for example, Blewitt *et al.* (1954) quote values of about $10^{-4}G$).

Although the Peierls' stress may be related in some way to the yield stress of single crystals it does not equal it, as the Peierls' stress is the force needed to move a length of dislocation line only if the line lies parallel to a close packed direction and if the dislocation moves as a rigid rod. Our particular concern is whether the Peierls' stress can be higher than the yield stress in material where the yield stress depends neither on impurities nor interactions between dislocations. To obtain appreciable plastic flow the stress must be at least sufficient to operate Frank–Read sources, and the critical stress is usually calculated from the line tension of the dislocation, the effect of potential wells associated with the lattice lines being ignored. This last effect is small for dislocations which run across lattice directions (Mott and Nabarro 1948) but in general some segments of a dislocation will lie parallel to lattice directions. If these segments are to move forward, and not hold back the rest of the line, then it might appear that a stress equal to the Peierls' stress must be applied. (Dislocations which are already present in a crystal and which lie across lattice directions will of course be able to sweep out a considerable area before being held up at a Peierls' barrier, but the total strain which can be produced in this way is negligible.) However there are at least two possibilities whereby the dislocations might cross the barrier under a lower applied stress than the Peierls' stress. The mechanism discussed in § 4.1 would enable the barriers to be crossed at high temperatures by the formation of bulges, but would imply a much stronger dependence of the yield stress on temperature than is observed. Nevertheless according to the figures given by Seeger *et al.*, the frequency at which bulges are formed increases considerably for values of σ/σ_p greater than about 1%, so that even at low temperatures the dislocation might be able to surmount the barriers comparatively easily. Another possibility (Granato, private communication) arises from the fact that a dislocation not originally parallel to lattice directions will have moved some distance before having to surmount a barrier, and may have sufficient kinetic energy to carry itself over.

§ 5. CONCLUSION

It has been shown above that the mechanism proposed by Seeger accounts qualitatively for our results, but leads to rather high values for the activation energy and the jump frequency. It may be that a more refined calculation, say taking into account the fact that the dislocations will be split into partials, would lead to better agreement, but one should also consider if there is any alternative mechanism which could be responsible. Our results seem to indicate that the friction arises from the motion of lengths of dislocation line which can move with a small activation energy, but only over small distances. As mentioned previously it is possible that the process responsible consists of dislocations being pinned and unpinned from impurity atoms, and such a mechanism may well have an activation energy of about 0·1 ev. Although this is in some ways an attractive suggestion, the experimental evidence is rather against it. Thus the magnitude of the friction would presumably be very dependent on the impurity concentration, but our specimens of copper from two sources and those of Bordoni all give the same order of friction. Also there is no marked amplitude dependence of the friction as might be expected if it arose from unpinning. Thus the evidence suggests that a mechanism of the type proposed by Seeger is responsible for the two peaks, and this could probably be confirmed by measurements on zone annealed copper when it becomes available. Seeger's theory does not explain the peak which is observed in some specimens at about 200°K, but the fact that it is not always observed (in contrast to the Bordoni peaks) implies that it arises from some other mechanism.

Finally it is worth noting that a very marked feature of the Bordoni peaks is their reproducibility and independence of strain amplitude, both of which characteristics are in marked contrast to the behaviour of the background friction. In this respect polycrystalline material is markedly superior to single crystals; although both peaks have been observed in single crystals (Niblett 1956) they are superposed on a greater amount of background friction and their analysis is correspondingly more difficult. Thus the present relaxation process, once fully understood, would appear to offer a useful way of observing the motion of dislocation lines under well defined conditions. For example, it is possible that the effect of neutron irradiation on internal friction might be more profitably studied by its effect on these peaks rather than by using annealed material.

ACKNOWLEDGMENTS

We are grateful to Dr. Alfred Seeger for his stimulating interest in this work; to Mr. D. E. Thomas of Aluminium Research Laboratories for assistance in the design of the apparatus; to the British Non-Ferrous Metals Research Association and the General Electric Company for supplying the copper ; and to the City of Oxford College of Technology Art and Commerce for the use of a tensometer. We also wish to express our thanks to Metropolitan-Vickers Electrical Company for a Research Fellowship (J.W.), to the Department of Scientific and Industrial Research for a maintenance grant (D.H.N.) and to the Pressed Steel Company for a Research Fellowship (D.H.N.).

REFERENCES

BENNEWITZ, K., and RÖTGER, H., 1938, *Z. tech. Phys.*, **19,** 521.
BERRY, B. S., 1955, *J. appl. Phys.*, **26,** 1221.
BILLINGTON, D. S., and SIEGEL, S., 1950, *Metal Progr.* **58,** 847.
BLEWITT, T. H., COLTMAN, R. R., and REDMAN, J. K., 1954, *Report of Bristol Conference on Defects in Crystalline Solids* (London : Physical Society) p. 369.
BÖMMEL, H. E., 1955, *Phys. Rev.*, **98,** 1136. See Mason, W. P., 1955.
BORDONI, P. G., 1949, *Ric. sci.* **19,** 851 ; 1954, *J. acoust. Soc. Amer.*, **26,** 495.
DIETZE, H. D., 1952, *Z. Phys.*, **131,** 156.
FELTHAM, P., and MEAKIN, J. D., 1957, *Phil. Mag.*, **2,** 105.
FOREMAN, A. J., JASWON, M. A., and WOOD, J. K., 1951, *Proc. phys. Soc. Lond.* A, **64,** 156.
FORSTER, F., and KÖSTER, W., 1937, *Naturwissenschaften*, **25,** 436.
HIRSCH, P. B., HORNE, R. W., and WHELAN, M. J., 1956, *Phil. Mag.* **1,** 677.
HUTCHISON, T. S., and FILMER, A. J., 1956, *Canad. J. Phys.*, **34,** 159.
JAMISON, R. E., and BLEWITT, T. H., 1952, *Phys. Rev.*, **86,** 641.
KÖSTER, W., and ROSENTHAL, K., 1938, *Z. Metallk.*, **30,** 345.
MARX, J., and KOEHLER, J. S., 1950, *Carnegie Inst. of Technology Symposium on the Plastic Deformation of Crystalline Solids* (Office of Naval Research).
MARX, J. W., COOPER, H. G., and HENDERSON, J. W., 1952, *Phys. Rev.*, **88,** 106.
MASON, W. P., 1955, *J. acoust. Soc. Amer.*, **27,** 643.
MOTT, N. F., and NABARRO, F. R. N., 1948, *Report of a Conference on the Strength of Solids* (London : Physical Society).
NIBLETT, D. H., 1956, *Thesis*, Oxford.
NIBLETT, D. H., and WILKS, J., 1955, *Conf. Phys. Basses Temp.*, Paris, 484 ; 1956, *Phil. Mag.*, **1,** 415.
READ, W. T., 1953, *Dislocations in Crystals* (McGraw-Hill), p. 53.
SEEGER, A., 1955 a, *Theorie der Gitterfehlsstellen, Handbuch der Physik*, **7**/**1,** 383 ; 1955 b, *Phil. Mag.*, **46,** 1194 ; 1956, *Ibid.*, **1,** 651.
SEEGER, A., DONTH, H., and PFAFF, F., 1957, *Proc. Faraday Society* (in the press).
STEHLE, H., and SEEGER, A., 1956, *Z. Phys.* **146,** 217.
ZENER, C., 1937, *Phys. Rev.*, **52,** 230 ; 1948, *Elasticity and Anelasticity of Metals* (Chicago).
ZENER, C., OTIS, W., and NUCKOLLS, R., 1938, *Phys. Rev.*, **53,** 100.

Structural Behaviour of Neutron Irradiated Quartz†

By M. C. Wittels
Solid State Division, Oak Ridge National Laboratory, Oak Ridge, Tennessee, United States

[Received June 25, 1957]

Summary

X-ray and density studies have been made on single crystals of quartz irradiated with fast pile neutrons at approximately 100°c. The structural effects of the irradiation follow at least two processes with doses up to $1{\cdot}2\times10^{20}$ neutrons/cm^2. Crystals irradiated with less than 3×10^{19} neutrons/cm^2 expand anisotropically in a manner that is similar to the thermal expansion of unirradiated quartz. In this dosage range the volume increase is the same, as determined by x-ray and hydrostatic methods, and little or no distortion is observed in x-ray diffraction patterns. The model which seems to fit these results best consists of point defects and slightly disordered regions which result in an elastic distention of the lattice.

After doses in excess of 3×10^{19} neutrons/cm^2 the damaging process is more complex since the volume change indicated by x-ray measurements of the host lattice becomes larger than the bulk volume change determined hydrostatically. After irradiation with 8×10^{19} neutrons/cm^2 an inhomogeneous shear strain is observed in the extreme skewing of the (22·0) reflection which is interpreted as being due to the crowding of oxygen ion interstitials into the open *c*-axis channels. Amorphous regions enmeshed in the host lattice are identified in crystals that still possess long range order after irradiation with 7×10^{19} neutrons/cm^2. The diffuse x-ray scattering halo associated with the amorphous material changes peak position, shape, and intensity with increasing dosages of irradiation. It is suggested that these changes result from a reorientation of disordered regions which is assisted by the increased expansion of the lattice and the presence of ruptured silicon–oxygen bonds. A second kind of diffuse scattering appears at these high doses which cannot be accounted for on the basis of a thermal origin but is probably related to scattering resulting from inhomogeneous lattice strains.

In a complementary study it was found that coesite, a high density crystalline silica remained stable under neutron irradiation dosages which completely disorder quartz. These results indicate that the rate of damage in silica solids is structure dependent.

---

† Communicated by the Author.

§ 1. INTRODUCTION

THE influence of different types of lattice imperfections upon the low temperature thermal conductivity of solids (Klemens 1951) has provided a sensitive method for determining the nature of disorder in neutron irradiated quartz (Berman 1951). As a result of these earlier investigations, the presence of defects with atomic dimensions and more complex regions of disorder were first indicated, and Berman's study also revealed that the low temperature thermal conductivity curve for neutron irradiated quartz was displaced towards the curve for unirradiated silica. By x-ray, x-ray density, and optical methods it was later shown that extensive neutron irradiation reduced several phases of silica, including quartz and glass, to a common amorphous phase (Wittels and Sherrill 1954) and that this material reverted to α-quartz upon annealing at 930°C.

The changes in density which accompanied the disordering process in quartz (Wittels and Sherrill 1954) followed a very peculiar behaviour, since, more often, the changes which are produced in solids as a result of high energy radiation follow a simple saturation curve when plotted as a function of irradiation dosage. In quartz, the relation of density change versus neutron flux exhibits a sigmoid curve with a maximum rate of density change occurring at $\sim 6\times 10^{19}$ neutrons/cm^2, and this rate approaches saturation with dosages in excess of $1{\cdot}2\times 10^{20}$ neutrons/cm^2. Kinchin and Pease (1955) have suggested that the breakdown of the structure occurs when a sufficient concentration of interstitial ions are produced to render the structure unstable. The anisotropy of expansion (Wittels 1953, Johnson and Pease 1954) was thought by Wittels to be related to the open c-axis channels in the quartz lattice. Recently Klemens (1956) presented a theoretical treatment of this effect which was based on a mechanism of plastic flow that would result in an accelerated volume expansion rate. In a study of the optical effects in quartz resulting from neutron irradiation Mitchell and Paige (1956) interpreted their data as indicating point defects, namely oxygen interstitials and vacancies, and suggested that amorphous regions were formed in irradiated crystals as a result of local melting phenomenon.

The purpose of the present paper is to discuss some recently obtained x-ray diffraction data on neutron irradiated quartz single crystals in relation to these hypotheses.

§ 2. EXPERIMENTAL METHOD

Single crystals of quartz were exposed to fast pile neutrons at 100°C with dosage increments of approximately 10^{19} neutrons/cm^2. The integrated fast flux dosages are estimated to include all neutrons whose energies are in excess of 50 kev. Before irradiation and between successive periods of cumulative bombardment, the crystals were examined using x-ray diffraction and hydrostatic density methods.

For purposes of making direct comparisons between the x-ray density data and the hydrostatic density measurements, cubes having an edge length of 0·25 in. were cut from Y-cut bars so that {00·1} and {11·0} surfaces were coincident with cube faces. Precision lattice parameters were measured by means of a spectrometer and geiger counter method employing a narrow incident beam (12 minutes total divergence). By the same technique, the shapes of several reflections were scanned by step counting in intervals of 0·01°(θ). Hydrostatic density measurements were made on the same cube specimens so that a relation might be established between the calculated densities taken from the x-ray data and the densities measured hydrostatically. As will be shown presently, the x-ray diffraction measurements on these cubes are primarily concerned with the host crystal lattice and the effects which the irradiation-induced imperfections have upon that lattice.

From the same crystal bars, thin plates varying between 0·003 in. and 0·007 in. were cut so that [00·1] and [11·0] directions were made perpendicular to the plate surfaces. These crystals were similarly irradiated and between successive stages of irradiation were examined by means of x-ray diffraction transmission methods that employed conventional single crystal film techniques on stationary and moving crystals at room temperature and at 78°K. When the appearance of ‘ vitreous inclusions ’ became apparent in film photographs, a geiger counter-step scanning method was used to determine the approximate shape of the diffuse x-ray scattering halo which is associated with the scattering of x-rays from an amorphous material. It will be seen that the x-ray diffraction transmission data furnish information concerning the irradiation-induced imperfections in addition to the long range order of the host crystal matrix.

In a complementary study, polycrystalline samples of coesite, a high density crystalline silica (Coes 1953, Sosman 1954, Ramsdell 1955) were exposed to heavy dosages of fast neutron flux and examined with Debye Scherrer x-ray diffraction methods. The purpose of these irradiations was to determine whether a possible structure dependence existed concerning the radiation stability of different phases of the silica system.

§ 3. Experimental Results

3.1. *X-Ray Diffraction and Density Measurements*

The results of the lattice parameter measurements are an extension of the earlier studies of the anisotropic expansion in irradiated quartz (Wittels 1953, Johnson and Pease 1954) and are shown in fig. 1. These measurements were taken from crystals irradiated with integrated fluxes only up to 8×10^{19} neutrons/cm². since beyond this dose, the reflections are too broad and diffuse for precision measurements. It is clear that the expansion in quartz resulting from neutron irradiation is anisotropic, and in addition, if one compares this irradiation-induced expansion (fig. 1) with the thermal expansion of unirradiated quartz (fig. 2) it is evident that a strong similarity exists between these two characteristics.

In both cases, the expansion perpendicular to the *c*-axis is significantly faster than the expansion parallel to the *c*-axis. Also, in both unirradiated and irradiated crystals, the rate of expansion increases with either increasing temperature or increasing neutron dosage.

Fig. 1

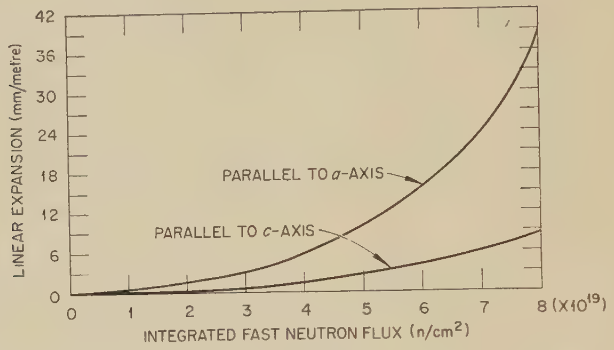

Lattice expansion of quartz due to neutron irradiation.

Fig. 2

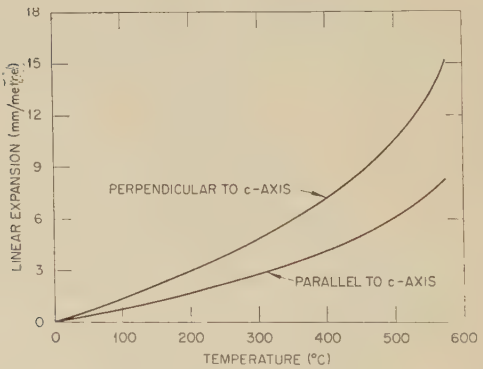

Thermal expansion of quartz (after Kozu and Saiki 1925).

In the case of either unirradiated or irradiated quartz, it is apparent that the restoring force for atomic motion perpendicular to the *c*-axis is less than the same force parallel to the *c*-axis and this is verified by the anisotropy of expansion in both cases. This relationship could hardly be fortuitous and probably indicates that the irradiated quartz lattice is distended as a result of defect introduction in a manner which is consistent with the directional binding forces of the unirradiated crystal.

Comparisons between the hydrostatic volume changes induced by irradiation and the volume changes calculated from the x-ray diffraction data are shown in fig. 3. In this figure percentage changes in volume obtained with hydrostatic measurements are accurate to ±0·02% while the same changes determined from x-ray data are accurate to ±0·03%. Within these experimental limits it is seen that for irradiation doses up to about 3×10^{19} neutrons/cm^2 the two kinds of measurements are in agreement, and further, that the changes in volume follow a trend that is similar to the thermal volume changes in unirradiated quartz (see inset fig. 3). The latter result is consistent with the observations of linear expansions previously given. The relationship between the unit cell reciprocal volume as calculated from x-ray data, and the measured hydrostatic densities, provides evidence of a general nature concerning radiation damage in quartz. In fig. 4 it is noted that with irradiations up to $\sim 3\times10^{19}$ neutrons/cm^2 the points fall on a straight line that is contiguous with the same straight line for unirradiated quartz, and

Fig. 3

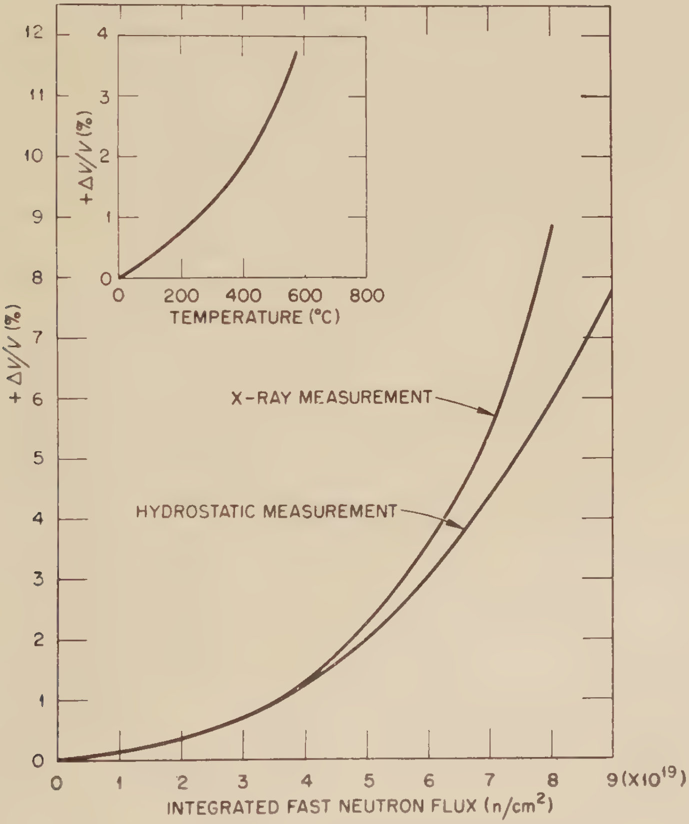

Volume changes in neutron irradiated quartz.

that at higher doses there is a marked deviation from this relationship. At low doses then, the molecular weights of irradiated crystals are identical to those of unirradiated crystals which contain three SiO_2 molecules per unit cell, and at higher doses, the increased concentration of defects having densities lower than those of the host crystal results in smaller calculated molecular weights.

Fig. 4

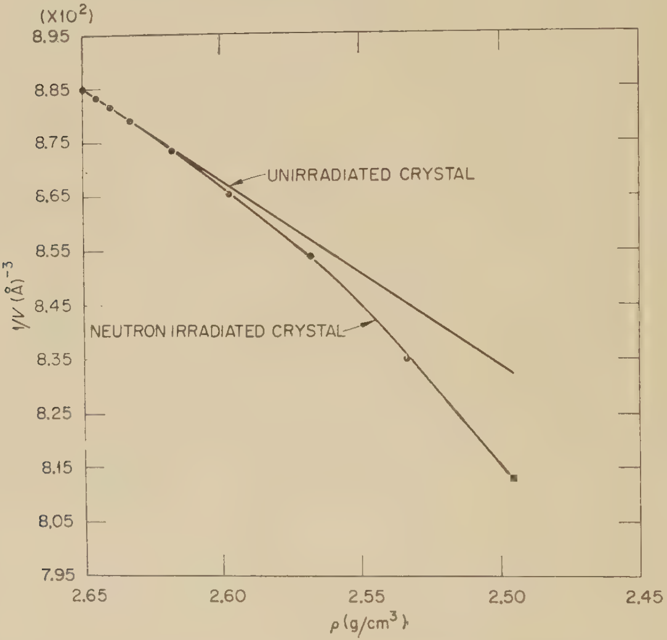

Reciprocal volume as a function of density in neutron irradiated quartz.

It has been theoretically demonstrated (Miller and Russell 1952, 1953. Eshelby 1953) that the presence of Frenkel defects in an isotropic medium should result in an agreement between x-ray density and hydrostatic density values. Although this agreement is found in quartz irradiated with less than 3×10^{19} neutrons/cm^2 is it not entirely clear that the theory is applicable to the highly anisotropic lattice of quartz. The steeper slope (fig. 3) of the volume change at high doses as determined by x-ray methods is in contradiction with Klemens' model (1956) since a relief of shear strain through plastic flow of the crystalline regions would be expected to give rise to a saturation in the expansion of the host crystal matrix as determined from x-ray lattice parameters.

Examination of the packing model of the quartz structure (Bragg and Gibbs 1925, Gibbs 1926) gives evidence suggesting that the configuration of interstitial space in the lattice may be related to the radiation damage process in quartz. Nearly half of the total volume of the unit cell is unoccupied and more than two-thirds of this unoccupied space comprises the screw channels which are roughly parallel to the c-axis in a hexagonal array. It was suggested earlier (Wittels 1953) that these sites might serve as interstitial traps and thus qualitatively explain the anisotropy of expansion. The oxygen ions which are situated immediately adjacent to the screw channels could be easily displaced to these sites by breaking only two bonds as against four bond ruptures for a silicon displacement. In addition, the large ionic diameter of oxygen would make it a more efficient defect for producing the anisotropic expansion.

Except for line shifts, the x-ray diffraction patterns of crystals irradiated with less than 3×10^{19} neutrons cm^2 are relatively unaltered. With the limitations imposed by the total divergence of the incident x-ray beam (12 minutes), little or no line broadening was observed in this dosage range. This indicates that the expansion does not involve severe distortion of the lattice at low doses, and that regions of highly disordered material of a vitreous nature are not present in concentrations sufficient for detection by this technique. It would be expected that the presence of large vitreous regions would set up inhomogeneous shear stresses (Klemens 1956) in the crystalline regions and result in the skewing of reflection peaks together with little or no peak shifting. For low doses at least, it is evident that this is not the case since the x-ray reflections remain sharp and are measurably shifted due to the lattice expansion. The x-ray diffraction patterns of crystals irradiated with neutron doses in excess of 6×10^{19} neutrons cm^2, however, reveal considerable lattice strain as the Laue and Bragg reflections (fig. 5 (*b*), Pl. 59) are smeared and peak intensities are diminished. Klemens' (1956) model predicts an extremely skew line broadening should result from inhomogeneous shear strain in the crystal matrix and experimental verification of this prediction is seen in x-ray diffraction lines of crystals irradiated with 8×10^{19} neutrons cm^2. Figures 6 and 7 show that in the direction of greatest expansion (a-axis) the Bragg reflection is shifted and smeared to give a long tail of low intensity in the direction of increasing diffraction angle, while in the c-direction the reflection is shifted, but otherwise is much less affected. It is conceivable that the extreme skewing of (hh·0) reflections results from an inhomogeneous shear strain that is predominant in directions perpendicular to the c-axis. This idea is also consistent with crowding of interstitial ions into the open c-axis channels to cause the anisotropic expansion. In addition, the lack of comparable line skewing for (00·l) reflections supports this contention. The lattice parameters were calculated from the peak positions of the lines rather than the mean positions. Using the reflection peaks to calculate the x-ray volumes one finds that the ratio of x-ray volume to hydrostatic volume after irradiation with 8×10^{19} neutrons/cm^2 is 1·48. By employing the mean positions of the reflections the ratio becomes approximately 1·14. This is in agreement with Klemens suggestion that line skewing should account for a portion of the lattice expansion observed. It should be noted, however, that this extreme line skewing (fig. 6) is not observed in crystals irradiated with less than 7 × 10^{19} neutrons/cm^2 and that lattice parameter measurements of these crystals are not exaggerated by the employment of reflection peaks. Although the calculated x-ray volume is reduced by employment of the mean positions of the reflections, it is evident that the x-ray volume is still greater than the hydrostatic volume after 8 × 10^{19} neutrons/cm^2 and that there is no early saturation in the expansion of the host crystal as expected from Klemens' model of plastic flow.

Fig. 6

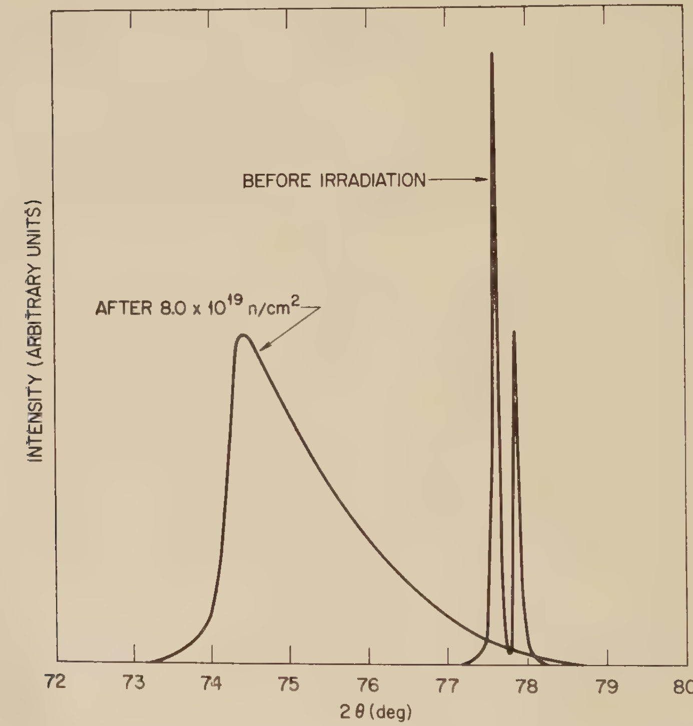

(22·0) of quartz single crystal irradiated with 8 × 10^{19} neutrons/cm^2.

3.2. *Diffuse X-Ray Scattering*

The studies of Berman (1951) suggest that disordered regions are produced in quartz by neutron irradiation and are observed in low temperature thermal conductivity measurements. In an optical investigation of irradiated quartz, Mitchell and Paige (1956) have suggested that amorphous regions are formed at all levels of irradiation. Although these defects are easily identified by x-ray measurements only on crystals irradiated with dosages in excess of 6×10^{19} neutrons/cm², this does not preclude their presence in lower concentration at lower doses or in regions which still retain a semblance of order, or both. The changing nature of the disorder within these regions, and the complete vitrification to the amorphous state upon prolonged bombardment can be qualitatively observed by diffuse x-ray scattering measurements.

Fig. 7

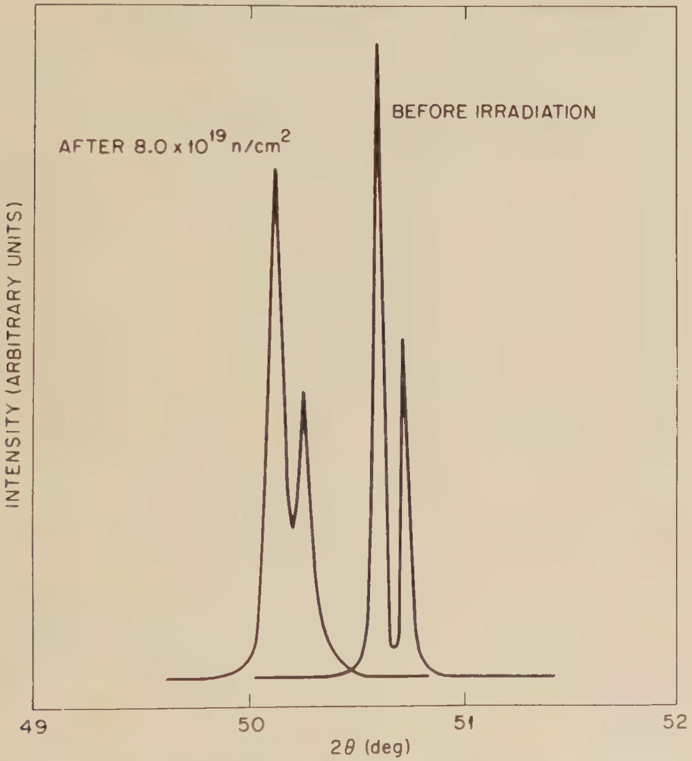

(00·3) of quartz single crystal irradiated with 8×10^{19} neutrons/cm².

The diffuse x-ray scattering halo which is characteristic of amorphous materials becomes evident in single crystals of neutron irradiated quartz that still possess considerable long range order. As shown in figs. 8 (*b*), (*c*), Pl. 59, there is a broad diffuse halo with a peak position close to that for unirradiated vitreous SiO_2 that appears in the reciprocal lattice photograph of irradiated quartz single crystals. The shape and peak position of this diffuse scattering from irradiated single crystals is progressively altered (fig. 9) until the rate of density change becomes zero. Qualitatively, it is evident from these changes that the configuration of the atoms within the amorphous regions changes upon increased irradiation. The shift in the peak position is indicative of an alteration of the average interatomic distances within these disordered regions and is probably related to the constraints of the host crystal lattice as suggested by Klemens

(1956). Since the crystal matrix expands sharply during the development of these amorphous regions, it seems reasonable to assume that the increased openness of the host lattice facilitates the changing configuration of the disordered atoms and atom groups. It is also believed that ruptured Si–O bonds aid this rearrangement not only by furnishing a higher degree of freedom to [SiO_4] tetrahedra, but also by providing the crystal lattice with a driving force that tends to reduce the number of ruptured bonds by means of suitable rearrangements. The suggestion of a higher degree of freedom for [SiO_4] tetrahedra has been proposed by Lukesh (1955) in studies on irradiated vitreous silica. In addition, the presence of ruptured bonds was also indicated by the magnetic susceptibility studies by Stevens (1955).

Fig. 9

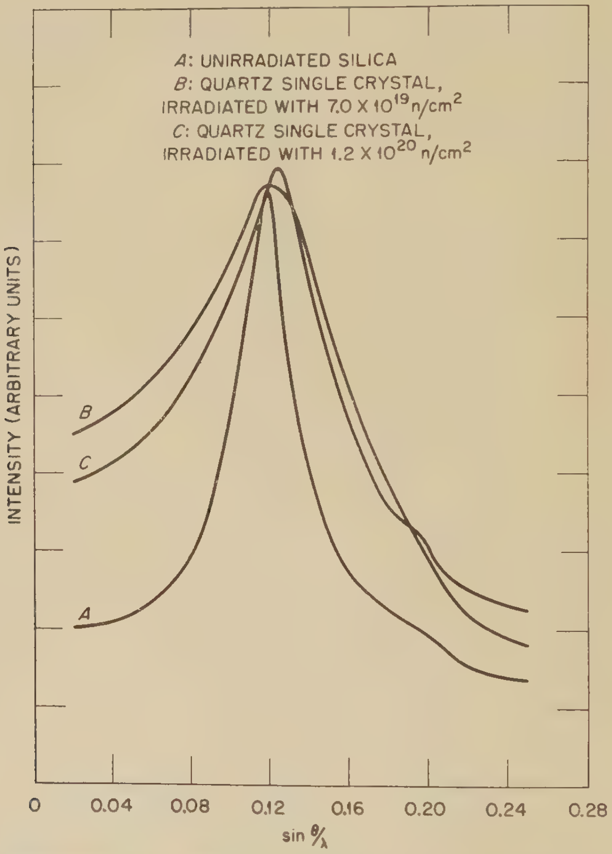

Diffuse x-ray scattering curves from vitreous inclusions in neutron irradiated single crystals of Quartz. Ni filtered Cu radiation employed. Uncorrected for temperature or Compton scattering.

Klemens (1956) has made estimates of the concentration of vitreous material in quartz as a function of neutron flux by two separate methods.

These values were found to agree within a factor of 2. From the observations of diffuse X-ray scattering in crystals studied here only qualitative estimates can be given concerning the fraction of vitreous material present in irradiated single crystals. These estimates tend to agree with the lower values presented by Klemens and indicate that 10–15% of the material is vitrified after irradiation with 5×10^{19} neutrons/cm².

The Laue photographs of crystals irradiated with 7×10^{19} neutrons/cm² (fig. 5 (*b*), Pl. 59) exhibit a diffuse scattering pattern of spots and streaks in addition to the halo that is associated with the amorphous regions of the crystal. This complex diffuse scattering pattern becomes even more evident when monochromatic radiation is used since Laue and Bragg diffraction is then suppressed. With single crystals oriented so that the incident monochromatic beam is parallel to the *c*-axis, a pattern of scattered radiation results which is outside the directions of selective reflection and which exhibits a hexagonal symmetry that is related to the pseudohexagonal symmetry of the quartz lattice.

In fig. 10 (*a*), Pl. 59, the six intense reflections of the outer hexagonal shell and the six strong inner spots are Bragg reflections while the remaining spots and streaks occur outside the zones of selective reflection. The appearance of the Bragg reflections is primarily due to the irradiation-induced distortion of those particular planes which happen to lie very close to the proper position for satisfying the Bragg equation. To a very minor extent this selective reflection is also due to a small divergence of the incident monochromatic beam.

The diffuse spots and streaks that fall outside the directions of selective reflection are remarkably similar to the anomalous scattering of a thermal origin reported by several workers (see Lonsdale 1942–43). It is unlikely that a thermal origin can be employed to describe the formation of this diffuse scattering in neutron irradiated quartz, however, and it is more probable that it is predominantly due to the displacement of the atoms from their mean positions by the presence of defects in the lattice. In this regard it should be emphasized that similar diffuse patterns, as in fig. 10 (*a*), Pl. 59, are conspicuously absent for unirradiated crystals under the same conditions of exposure time and monochromatic radiation. Under these conditions the photographs do not contain the Bragg spots of fig. 10 (*a*), Pl. 59, because of the lack of distortion of the unirradiated lattice, and the diffuse pattern is not even weakly evident. In addition, since the intensity of diffuse scattering from the irradiated crystals is hardly affected by cooling the crystals to 78°K, this is further evidence for ruling out a thermal origin in quartz which has a characteristic temperature, Θ, of approximately 300°K based on acoustical mode frequencies. It appears from the oscillator data of Johnson and Pease (1954) that changes of less than 1% are produced in the elastic constants, and it is therefore inconceivable that these small changes could alter significantly the thermal diffuse scattering. From these results, it appears that the anomalous diffuse X-ray scattering observed in heavily irradiated quartz is not of thermal origin but probably results from the inhomogeneous strains induced by the bombardment-produced defects.

3.3. *Neutron Irradiation of Coesite*

The classical studies of Bragg (1930) demonstrated the unique role of the [SiO_4] tetrahedral group in silicate crystals. In the crystalline phases of silica these structural entities are joined together by a sharing of all tetrahedral corners to form a rigidly bonded network which simply means that each oxygen ion forms a bridge between adjoining tetrahedra. The same structural unit is an integral part of vitreous silica as well (Warren *et al.* 1936), but in this case the tetrahedra are irregularly linked to form a random network configuration. From a structural viewpoint it is therefore evident that the basic difference between silica solids is primarily due to the Si–O–Si bond angle relationships and bond distances which in large part determine the closeness or openness of atom packing.

In quartz, low tridymite, low crystobalite and vitreous silica, the atom packing is markedly open and results in 50% or more void space in all of these solids. Since these materials are reduced to a common amorphous solid following prolonged neutron bombardment (Wittels and Sherrill 1954) it was of interest to determine whether the radiation damage process in silica structures was related to the openness of structure. For this purpose, polycrystalline specimens of coesite, a high density synthetic silica, were exposed to 2×10^{20} neutrons/cm², the dosage which is sufficient to vitrify three ‘ open ’ silica structures. Before and after irradiation Debye–Scherrer x-ray diffraction patterns were taken to ascertain whether any structural changes had occurred in the material as a result of the neutron bombardment, and it was determined that no appreciable damage had been frozen-in since diffraction patterns remained relatively unaltered. Lattice expansions in excess of 0·1% were not observed and the diffraction lines were not noticeably broadened.

Although the structure of coesite (Ramsdell 1955) is not clearly understood it is reasonable to assume that the crystal is composed of linked [SiO_4] tetrahedra similar to the natural silica forms. The essential difference between coesite and these natural forms of silica is therefore displayed by the packing of atoms in the structure. The synthetic material has a density of 3·01 g/cm³ and must be considered close-packed when compared to the other phases of silica. Presumably the binding energies in coesite are not considerably greater than the binding energies in the natural silica phases, and if this is true, the production of displacements by knock-on collision should not be significantly different for either case. And since the basic physical differences between these structures concerns the packing of atoms it seems reasonable to believe that the radiation damage process in silica structures is primarily concerned with the ease or difficulty with which [SiO_4] tetrahedra may be reoriented. In the open silica lattices it is conceivable that these normal voids furnish ideal trapping sites for interstitial ions while the acompanying rupturing of bonds assists in ‘loosening’ the lattice to make the structure more susceptible to further damage. This process is necessarily obscure but it is suggested that the radiation stability of coesite offers evidence supporting the suggestion that both the rate of damage and the location of lattice defects have a structure dependence in neutron irradiated silica solids.

§ 4. DISCUSSION OF RESULTS

The structural effects of the neutron irradiation of quartz with doses up to $1{\cdot}2\times10^{20}$ neutrons/cm^2 follow at least two processes: (i) an anisotropic expansion that is essentially elastic at doses less than $\sim3\times10^{19}$ neutrons/cm^2, and (ii) a more complex anisotropic expansion at higher doses. Associated with the first process is a direct relation between x-ray densities and hydrostatic densities. With the second process one observes: (*a*) inhomogeneous shear strain in the crystalline matrix perpendicular to the *c*-axis, (*b*) a growth and changing configuration of amorphous regions within the host lattice, and (*c*) a diffuse x-ray scattering pattern indicative of inhomogeneous lattice strains that result from the presence of defects. Coesite, a high density crystalline silica is stable under neutron irradiation doses which completely disorder quartz.

4.1. *Effects after Doses Less than* 3×10^{19}

A model of the radiation damage process in quartz is developed on the basis of point defects and slightly disordered regions in crystals irradiated with $\sim10^{19}$–3×10^{19} neutrons/cm^2, in the range where the lattice distentions appear to be elastic. This analysis appears to fit the annealing studies of Berman (1951), Johnson and Pease (1954) and Mitchell and Paige (1956) on crystals irradiated with $\sim1\times10^{19}$ neutrons/cm^2. Berman found that the complex defects annealed more rapidly than the simple defects and this is consistent with a picture of only slightly disordered regions plus simple defects. Primak (1955) argues that the absence of any stored energy release is proof for the non-existence of interstitial-vacancy defects in neutron irradiated quartz. It is conceivable, however, that a possible stored energy release would remain undetected, either because of its small magnitude, or by virtue of the fact that a slow release over a broad spectrum of temperature would be difficult to determine experimentally. The presence of point defects, first observed by Berman, tends to be confirmed by the annealing recovery of the lattice parameter and piezoelectric properties (Johnson and Pease 1954) as well as the optical properties (Mitchell and Paige 1956) in irradiated crystals. More recently, magnetic studies (Weeks *et al.* 1957) have also revealed the presence of point defects in irradiated quartz. It is suggested that the essentially complete recovery of order by thermal annealing would be unlikely if all the defects were of large and complex configuration since the rigidity and short range character of binding in the silicon–oxygen system is not amenable to an annealing process that requires mobility. In the present study the lack of distortion seen in x-ray diffraction patterns of crystals irradiated with less than 3×10^{19} neutrons/cm^2 also supports these conclusions.

The displacement calculations of Mitchell and Paige (1956) indicate that on the order of twice as many oxygen ions would be displaced by knock-on collision than silicon ions. Although this may not be considered a large enough factor to insure the suggestion that oxygen ions form the predominant interstitials, it is still evident that the large ionic diameter of oxygen makes it a very efficient agent for inducing expansions of the lattice. Tentatively, therefore, the present author is in agreement with the suggestion of Mitchell and Paige concerning the presence of oxygen ion interstitials and vacancies in neutron irradiated quartz.

4.2. *Effects after Doses in Excess of* 3×10^{19} *neutrons/cm*^{2}

The effects of irradiation with doses in excess of 3×10^{19} neutrons/cm^2 are exceedingly complex and still not well understood. Nevertheless, the experimental results at these high doses are compatible with the conclusions given concerning crystals having suffered less damage. The extreme skewing of the (22·0) reflection compared to the rather slight broadening of the (00·3) reflection indicates that an inhomogeneous shear strain is present in crystals irradiated with 8×10^{19} neutrons/cm^2. In part, this line skewing is in accord with the prediction of Klemens (1956) but it is even more consistent with the anisotropic expansion of the lattice and is propably due to the crowding of interstitial oxygen ions into the open *c*-axis channels.

It is inherent that ruptured silicon–oxygen bonds are associated with the production of point defects and ' vitreous ' regions since the unirradiated perfect crystal is composed of a rigidly bonded network of [SiO_4] tetrahedra. It is difficult to conceive of the disordering of four phases of silica (Wittels and Sherrill 1954) to a common amorphous phase without the action of some rearrangement process that would promote the formation of a common silicon–oxygen configuration. This process is probably assisted by the presence of ruptured silicon–oxygen bonds. It is also suggested that the thermal recrystallization of quartz from heavily irradiated silica phases (Wittels and Sherrill 1954) also is aided by the presence of broken silicon–oxygen bonds since, in either case, the processes would be promoted by the presence of ruptured bonds which would result in a loosely held array rather than a rigid network.

The appearance of a diffuse x-ray scattering halo in diffraction patterns of heavily irradiated quartz (7×10^{19} neutrons/cm^2) confirms the presence of amorphous regions in crystals that still possess considerable long range order. With increasing dosages of irradiation the growth and modification of these amorphous regions is indicated by the change in peak position, shape, and relative intensity of the diffuse halo. The exact nature of this phenomenon is not clear, but it is evident that the average interatomic distances and atomic configuration within these regions changes as the host lattice rapidly expands. Qualitatively, the shift of the diffuse peak to higher values of sin θ/λ means that the average interatomic distances within the amorphous regions is smaller than that found in unirradiated vitreous silica. Perhaps it is unusual to find that the specific volume of these amorphous regions does not increase sharply as the host lattice rapidly expands but since the density of irradiated fused silica increases upon neutron irradiation (Primak *et al.* 1953) it appears that the process is not one of simple expansion. It is probably also related to the suggestion by Klemens (1956) that the volume expansion of these disordered regions is constricted by the surrounding crystalline matrix. The diffuse scattering studies of Simon (1956) on totally disordered quartz indicated that the amorphous material showed a shorter Si nearest Si neighbour distance, and a smaller Si–O–Si bond angle than that given in the model of silica by Warren *et al.* (1936). In addition, his study showed a wider distribution of both O–O distances and more distant Si–O coordination distances which might be considered as evidence for randomly placed point defects and ruptured Si–O bonds.

There is no positive evidence in the present investigation which would indicate that a thermal spike mechanism (Primak 1955) is the cause for the irradiation-induced disordering of quartz. Moreover, it is difficult to see how the defects produced by Seitz' knock-on mechanism could be distinguished from the disordering due to thermal spikes (Seitz 1949, Brooks 1950) or displacement spikes (Brinkman 1954). If an oxygen ion were displaced to an interstitial position by the knock-on process, in the vicinity of the oxygen ion vacancy the first oxygen coordination shell for two adjoining [SiO_4] tetrahedra would be disrupted and this would probably be followed by a rearrangement of these shells to better satisfy the binding requirements. The coordination shell rearrangements would result in an alteration of the Si–O–Si bond angles as well as bond distances in a small region about the vacancy and would cause a sharp decrease, locally, of short range order, and a much smaller decrease in long range order. In addition, a distortion would be affected in the region of the interstitial oxygen ion which would also give rise to local disorder. In a necessarily naive sense, these disordering effects in a refractory crystal like quartz would be much like a 'vitrification,' in local areas the sizes of which would depend upon the local concentration of interstitials and vacancies. Where displacements are more closely spaced near the end of the track of the primary recoil ion these 'vitrified' regions would occupy a larger volume, as suggested by Klemens.

§ 5. CONCLUSIONS

X-ray diffraction studies of neutron irradiated quartz indicate that at least two damaging processes occur with doses up to $1 \cdot 2 \times 10^{20}$ neutrons/cm^2. Crystals irradiated with less than $\sim 3 \times 10^{19}$ neutrons/cm^2 exhibit an anisotropic lattice expansion which is similar to the thermal expansion of unirradiated quartz, and it is suggested that this is related to the directional binding forces of the unirradiated crystals. In this dosage range, the volume increase is the same, as determined by x-ray and hydrostatic methods, which might be interpreted as indicating the presence of point defects. Except for line shifts, x-ray diffraction patterns from single crystals show no observable distortions and indicate that the expansion is essentially elastic. Although it is felt that point defects and ‘ vitreous ’ regions are produced by knock-on collisions at all doses, it is believed that the total disorder of the complex defects is relatively slight in crystals irradiated with less than 3×10^{19} neutrons/cm^2.

At doses in excess of 3×10^{19} neutrons/cm^2 the damaging process is more complex since the volume change indicated by x-ray measurements of the host lattice becomes larger than the bulk volume change measured hydrostatically. The inhomogeneous shear strain induced by the large anisotropic expansions after 8×10^{19} neutrons/cm^2 is seen in the skewing of the (22·0) reflection and reveals the anisotropy of the damaging process after high doses. Amorphous regions enmeshed within the host lattice are identified in crystals that still possess long range order after irradiation with 7×10^{19} neutrons/cm^2. The diffuse x-ray scattering halo associated with this amorphous material changes peak position, shape, and intensity as the host lattice is distended and strained, and is probably due to the rearrangement of the atoms within the disordered regions as the host matrix expands. In addition, a second kind of diffuse scattering appears which cannot be accounted for on the basis of a thermal origin but is evidently related to scattering as a result of inhomogeneous strains in the damaged lattice.

The stability of polycrystalline samples of coesite, a high density synthetic silica after irradiation dosages sufficient to completely disorder the natural ‘ open ’ phases of silica suggests that the rate of damage has a structure dependence in neutron irradiated silica solids. In neutron irradiated quartz, there is some evidence that the lattice defects may be structure dependent as well, but this is less certain for the other phases of silica and coesite.

Acknowledgments

The author is indebted to several colleagues at this Laboratory. Dr. D. S. Billington and Dr. J. H. Crawford, Jr., have encouraged and counselled these studies, and to them the author is deeply indebted. Many thanks are due to Mr. F. A. Sherrill for x-ray measurements, and to Dr. R. H. Silsbee and Dr. H. C. Schweinler for numerous stimulating discussions.

Several quartz crystals were secured through the kind courtesy of Dr. George Switzer of the U.S. National Museum and the coesite samples were obtained through the efforts of Dr. Tracy Hall of the General Electric Co., Schenectady, New York,

REFERENCES

BERMAN, R., 1951, *Proc. roy. Soc.* A, **208,** 90.

BRINKMAN, J. A., 1954, *J. appl. Phys.*, **25,** 961.

BRAGG, W. L., 1930, *The Structure of Silicates* (Leipzig: Acad. Publ. Soc.).

BRAGG, W. L., and GIBBS, R. E., 1925, *Proc. roy. Soc.* A, **109,** 405.

BROOKS, H., 1950, *Knolls Atomic Power Laboratory Report*, KAPL 360 (unpublished).

COES, L., Jr., 1953, *Science*, **118,** 131.

ESHELBY, J. D., 1953, *J. appl. Phys.*, **24,** 1249.

GIBBS, R. E., 1926, *Proc. roy. Soc.* A, **110,** 443.

JOHNSON, F. B., and PEASE, R. S., 1954, *Phil. Mag.*, **45,** 651.

KINCHIN, G. H., and PEASE, R. S., 1955, *Rep. Progr. Phys.*, **18,** 1.

KLEMENS, P. G., 1951, *Proc. roy. Soc.* A, **208,** 108; 1956, *Phil. Mag.*, **1,** 938.

KOZU, S., and SAIKI, S., 1925, *Sci. Rep. Tohoku Imp. Univ.*, Third Ser., **2,** 203.

LONSDALE, K., 1942–43, *Rep. Progr. Phys.*, **9,** 256.

LUKESH, J. S., 1955, *Phys. Rev.*, **97,** 345.

MILLER, P. H., and RUSSELL, B. R., 1952, *J. appl. Phys.*, **23,** 1163; 1953, *Ibid.*, **24,** 1248.

MITCHELL, E. W. J., and PAIGE, E. G. S., 1956, *Phil. Mag.*, **1,** 1085.

PRIMAK, W., 1955, *Phys. Rev.*, **98,** 1854.

PRIMAK, W., FUCHS, L. H., and DAY, P., 1953, *Phys. Rev.*, **92,** 1064.

RAMSDELL, L. S., 1955, *Amer. Min.*, **40,** 975.

SEITZ, F., 1949, *Disc. Faraday Soc.*, No. 5, 271.

SIMON, I., 1956, *Phys. Rev.*, **103,** 1587.

SOSMAN, R. B., 1927, *The Properties of Sicila* (New York: Chemical Catalogue Co.); 1954, *Science*, **119,** 738.

STEVENS, D. K., 1955, *Phys. Rev.*, **98,** 1541.

WARREN, B. E., KRUTTER, J., and MORNINGSTAR, O., 1936, *J. Amer. ceram. Soc.*, **19,** 202.

WEEKS, R. A., SISLBEE, R. H., STEVENS, D. K., and SONDER, E., 1957, *The Defect Structure of Quartz and Glassy Silica* (New York: John Wiley and Sons, Inc.) (to be published).

WITTELS, M. C.,1953, *Phys. Rev.*, **89,** 656.

WITTELS, M. C., and SHERRILL, F. A., 1954, *Phys. Rev.*, **93,** 1117.

Thermoelectric Power of Ionic Conducting Crystals†

By R. E. Howard
Clarendon Laboratory, Oxford

and A. B. Lidiard
Atomic Energy Research Establishment, Harwell, Berkshire‡

[Received August 22, 1957]

§ 1. Introduction

Crystals which conduct electricity by movement of the *ions* in the crystal have proved rather favourable subjects for the study of lattice defects such as interstitial ions, vacancies and foreign ions. In particular, much is now known about their concentrations, their mobilities and their interactions with one another. With the aim of extending this knowledge, particularly of the kinetic properties of the lattice defects, we have studied the thermoelectric power of ionic conducting crystals. Previous work on this topic has been almost entirely from the point of view of the theory of irreversible thermodynamics (de Groot 1951, Holtan 1953). We have approached the subject theoretically by making use of the models of Frenkel and Schottky lattice disorder and have obtained results which are consistent with the thermodynamic analysis but which allow more detailed predictions to be made.

We shall here confine ourselves to a crystal MX fitted with electrodes of metal M, the experimental arrangement being as shown schematically in fig. 1. The thermoelectric potential is the difference in potential V_B-V_A, made of up five parts: (1) the 'homogeneous' potential difference V_P-V_A due to the temperature difference between P and A; this term is small by comparison with the others and will be dropped; (2) the contact potential difference $V_Q-V_P\equiv-\Phi(T)$; (3) the homogeneous potential difference V_R-V_Q due to the temperature gradient in the salt; (4) the contact potential difference $V_S-V_R=\Phi(T+\Delta T)$; (5) the homogeneous term in the electrode and wire which we shall again neglect. The total is then

$$V_B-V_A=(V_R-V_Q)+\Phi(T+\Delta T)-\Phi(T).$$

The quantity $(V_B-V_A)/\Delta T$ is the thermoelectric 'power' θ and is composed of a homogeneous part $\theta_{\text{hom}}=(V_R-V_Q)/\Delta T$ and a heterogeneous part $\theta_{\text{het}}=\Delta\Phi/\Delta T$. We shall discuss these two components separately. In this discussion it will be convenient to have a particular system in mind; we shall therefore suppose we are dealing with a cationic conductor displaying Frenkel disorder, i.e. containing mobile interstitial cations and cation vacancies. This is typified by AgBr or AgCl. In addition we shall deal with crystals containing foreign ions of a different valency, e.g. Cd^{2+} in AgBr. The importance of this case comes from the creation of one Ag^+ vacancy for every molecule of $CdBr_2$ incorporated in the AgBr crystal; the vacancy concentration can therefore be altered at will.

---

† Communicated by the Authors.

‡ Present address: Department of Physics, University of Reading, Berkshire.

Fig. 1

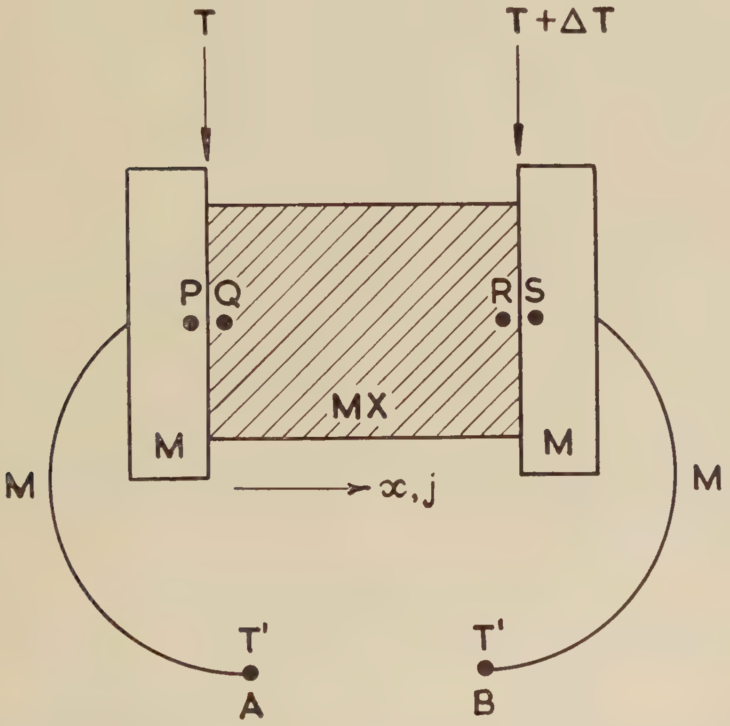

Schematic diagram of the experimental arrangement for the measurement of the thermoelectric power of an ionic conductor MX fitted with electrodes of metal M. In the equations of § 2, the currents j and the spatial coordinate x are referred to left to right as positive direction.

§ 2. HOMOGENEOUS POWER, θ_{hom}

The thermoelectric potential is measured with no current flowing, so we therefore write down phenomenological equations for the current densities of the two charge carriers (interstitials and vacancies)

$$j_i = L_i\left[-(\text{grad}\,\mu_i)_T - e\,\text{grad}\,V - q_i{}^*\frac{\text{grad}\,T}{T}\right], \quad . \quad . \quad (2.1)$$

$$j_v = L_v\left[-(\text{grad}\,\mu_v)_T + e\,\text{grad}\,V - q_v{}^*\frac{\text{grad}\,T}{T}\right], \quad . \quad . \quad (2.2)$$

and determine the power $\theta_{\text{hom}}=(\text{grad } V)/(\text{grad } T)$, by setting the total electric current equal to zero, i.e.

$$j_i-j_v=0. \qquad (2.3)$$

The coefficients L_i and L_v are proportional to the mobilities of interstitials and vacancies respectively and q_i^* and q_v^* are 'heats of transport', i.e. coefficients of proportionality between the defect current densities and the 'reduced' heat flow under isothermal conditions†. The chemical potentials μ_i and μ_v are defined as the change in the Gibbs free energy of the crystal on adding respectively one interstitial and one vacancy. From the statistical theory of Frenkel disorder we obtain the expressions

$$\mu_i=g_i+kT\ln\left(\frac{n_i}{N'}\right), \qquad (2.4)$$

$$\mu_v=g_v+kT\ln\left(\frac{n_v}{N}\right), \qquad (2.5)$$

where g_i is the work required to bring a cation from a state of rest at infinity into a particular (but arbitrary) interstitial position in the crystal (constant T, P). Similarly g_v is the work required to remove a normal ion to a state of rest at infinity. N and N' are the numbers of normal and interstitial sites per unit volume and n_i and n_v are the numbers of interstitial ions and vacancies per unit volume. Equations (2.4) and (2.5) allow us to write eqns. (2.1) and (2.2) in terms of grad n_i and grad n_v and these quantities are related to each other and to grad T through the condition of local thermodynamic equilibrium which gives the familiar equation

$$n_in_v=NN'\exp\left[-\frac{1}{kT}(g_i+g_v)\right]. \qquad (2.6)$$

This procedure gives for θ_{hom} the expression

$$\theta_{\text{hom}}=\frac{\text{grad } V}{\text{grad } T}=-\frac{kT\,\text{grad } n_i}{en_i\,\text{grad } T}+\frac{\{(q_v^*+h)\xi-\phi q_i^*/\xi\}}{eT\{\xi+\phi/\xi\}}, \qquad (2.7)$$

where

$$h=(g_i+g_v)-T\frac{\partial(g_i+g_v)}{\partial T},$$

is the heat of formation of a Frenkel pair, and where ϕ is the ratio of interstitial mobility to vacancy mobility and ξ the vacancy concentration relative to its value in the pure crystal at that temperature (this may differ from unity owing to the presence of foreign ions of different valency).

---

† Holtan (1953). The movement of a defect from one site to another is a thermally activated process and requires that energy be given to the defect at the initial position and given up again at the final position. There is therefore a heat flow associated with a flow of defects, additional to that resulting from the dependence of free energy on concentration (which in (2.1) and (2.2) gives the grad μ terms). It is this additional part which corresponds to the 'reduced' heat flow of the thermodynamic treatment.

§ 3. INHOMOGENEOUS POWER, θ_{het}

This is found from the contact potential $\Phi(T)$ by differentiation with respect to T. The contact potential is determined from the condition that the electrochemical potential of M^+ be the same in the salt and in the metal electrode, i.e.

$$\Phi(T)=\frac{1}{e}\{\mu_i-\mu(M^+\text{ in }M)\}. \qquad (3.1)$$

Therefore

$$\theta_{\text{het}}=\frac{1}{e}\frac{\partial\mu_i}{\partial T}+\frac{1}{e}s(M^+\text{ in }M), \qquad (3.2)$$

where $s(M^+\text{ in }M)$, the partial entropy of M^+ ions in the metal, can be identified with the entropy of the metal since the free electrons make only a small contribution. The derivative $\partial\mu_i/\partial T$ is found from (2.4); we get finally

$$\theta_{\text{het}}=-\frac{s_i}{e}+\frac{k}{e}\ln\left(\frac{n_{i0}}{N'}\right)+\frac{kT\,\text{grad}\,n_i}{en_i\,\text{grad}\,T}+\frac{1}{e}s(M^+\text{ in }M)-\frac{k}{e}\ln\xi, \quad (3.3)$$

where $s_i=-\partial g_i/\partial T$, and n_{i0} is the value of n_i for the pure crystal.

§ 4. TOTAL POWER, θ

This is obtained by adding together (2.7) and (3.3). We obtain

$$\theta(\xi)=\frac{\{(q_v{}^*+h)\xi-\phi q_i{}^*/\xi\}}{eT\{\xi+\phi/\xi\}}-\frac{k}{e}\ln\xi-\frac{s_i}{e}+\frac{1}{e}s(M^+\text{ in }M)+\frac{k}{e}\ln\left(\frac{n_{i0}}{N'}\right). \qquad (4.1)$$

We shall not discuss here the value $\theta(1)$ of the power for the pure crystal (Howard and Lidiard 1957) but will consider the *difference* in power between a crystal containing a certain concentration of foreign ions (giving ξ different from unity) and a pure crystal. From (4.1) it follows that

$$\Delta\theta\equiv\theta(\xi)-\theta(1)=\frac{(\xi^2-1)}{(\xi^2+\phi)}\frac{\phi(q_i{}^*+q_v{}^*+h)}{(\phi+1)eT}-\frac{k}{e}\ln\xi. \qquad (4.2)$$

The relative vacancy concentration ξ may be obtained from a theoretical discussion of the influence of foreign ions on the defect concentrations or, in favourable cases, can be derived directly from experimental results on ionic conductivity, e.g. in AgBr and AgCl (Teltow 1949, Ebert and Teltow 1955). In these systems the conductivity isotherms are described by the equation

$$\frac{\sigma}{\sigma_0}=\frac{\xi+\phi/\xi}{1+\phi}, \qquad (4.3)$$

where σ is the conductivity of the impure crystal, σ_0 is the conductivity of the pure crystal and ϕ as before is the ratio of mobilities. For both AgBr and AgCl the curves of σ/σ_0 against impurity concentration show minima, the positions of which enable ϕ to be determined directly (Teltow 1949). It is then possible to use the experimental conductivity isotherms to give ξ as a function of impurity concentration c and then to calculate $\theta(\xi)-\theta(1)$ as a function of c using (4.3). Typical results for AgBr containing $CdBr_2$ are shown in fig. 2. There is one unknown parameter $(q_i^*+q_v^*+h)$, whose value should be given rather accurately by measurements of thermoelectric power as function of concentration. For reasonable values of this parameter the changes in power are large and have a very characteristic variation with c.

Fig. 2

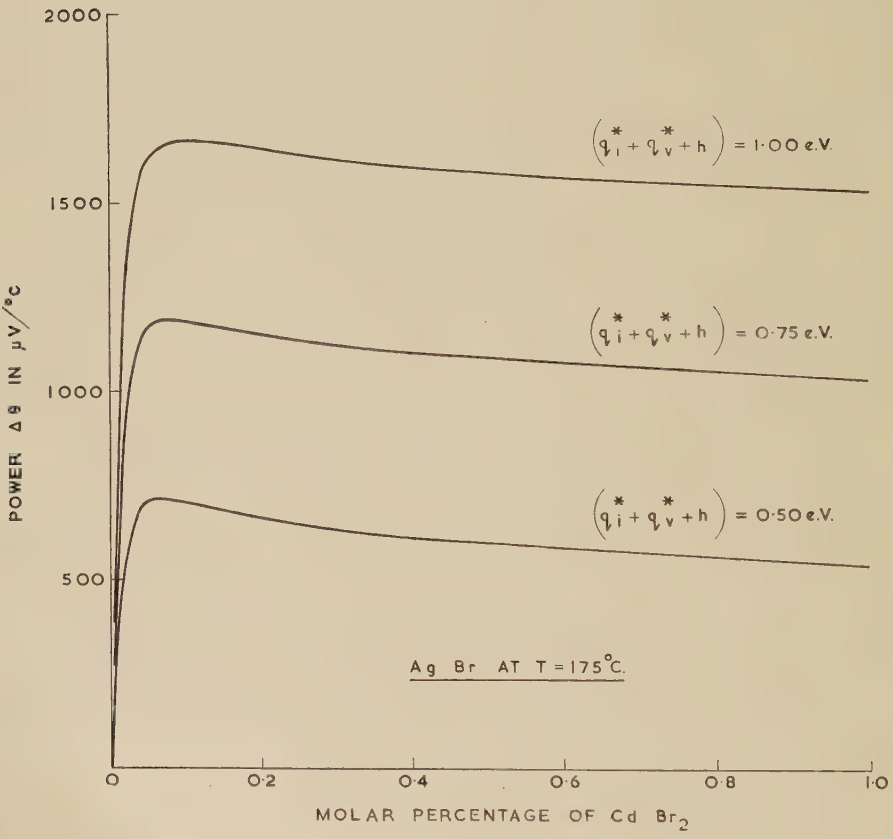

The thermoelectric power of AgBr containing $CdBr_2$ relative to the power of pure AgBr at 175°c. These curves have been constructed by assuming values for the parameter $(q_i^*+q_v^*+h)$ and by finding ξ from the conductivity measurements of Teltow (1949). It may be noted that the power of pure AgBr at 175°c is -1365 μv/°c (Patrick and Lawson 1954).

More generally the dependence of $\theta(\xi)-\theta(1)$ on c can easily be discussed qualitatively since ξ is a monotonically increasing function of c. We find that whenever $(q_i^*+q_v^*+h)/kT \geqslant (1+\phi)^2/2\phi$ then $\theta(\xi)-\theta(1)$ initially increases with c before passing through a flat maximum as in fig. 2. When $(q_i^*+q_v^*+h)/kT < (1+\phi)^2/2\phi$ then $\theta(\xi)-\theta(1)$ initially decreases with increasing c; a minimum and a maximum occur at ξ_- and ξ_+ given by

$$\xi_\pm{}^2=\phi(\kappa-1)\pm\phi\{(\kappa-1)^2-1\}^{1/2},$$

where $\kappa\equiv(q_i^*+q_v^*+h)/kT$. ξ_+ and ξ_- are real if $\kappa>2$. For $\kappa<2$, $\theta(\xi)-\theta(1)$ is a monotonically decreasing function. In assessing the magnitude of $(q_i^*+q_v^*+h)$ it may be noted that q_v^* is a negative quantity whose magnitude is probably close to the activation energy for vacancy movement; q_i^* is positive and probably rather smaller than the activation energy for interstitial movement.

§ 5. CONCLUSION

In conclusion we propose that measurements of thermopower of 'doped' ionic conductors will (*a*) provide a rather general and unambiguous check on the theory of lattice disorder in these crystals, and (*b*) provide a good value for $q_i^*+q_v^*$ since h can be determined independently. The values of q_i^* and q_v^* are closely related to the details of the movement of lattice defects from one position to another. At present there exists only a very qualitative theory of q_i^* and q_v^*, and the development of crystal dynamical theory to improve on this situation would seem very desirable. Measurements of thermoelectric power in the systems we have described might provide a good stimulus for that development.

ACKNOWLEDGMENT

The authors would like to thank Dr. W. M. Lomer for his comments on the manuscript.

REFERENCES

DE GROOT, S. R., 1951, *Thermodynamics of Irreversible Processes* (Amsterdam: North-Holland Publishing Co.).

EBERT, I., and TELTOW, J., 1955, *Ann. Phys., Lpz.*, **15,** 268.

HOLTAN, H., 1953, *Thesis*, University of Utrecht; alternatively see *Proc. K. Ned. Akad. Wetensch.*, **56,** 498, 510 (1953) and **57,** 138 (1954).

HOWARD, R. E., and LIDIARD, A. B., 1957, *Disc. Faraday Soc.*, **23,** 113.

PATRICK, L., and LAWSON, A. W., 1954, *J. chem. Phys.*, **22,** 1492.

TELTOW, J., 1949, *Ann. Phys., Lpz.*, **5,** 63, 71.

Lifetime of the 3·56 MeV State of Lithium 6†

By H. J. Rose‡ and E. K. Warburton
Brookhaven National Laboratory, Upton, New York

[Received August 6, 1957]

Recently Browne and Bockelman (1957) obtained the first precise location of the second excited state of ^{6}Li—3·560±0·006 Mev—from an average of several observations on the reactions ^{6}Li(p, p′)^{6}Li and ^{9}Be(p, α)^{6}Li. They compared this value to the previously determined (Mackin 1954) gamma-ray energy of 3·572±0·012 Mev and concluded that the agreement in energy indicates that the 3·56 Mev level is relatively long-lived (comparable to the stopping time of the ^{6}Li nuclei)§. The 3·56 Mev level of ^{6}Li is almost certainly the analogue of the ^{6}He ground state and thus has $J^\pi = 0^+$, $T = 1$. In L–S coupling the M1 lifetime of the 3·56 Mev level of ^{6}Li is calculated to be $5{\cdot}5 \times 10^{-17}$ sec. The lifetime can also be calculated using the M1 lifetime formula given by Sherr *et al.* (1955) which is valid for p^2 and p^{-2} configurations in any degree of intermediate coupling. If the ^{6}He beta decay *ft* value and the ^{6}Li magnetic and quadrupole moments are used to estimate the wave functions of the ^{6}Li levels involved, it is found that the lifetime calculated from the formula of Sherr *et al.* differs negligibly from that obtained in pure L–S coupling. Therefore, a Doppler shift less than the maximum possible would indicate either that the transition were not M1 and thus the 3·56 Mev level were not 0^+ as expected, or that the M1 lifetime was in serious disagreement with theoretical predictions. It should be noted that the above quoted energy measurements do not demand a relatively long-lived level since the quoted errors in the two measurements are also consistent with the full Doppler shift of 26 kev. However, in view of the serious consequences if, in actual fact, the 3·56 Mev level were found to be relatively long-lived, it was felt worthwhile to investigate the lifetime by a Doppler shift measurement using the ^{9}Be(p, α)^{6}Li reaction.

---

† Communicated by the Authors. Work performed under the auspices of the U.S. Atomic Energy Commission.

‡ Guest Physicist at Brookhaven National Laboratory on a fellowship of Deutsche Forschungsgemeinschaft.

§ The gamma-ray energy was obtained using the ^{9}Be(p, α)^{6}Li reaction at the 2·56 Mev resonance. Stoltzfus *et al.* (1956) have shown that the 3·56 Mev gamma-rays following this reaction have an isotropic distribution and that the alpha–gamma correlation in the plane containing the beam is isotropic to 4%. Since the reaction proceeds through the ^{10}B 8·89 Mev level, the angular distribution of the excited ^{6}Li nuclei must be symmetric about 90° in the centre-of-mass system, and thus the full Doppler shift (defined as the shift expected for a lifetime short compared to the stopping time of the excited nuclei) is given by $\Delta E = E\{(v/c)\cos\theta\}$, where v is the velocity of the centre-of-mass system. The full Doppler shift expected for Mackin's measurement (made at 0° to the proton beam) is 26 kev.

Three different targets were used in this experiment. A thick beryllium target, a thick copper–beryllium target containing 2% beryllium, and a 460 Å beryllium target evaporated onto a 0·00005 in. nickel foil. For the thick target measurements, protons of initial energy 2·67 Mev were used. This energy was picked so that an integration of the measured cross section (Day and Walker 1952) along the proton path gave an effective proton energy corresponding to the peak of the 2·56 Mev resonance. For the thin target measurements, the beryllium was bombarded through the nickel foil and the proton energy was adjusted for maximum gamma-ray intensity. The gamma-rays were detected using a 2 in. right cylinder of NaI(Tl) mounted on a DuMont type 6292 photomultiplier which was picked for its non-rate-dependent gain. The crystal was irradiated with its centre 14·7 cm from the target, at 0° to the proton beam and at backward angle of 160°. The gamma-ray spectra were recorded using a hundred channel analyser with a bias of 400 channels. Only the full-energy-loss peak was investigated. A typical set of spectra obtained from the thick beryllium target is shown in the figure.

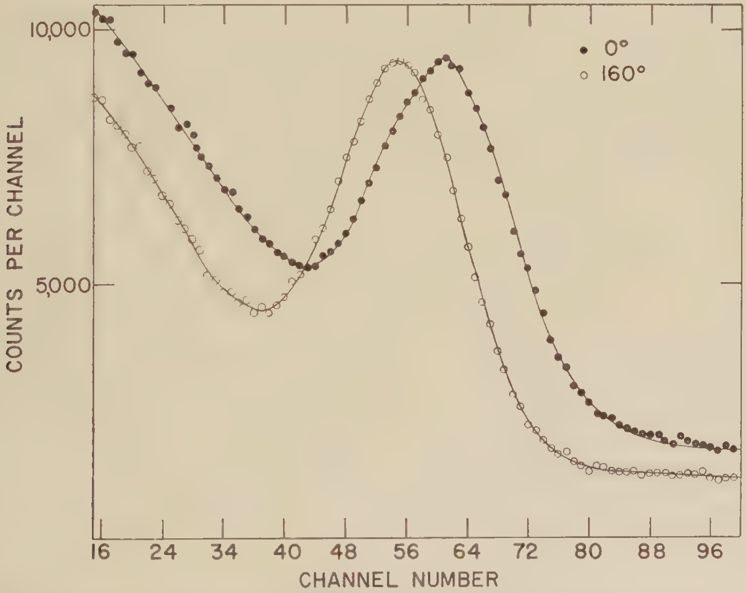

The full-energy-loss peak of the ^{6}Li 3·56 Mev gamma-ray produced by the ^{9}Be(p, α)^{6}Li reaction. The spectra were recorded by a 2 in. × 2 in. NaI(Tl) crystal and a 100 channel analyser with a bias of 400 channels at angles of 0° and 160° to the proton beam.

To obtain the pulse height of the full-energy-loss peak, the background was subtracted and the centre of gravity of the remaining peak was found numerically. This method was possible because of the large number of experimental points in each peak. The gain of the system was monitored and corrections were made for shifting of the gain with time and position by comparison with the gamma-rays from the decay of ^{60}Co in a manner similar to that used by Wilkinson (1957) in his measurement of the Doppler shift of the first excited state of ^{11}B. In all, 16 spectra were obtained in one sequence from the Be target, 44 spectra were obtained in four sequences from the Cu–Be target, and 27 spectra were obtained in two sequences from the Ni–Be target. The mean absolute shift in the pulse height of the full-energy-loss peak obtained from these three targets is shown in the second column of the table.

Results of the Doppler Shift Measurement on the
3·56 Mev Gamma-Ray from ^{6}Li

Target	Measured absolute shift (in channels)	Percent shift
Be	$5{\cdot}83 \pm 0{\cdot}2$	$1{\cdot}43 \pm 0{\cdot}05$
Cu–Be	$5{\cdot}54 \pm 0{\cdot}1$	$1{\cdot}40 \pm 0{\cdot}03$
Ni–Be	$5{\cdot}62 \pm 0{\cdot}1$	$1{\cdot}42 \pm 0{\cdot}03$

The uncertainty given is the standard deviation. Because the amplifier–analyser system was found to be slightly non-linear, the analyser region between 400 and 500 channels was calibrated from the ^{60}Co 1·17 and 1·33 Mev and the ^{22}Na 1·27 Mev gamma-ray lines. In order that the pulse heights of these gamma-rays would be comparable to the beryllium gamma-ray, the beryllium spectra were taken using a precision attenuator which was removed when the radioactive spectra were taken. The attenuator was calibrated by comparing pulse heights of different gamma-ray lines, obtained with and without the attenuator, in a region of pulse height where the system was linear. The Doppler shifts expressed in percent, which are given in the last column of the table, were then obtained by converting the channel shifts to Mev by means of the calibration and dividing by 3·56 Mev. The errors here given include the uncertainty in the calibration as well as the uncertainties in the channel shifts. The observed shifts are to be compared to the calculated full shift of 1·44% (which includes a 0·5% correction for finite counter size).

It is seen from the table that the measured Doppler shift is constant within the experimental error over a wide range of stopping material density, and thus of ^{6}Li stopping time, and agrees, within the experimental error, with the calculated full Doppler shift. Therefore it is concluded that the lifetime of the 3·56 Mev level is short compared to the stopping time of the ^{6}Li nuclei. The sharpest upper limit for the lifetime of the 3·56 Mev level can be obtained from the Cu–Be measurement since the stopping time of the ^{6}Li nuclei is shortest in the copper target. The stopping time of the ^{6}Li nuclei in copper for the pertinent velocity region was extrapolated from data on the slowing down of ^{7}Li nuclei in copper measured for slightly higher velocities (Devons and Towle 1956), and from the slowing down of ^{7}Li in gases (Allison and Littlejohn 1956) measured in the pertinent velocity region. Before constructing a velocity *versus* stopping power curve covering the pertinent velocity region, the gas stopping power data was lowered by approximately 20%. This correction for the difference in the stopping powers of metals and gases was estimated from the published (Allison and Warshaw 1953) dependence of the stopping power of gases and solids for alpha particles which covers a wide range of velocities and densities. From these data it is found that a Doppler shift of 1·30% for the copper target would give a limit $T_{1/2} \leqslant 3 \times 10^{-14}$ sec. Since 1·30% is three standard deviations below the measured shift of $1{\cdot}40 \pm 0{\cdot}03\%$, it is concluded that the lifetime of the ^{6}Li 3·56 MeV level is less than 3×10^{-14} sec. This limit is sharp enough to give strong evidence against an E2 transition.

The Weisskopf formula would present 9×10^{-13} sec if the transition were E2. The worst possible (and hardly imaginable) inhancement of this transition due to collective motion would arise if all three protons contributed to the transition, in which case the E2 lifetime would be 10^{-13} sec. Therefore, it is concluded that the transition is predominantly M1 in character in agreement with the results (Mackin 1954) obtained from the internal pair spectrum of the ^{6}Li 3·56 MeV gamma-ray.

ACKNOWLEDGMENT

We wish to express our thanks to D. H. Wilkinson for helpful discussion concerning this work.

REFERENCES

ALLISON, S. K., and LITTLEJOHN, C. S., 1956, *Phys. Rev.*, **104**, 959.
ALLISON, S. K., and WARSHAW, S. D., 1953, *Rev. mod. Phys.*, **25**, 779.
BROWNE, C. P., and BOCKELMAN, C. K., 1957, *Phys. Rev.*, **105**, 1301.
DAY, R. B., and WALKER, R. L., 1952, *Phys. Rev.*, **85**, 582.
DEVONS, S., and TOWLE, J. H., 1956, *Proc. phys. Soc. Lond.* A, **69**, 345.
MAKIN, R., 1954, *Phys. Rev.*, **94**, 648.
SHERR, R., GERHART, J. B., HORIE, H., and HORNYAK, W. F., 1955, *Phys. Rev.*, **100**, 945.
STOLTZFUS, J., FRIICHTENICHT, J., and NELSON, E. B., 1956, *Bull. Amer. phys. Soc.*, **1**, 329.
WILKINSON, D. H., 1957, *Phys. Rev.*, **105**, 666.

Scattering of Polarized Positrons by Polarized Electrons†

By J. M. C. Scott
Cavendish Laboratory, Cambridge

[Received August 26, 1957]

Abstract

The cross sections for the scattering of polarized positrons and electrons by polarized electrons have been calculated.

---

§ 1. Introduction

The usual methods of measuring the spin orientation in beta rays depend on scattering by heavy nuclei. The spin effect in this phenomenon, however, is quite small in the case of positrons (Massey 1943). As an alternative method for detecting the spin-orientation, Dicke (1950), Frauenfelder (1957) and others have suggested methods depending on scattering by polarized electrons.

Since there has been some doubt as to whether the discrimination would be big enough, especially with positrons, we have calculated the cross sections for each kind of polarization and for both e^+ and e^-. The electron–electron cross section given by Møller (1932) and the positron–electron cross section given by Bhabha (1936) refer of course to unpolarized electrons; their results follow from ours after averaging over the spins. The calculation is a straightforward one (Jauch and Rohrlich 1955); it was in fact carried out using eigenfunctions of $\boldsymbol{\sigma p}$ in the standard representation rather than by the usual method of traces.

One or two errors were found in the literature; in particular we are not aware of any reference in which the last two terms of Bhabha's formula are quoted correctly.

§ 2. Results

A positron with total energy γmc^2 collides with an electron at rest, whose spin in the direction of motion of the positron is $+\frac{1}{2}$. The spin of the positron in this direction may be (a) $+\frac{1}{2}$ or (b) $-\frac{1}{2}$. The positron loses a fraction w of its kinetic energy $(\gamma-1)\,mc^2$, and is deflected through an angle λ in the laboratory frame of reference; θ is the scattering angle in the centre-of-mass system of coordinates. Thus

$$w=\tfrac{1}{2}\,(1-\cos\theta) \qquad (1)$$

and

$$\tan\tfrac{1}{2}\theta=[\tfrac{1}{2}(\gamma+1)]^{1/2}\tan\lambda. \qquad (2)$$

---

† Communicated by the Author.

The differential cross section is then

$$d\sigma=\frac{r_0^2}{2(\gamma+1)}Q\,.\,2\pi\sin\theta\,d\theta=\frac{r_0^2\cos\lambda}{[1+\frac{1}{2}(\gamma-1)\sin^2\lambda]^2}Q\,.\,2\pi\sin\lambda\,d\lambda \qquad (3)$$

where $r_0^2=(e^2/mc^2)^2$ and Q is given by the following formulae :

$$(a)\ \ Q(\rightarrow\rightarrow)=\frac{\gamma^2}{(\gamma-1)^2}\frac{1}{w^2}-\frac{4\gamma+1}{\gamma-1}\frac{1}{w}+\frac{6\gamma-5}{\gamma-1}-\frac{4\gamma}{\gamma+1}w+\frac{2(\gamma-1)}{\gamma+1}w^2 \qquad . \quad . \quad . \quad (4\,a)$$

$$(b)\ \ Q(\rightarrow\leftarrow)=\frac{\gamma^2}{(\gamma-1)^2}\frac{1}{w^2}-\frac{3\gamma+1}{\gamma^2-1}\frac{1}{w}-\frac{1}{(\gamma+1)^2}\left[\frac{\gamma^2+3}{\gamma-1}-8\gamma w+4(\gamma-1)w^2\right]. \qquad . \quad . \quad . \quad (4\,b)$$

The average of these is equivalent to Bhabha's formula (Bhabha 1936, Ashkin *et al.* 1954) ; it is

$$\bar{Q}=\frac{\gamma^2}{(\gamma-1)^2}\frac{1}{w^2}-\frac{2(\gamma+1)^2-1}{\gamma^2-1}\frac{1}{w}+3+\frac{1-2\gamma(\gamma-1)w+(\gamma-1)^2w^2}{(\gamma+1)^2}. \qquad (5)$$

If the incident particle is a negative electron, the values of Q to be inserted in (3) are :

$$Q(\rightarrow\rightarrow)=\frac{2}{(\gamma-1)^2}\frac{(\gamma-1)^2+2\gamma(3\gamma+1)\cos^2\theta+(\gamma^2-1)\cos^4\theta}{\sin^4\theta} \qquad (6\,a)$$

$$Q(\rightarrow\leftarrow)=\frac{4}{(\gamma-1)^2}\frac{4\gamma^2-4\gamma+2+(5\gamma-3)\cos^2\theta-(\gamma-1)\cos^4\theta}{\sin^4\theta} \qquad (6\,b)$$

$$\bar{Q}=\frac{4\gamma^2\,(1+3\cos^2\theta)+(\gamma-1)^2\sin^2\theta\,(5-\cos^2\theta)}{(\gamma-1)^2\sin^4\theta}. \qquad . \quad . \quad . \quad (7)$$

This last corresponds to the original Møller formula.

§ 3. DISCUSSION

The ratio $Q(\rightarrow\rightarrow)/Q(\rightarrow\leftarrow)$ at the most favourable angle ($\theta=90°$ in the centre-of-mass system) is equal to $\frac{1}{8}$ in the limit of high energy for both e^+ and e^-. As the energy of the electron decreases, this ratio decreases further, to zero in the low energy limit (cf. Mott and Massey 1949). This may be regarded as due to the effect of the Pauli principle on the probability of the electrons being close together. The ratio for positrons tends to 1 at low energies. But the notion that there should be no polarization effect because the positron and the electron are 'different' particles would be quite misleading at energies of the order of mc^2, where the virtual annihilation term is far from negligible.

The cross sections have also been calculated by A. Bincer, according to a recent communication by Dr. Frauenfelder. The ratio quoted agrees with ours for electrons, but not in the case of positrons†.

---

† *Note added in proof.*—These authors now obtain a slightly different formula (*Phys. Rev.*, **107**, 644). This is consistent with our (4) and there is no longer any discrepancy.

ACKNOWLEDGMENT

This work was carried out at the Atomic Energy Research Establishment, Harwell, and the author would like to thank the authorities for the hospitality of their laboratory.

REFERENCES

ASHKIN, A., PAGE, L. A., and WOODWARD, W. M., 1954, *Phys. Rev.*, **94,** 357.
BHABHA, H. J., 1936, *Proc. roy. Soc.* A, **154**, 195.
DICKE, R. H., 1950, quoted by Tolhoek 1956, *Rev. mod. Phys.*, **28,** 293.
FRAUENFELDER, H., 1957, private communication from Drs. C. F. Coleman and T. H. R. Skyrme.
JAUCH, J. M., and ROHRLICH, F., 1955, *Theory of Photons and Electrons* (Cambridge, Mass.: Addison-Wesley).
MASSEY, H. S. W., 1943, *Proc. roy. Soc.* A, **181,** 14.
MØLLER, C., 1932, *Ann. Phys.*, **14,** 531.
MOTT, N. F., and MASSEY, H. S. W., 1949, *Theory of Atomic Collisions*, 2nd ed. (Oxford), p. 104.

On the Mechanical Properties of Indium Antimonide†

By J. W. Allen
Services Electronics Research Laboratory, Baldock, Herts.

[Received August 30, 1957]

Summary

The deformation properties of indium antimonide have been studied under a variety of conditions. At room temperatures elastic behaviour is observed up to the fracture point, while at higher temperatures glide occurs on {111} planes. Impact at room temperature can cause glide on {110} planes. A method of observing individual dislocations is described, and the dislocation distributions after the various deformations have been studied.

§ 1. Introduction

The mechanical properties of the semiconductors silicon and germanium have been studied by several investigators. At room temperature these are brittle solids showing elastic behaviour up to the fracture point (Pearson *et al.* 1957), while at higher temperatures they show plastic behaviour with a sharp yield point and, for stresses below this yield point, flow with a temperature and stress-dependent incubation period (Gallagher 1952). These features naturally suggest an interpretation in terms of a Cottrell atmosphere locking mechanism, although this is not the only possibility. Similar behaviour has now been observed in indium antimonide, a semiconductor with zinc-blende structure. In addition plastic deformation has been observed at room temperature under certain special conditions.

§ 2. Observation of Dislocations

The plastic properties of crystals can usually be described in terms of the theory of dislocations but often more than one mechanism can be proposed to explain a given set of macro-properties. It is therefore useful if the actual numbers and positions of the dislocations can be determined experimentally. To this end we have devised an etch which produces on suitable crystal faces of InSb pits which mark the point of emergence of dislocations, this etch being a modification of CP4 as used by Vogel *et al.* (1953) to show dislocations in germanium.

In this method the crystal is first ground with 850 grade Unirundum in aqueous Teepol suspension on a glass plate. It is then polished chemically with CP4A or with CP4A diluted with water and nitric acid, after which it is placed in the etchant for one minute. (The composition of

---

† Communicated by the Author.

CP4A and of the etchant are given in an Appendix.) Best results are obtained if the solution is not agitated during this last process. After washing and drying clearly visible circular pits are observed on faces of the form $\{\bar{1}11\}$. Their visibility decreases as the angle between the face and $\{1\bar{1}\bar{1}\}$ increases, but they may be seen as elongated ellipses on faces of the form $\{11\bar{2}\}$. It is interesting that the form $\{111\}$ does not show these pits. This provides a rapid means of distinguishing between the two tetrahedral forms, a distinction necessary for the complete orientation of the non-centrosymmetrical class $\bar{4}3m$ but one which cannot be obtained by x-ray methods. (The convention adopted here as to which is the positive direction of the crystallographic axes conforms with that of Dewald (1957).)

Fig. 1

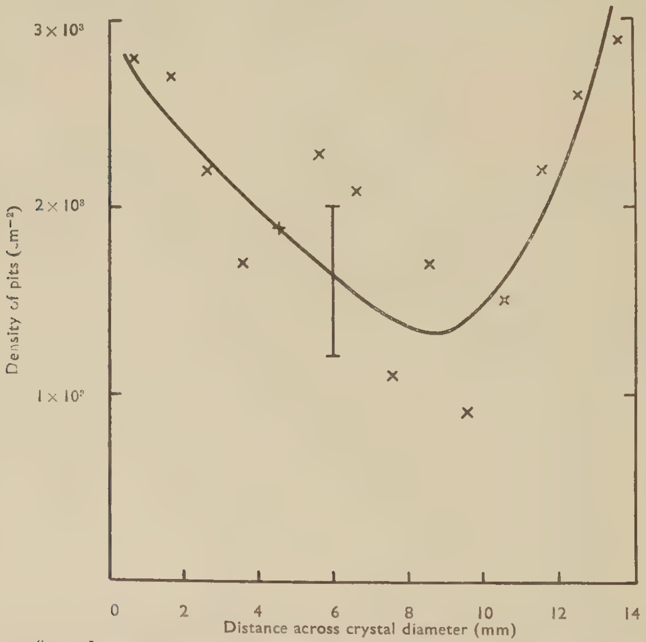

Variation of etch-pit density across the diameter of an indium antimonide crystal which was grown in a [111] direction. The vertical line indicates the statistical scatter expected.

These etch pits are quite reproducible, in that if a surface treated in the above manner is ground to a depth sufficient to remove them then on re-etching they reappear at the same positions. By continuing the grinding and etching process they may be traced through a crystal and therefore they correspond to line imperfections. As will be shown below, their disposition throughout the crystal is in accord with the expected disposition of an array of dislocations. We therefore conclude that the position of a pit marks the intersection of a dislocation with the surface. The converse of this proposition, namely that every dislocation site produces a pit, is much more difficult to prove, but experiments on bent bars have shown that the pit density is of the same order of magnitude as the expected dislocation density.

Single crystals of InSb grown at S.E.R.L. by the Czochralski pulling technique with [111] as the growth axis have dislocation densities of the order of 2×10^3 cm^{-2}, which is of the same order as is observed in silicon crystals grown here by the same method, but is about three orders of magnitude smaller than the densities commonly observed in well-annealed metal single crystals. The variation of pit density across a face perpendicular to the crystal growth axis for a typical crystal of InSb is shown in fig. 1. This is qualitatively similar to that obtained with pulled silicon or germanium crystals and is the result of deformation under thermal stresses caused by radial temperature gradients as the crystal is withdrawn from the melt. The small number of dislocations in this material helps considerably in interpreting plastic deformation experiments, since the density of introduced dislocations may then be three or four orders of magnitude greater than the density of those initially present.

§ 3. Room Temperature Fracture

Bars of InSb about 1 mm × 0·5mm × 11mm were supported at their ends and loaded quasi-statically at their centre. Measurements were made of the displacement at the centre as a function of load. Several specimens cleaved on (110) planes at comparatively low loads. Since cleavage occurred at only one place in such specimens and since the load at cleavage varied widely for different specimens it was assumed that this behaviour was due to adventitious stress concentration. Other specimens showed elastic behaviour up to the fracture point, at which they broke into several small pieces, not bounded by crystallographically important planes. The maximum strains at fracture were of the order of ½%, about the value obtained for silicon bars of similar dimensions (Pearson *et al.* 1957). Some of the fractured pieces were etched and it was found that no appreciable movement of dislocations had occurred, nor were fresh dislocations introduced in the bulk of the material. However, some ‘ dislocation-cracks ’ were seen to run from the fractured edges. This type of deformation will be discussed below. It is evident that at room temperature there are considerable forces locking dislocations in fixed positions. This fact is of importance in those experiments in which the positions of dislocations are to be studied, since these positions are not changed by handling the crystals provided that reasonable care is taken not to subject them to violent stresses.

§ 4. High-Temperature Flow

At temperatures of 200°C or more InSb becomes plastic, and single-crystal bars of it can be bent through large angles. On the absolute scale 200°c is about two-thirds of the melting temperature, and approximately the same ratio of temperature required for plastic flow to melting temperature is observed in silicon and germanium. In a typical experiment a bar 0·5 mm × 1 mm × 15 mm is supported at its ends and a fixed load is applied at its centre, this load being of the order of 50 gm wt, i.e. about a tenth of that which would cause fracture at room temperature. This system is placed in an oven containing a window and measurements of displacement at the centre as a function of time are taken. The variation obtained is shown diagrammatically in fig. 2; it is very similar to that observed in germanium (Gallagher 1952). This graph has three different regions corresponding to an incubation period, plastic flow, and work hardening.

Fig. 2

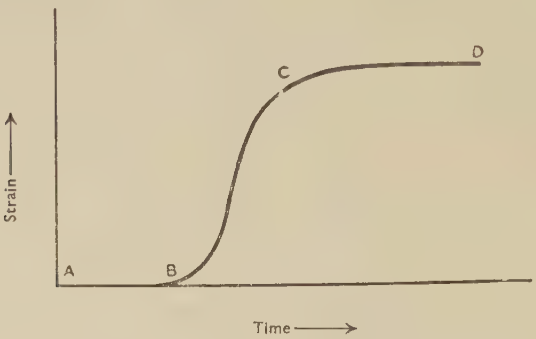

Strain–time curve for an InSb bar bent at an elevated temperature.

During the incubation period AB there is no appreciable deformation. The length of this period decreases as the stress or the temperature increases, and for the system described above is of the order of twenty minutes. It does not appear to be changed by preheating, i.e. by holding the crystal at the temperature of the experiment for some time without a load. Seitz (1952) has put forward an interpretation of the incubation in terms of the diffusion of locking impurities away from dislocation sources, while Pearson *et al.* (1957) suggest the Peierls force as being the source of locking. Experiments are in hand to determine, by the etch-pit technique, the number and disposition of dislocations introduced under various conditions of deformation and in this manner to unravel the processes involved.

The period of incubation is followed by one of plastic flow, BC. After deformation slip lines can be seen on the crystal which serve to establish the glide planes as being {111}, the planes of closest packing. The visibility of the slip lines on different faces of the bar depends on the crystallographic orientation and on their orientation with respect to the bend axis. This effect may be used to determine the slip direction, and this appears to be [110], the direction of the shortest translation vector in the zinc-blende lattice. On etching, the dislocations introduced may be seen. Their general disposition is shown in fig. 3, Pl. 60, which is a $(1\bar{1}\bar{1})$ face of InSb viewed along the bend axis. It will be seen that dislocations approach the neutral plane from both sides; they are generated mainly by sources at or near the upper and lower surfaces which are, of course, regions of maximum stress. While many of the dislocations are concentrated into relatively few slip lines an appreciable number are not. Another point of interest is that the arrays are not strictly linear, the deviations from linearity being of the order of a few microns. This is not due to interaction with the surface during slip, since by grinding off the surface the same effect may be seen to have taken place within the bulk of the crystal. Nor is climb out of the glide pane by thermal diffusion a likely explanation since this specimen was bent under conditions such that the incubation period was very short, and was air-quenched immediately after deformation so that the total time from applying a load to the crystal to its returning to room temperature was about three minutes. At 260°c. the temperature used in this particular experiment, the distance through which a dislocation will diffuse thermally in three minutes is certainly less than the distances with which we are here concerned. One possible explanation is that there is cooperative slip on parallel glide planes, although the scale here is much larger than is observed in multiple slip in aluminium (Heidenreich and Shockley 1948). Some credence is lent to this hypothesis by fig. 4, Pl. 60 which shows part of fig. 3, Pl. 60 at greater magnification, and in which some sort of cooperative slip may be seen. Another possibility is that the obstacles to movement presented by impurities are sufficient to make short lengths of dislocation climb out of their glide plane into another parallel one, although the magnitudes of the deviations are rather large to be accounted for by such a process. It should also be noted that the dislocations do not lie in the equilibrium positions calculated by Eshelby *et al.* (1951), which implies that there is considerable resistance to their motion even in the glide plane.

Plastic flow continues for some time, after which work-hardening sets in, as indicated by CD in fig. 2. If neither temperature nor load are too great this part of the strain–time curve becomes essentially flat. If now either temperature or load is increased further deformation takes place, after which the curve flattens off at a higher value of the strain. The amount of deformation before work-hardening also depends on orientation: if the orientation is chosen so that slip on one set of glide planes is preferred the section BC of fig. 2 is considerably extended. By etching to reveal dislocations it can be shown that work-hardening is associated with slip on two or more intersecting glide planes. An example of such an intersection is illustrated in fig. 5, Pl. 60; a short etching time has been used in order to show more clearly details of the dislocation positions at the crossing point. Some 'piling-up' can be seen. This not so pronounced as in a metal, for in InSb under these conditions the resistance to glide is high in any case so the intersecting glide plane does not increase this resistance by a large factor. Observations of these intersections also provide evidence that the dislocations themselves must to some extent have crossed during slip, and the jogs thereby produced presumably contribute to work-hardening.

§ 5. Room-Temperature Flow

It has been shown above that quasi-static bending of InSb at room temperature causes fracture before an elastic limit is reached. However, if InSb crystals are subjected to sudden local impact 'dislocation-cracks' may be formed. These are observed as line markings on the surface and have the appearance of fine cracks under low magnification, while under high magnification after etching individual dislocations may be resolved along their length, or part of it. In general these 'dislocation-cracks' are not straight, although they show a strong preference to lie in {110} planes. The dislocation density is not uniform along them, although short sections may show uniform spacing. They rarely run right across a crystal, and they are sometimes the continuation of an actual crack. Normally two or three more widely spaced dislocations may be seen along the continuation of the line some microns beyond its termination. Preliminary experiments suggest that the most favourable conditions for their formation are that a stress of the order of the fracture stress should be applied suddenly to a small region of the crystal, the rest of the crystal being comparatively stress-free. The dislocations are then propagated from some source and run into the crystal until the applied stress is removed or until they reach a region where the internal stress is insufficient to keep them in motion. The fact that on removal of the applied stress the dislocations do not run out again, and also that their spacing in the slip plane is very non-uniform, shows that there is a strong locking force which in this case cannot be a Cottrell atmosphere, since the times involved are far too short for the formation of such an atmosphere.

§ 6. Conclusions

Indium antimonide is a convenient substance for studying the production and properties of arrays of dislocations and for comparing these with theoretical ideas; experimentally, dislocations may be introduced under controlled conditions, they retain their positions and these positions are easily determined, and theoretically, the structure is not of intractable complexity. The low density of dislocations in our grown crystals is also of considerable advantage. As an example, a sample of reasonable size may only contain of the order of ten dislocations, and so nucleation of further dislocations at the surface is not masked by nucleation at Frank–Read or other internal sources. The mechanical properties of InSb are similar in many respects to those of a face-centred cubic metal and to those of silicon and germanium, although it shows some characteristic differences ; we may therefore hope that investigations of these properties in InSb will not only be of intrinsic interest but will shed light on the behaviour of these other materials.

ACKNOWLEDGMENT

Acknowledgment is made to the Admiralty for permission to publish this paper.

REFERENCES

DEWALD, J. F., 1957, *J. Electrochem. Soc.*, **104**, 244.
ESHELBY, J. D., FRANK, F. C., and NABARRO, F. R. N., 1951, *Phil. Mag.*, **42**, 351.
GALLAGHER, C. J., 1952, *Phys. Rev.*, **88**, 721.
HEIDENREICH, R. D., and SHOCKLEY, W., 1948, *Report on Strength of Solids* (London : Physical Society), p. 57.
PEARSON, G. L., READ, W. T., and FELDMANN, W. L., 1957, *Acta Metall.*, **5**, 181.
SEITZ, F., 1952, *Phys. Rev.*, **88**, 722.
VOGEL, F. L., PFANN, W. G., COREY, H. E., and THOMAS, E. E., 1953, *Phys. Rev.*, **90**, 489.

APPENDIX

CP4A polishing etch
5 parts HNO_3 aq.
3 parts HF aq.
3 parts CH_3COOH glacial

111 etch to show dislocations
1 part CP4A
1 part H_2O dist.
1 part CH_3COOH glacial

CORRESPONDENCE

Electron Microscopic Observation of Periodic Structures below 10 Å.

By G. A. Bassett and J. W. Menter
Tube Investments Research Laboratories, Hinxton Hall, Cambridge

[Received August 19, 1957]

In his initial studies on the direct resolution of lattice planes in crystals by electron microscopy one of the authors (Menter 1956) worked with metal phthalocyanines, principally because of their relatively large lattice parameters (e.g. $d_{(20\bar{1})}$ in platinum phthalocyanine=11·94 Å). The remarkable clarity of the images obtained suggested that it should be possible to resolve more closely spaced lattice planes. This was supported by an elementary consideration of the effect of the lens aberrations on the resolution of periodic structures which showed that these are less deleterious than with non-periodic structures.

However, for the practical realization of improved resolution a number of exacting conditions must be fulfilled by the specimen. It must be reasonably stable in vacuum and able to withstand electron bombardment without decomposition. The habit of the crystal must be such as to present the lattice planes it is hoped to resolve closely parallel to the electron beam when the crystal is resting on a support film. The crystal must be thin (a few hundred Å) in the direction of the electron beam. The number of crystals fulfilling these conditions with planar spacings between 5 and 10 Å is not great. At the present time the most successful results have been obtained with crystals of molybdenum trioxide in which the (020) planes (d=6·93 Å) have been clearly resolved. Molybdenum trioxide has perfect cleavages on (010) and (100) and a less perfect but distinct cleavage on (001) so that there is a reasonable probability of obtaining suitably oriented fragments. Crystals have been prepared by two methods. (1) A large crystal kindly supplied to us by Mr. H. P. Rooksby of G.E.C. Research Laboratories, Wembley was broken down mechanically by grinding. (2) Small crystals were prepared by thermal decomposition of ammonium molybdate followed by resublimation. In both cases the final preparation was suspended in alcohol for deposition on electron stabilized nitrocellulose support films containing many holes.

A considerable number of micrographs have been taken using a Siemens Elmiskop I with an instrumental magnification of × 160 000, accelerating voltage 80 kv. objective aperture 50 μ. They were recorded on Ilford

Contrasty Special Lantern plates developed in Ilford developer ID36. About 10% of the plates show fragments of crystal in which the lattice has been resolved. The spacing measured from the micrographs lies within ∓10% of the x-ray value quoted above. Due to the decomposition of the crystals in the microscope it has not been possible to record an electron diffraction pattern and a micrograph showing the resolved lattice from the same crystal in order to establish the orientation unambiguously. Assuming the habit surfaces are as defined by the cleavages given above then (020) planes may be resolved in crystals lying either on (001) or (100).

The clearest micrograph obtained in this investigation is shown in fig. 1, Pl. 61. The crystal is attached to the edge of a larger crystal itself spanning a hole in the support film. The background structure of the latter has been avoided in this way but the quality of the image is still seriously impaired by the structure of the contaminant carbon film C which envelops the crystal rapidly in the course of examination. A projection of the crystal structure on (001) as determined by Wooster (1931) showing only the positions of the molybdenum atoms is shown in fig. 2 to the same scale as the electron micrograph. It is clear from this how far the electron microscope image still is from representing the true structure of the crystal due to the limited number of diffraction spectra contributing to the image.

Fig. 2

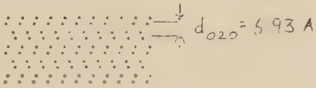

Schematic projection of molybdenum trioxide structure on (001), showing positions of molybdenum atoms only (after Wooster 1931). Same scale as fig. 1, Pl. 61.

It is considered that this resolution of a singly periodic structure of 6·9 Å by no means represents the limit of what is possible with existing microscopes. In the course of other experiments in our laboratory, moiré patterns formed by (422) planes in a gold/nickel specimen have been clearly resolved with a spacing of 5·3 Å† (Pashley *et al.* 1957). Furthermore doubly periodic moiré patterns with a spacing of 9·2 Å† from the (220) planes of the same combination of metals have also been resolved showing that lens astigmatism is not yet a limiting factor. The clarity of these micrographs suggests that doubly periodic structures below 9 Å should be readily resolvable. Since the mechanism of formation of the moiré image by recombination of diffracted spectra is essentially similar to that of a directly resolved lattice, we believe that with suitable crystals direct observation is possible at least down to 5 Å.

---

† These micrographs are in the course of publication elsewhere.

ACKNOWLEDGMENT

This note is published by permission of the Chairman of Tube Investments Limited.

REFERENCES

MENTER, J. W., 1956, *Proc. roy. Soc.* A, **236,** 119.

PASHLEY, D. W., MENTER, J. W., and BASSETT, G. A., 1957, *Nature, Lond.*, **179,** 752.

WOOSTER, N., 1931, *Z. Kristallogr.*, **78,** 484.

[*The Editors do not hold themselves responsible for the views expressed by their correspondents.*]

Fig. 3

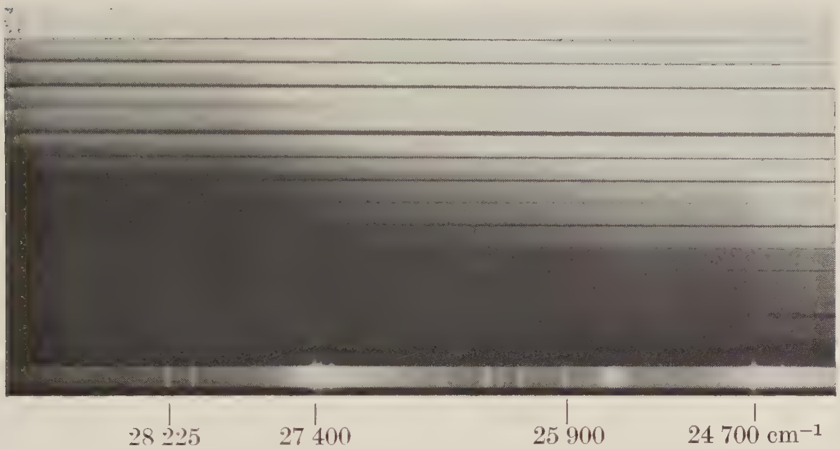

Absorption lines of $MnSO_4.4H_2O$ at room temperature.

Fig. 4

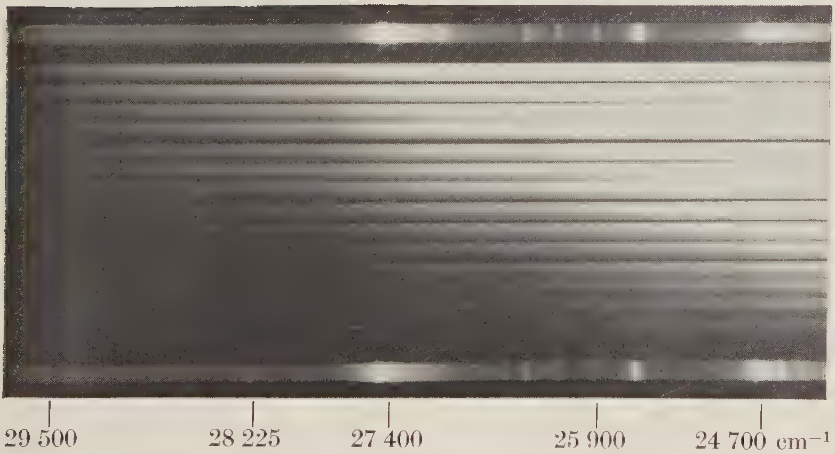

Absorption lines of $MnSO_4.4H_2O$ at 78°K.

Fig. 5

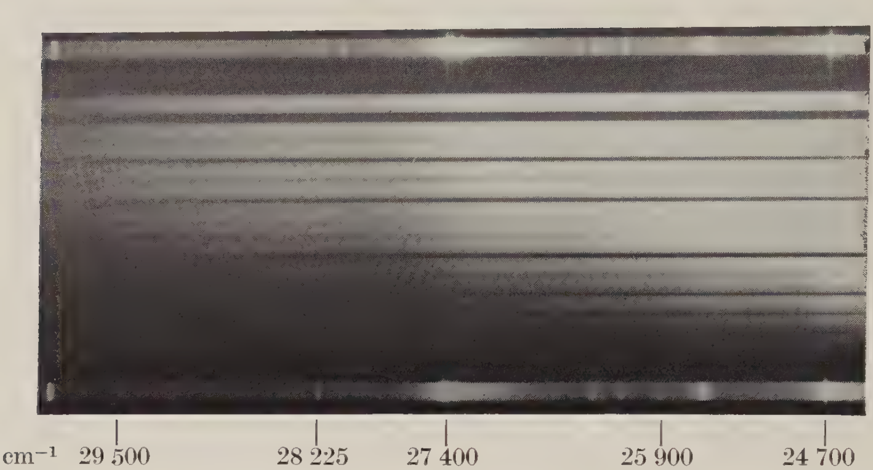

Absorption lines of $MnSO_4.4H_2O$ at 20°K.

Fig. 6

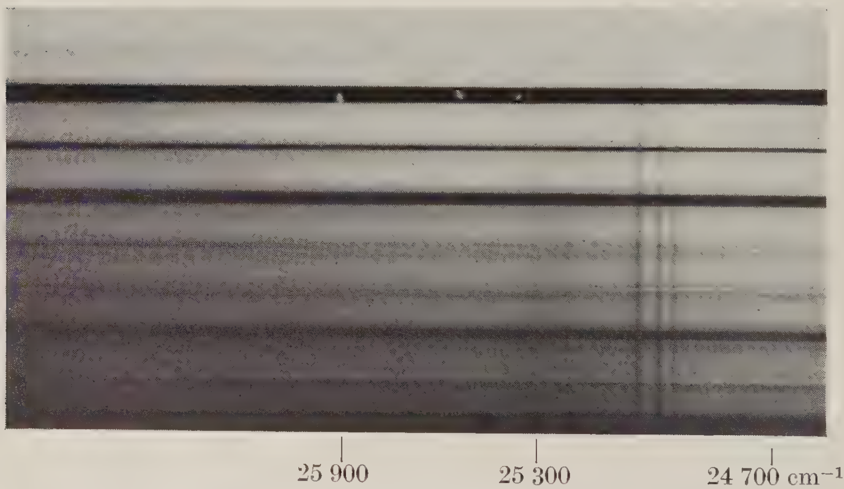

Absorption lines of $MnSO_4.4H_2O$ at 20°K (25 000 cm⁻¹ region).

Fig. 7

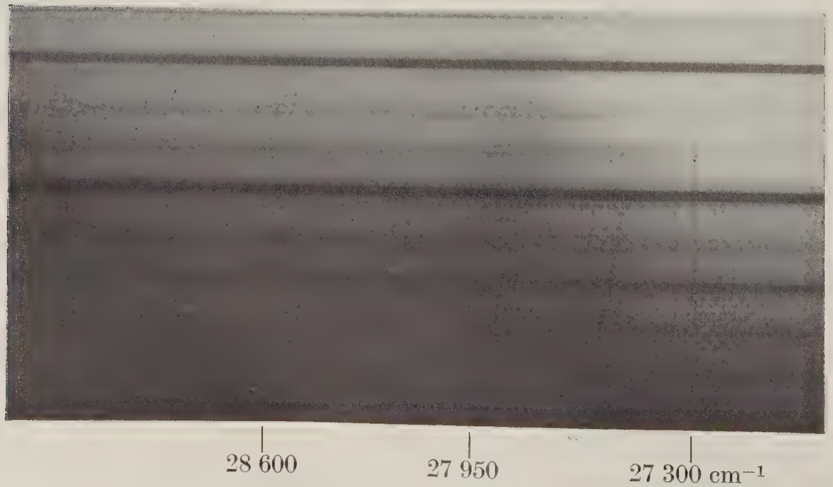

Absorption lines of $MnSO_4.4H_2O$ at 20°K (27 000 cm⁻¹ region).

Fig. 10

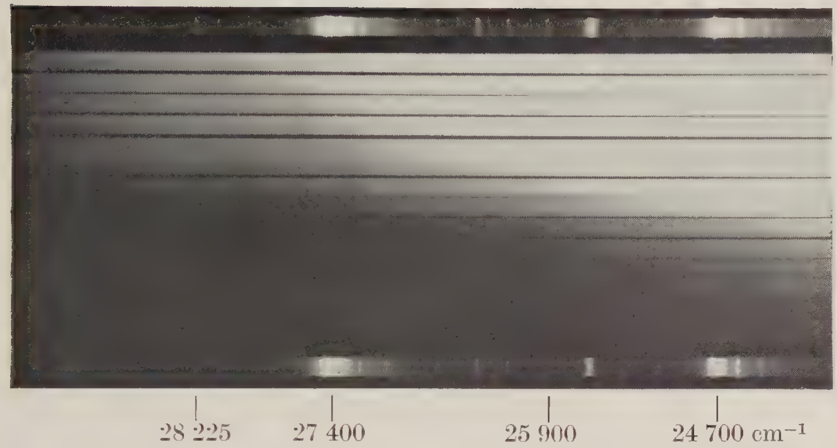

Absorption lines of $MnCl_2.4H_2O$ at 78°K.

Fig. 11

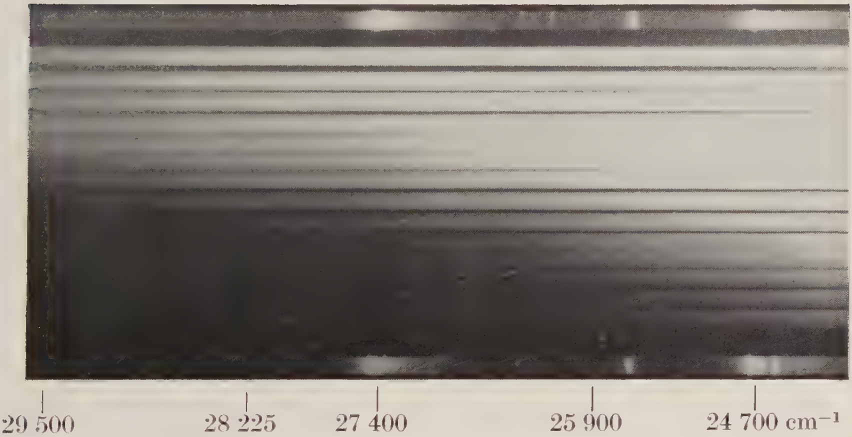

Absorption lines of $MnCl_2.4H_2O$ at 20°K.

Fig. 12

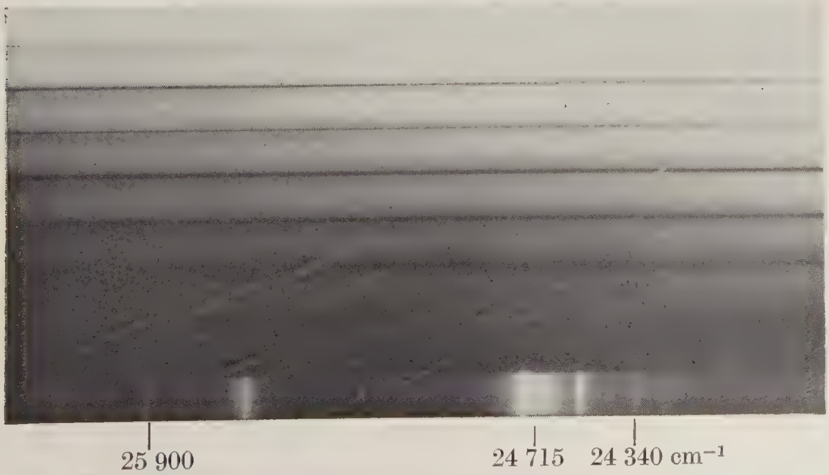

Absorption lines of $MnCl_2.4H_2O$ at 20°K (24 500 cm⁻¹ region).

Fig. 13

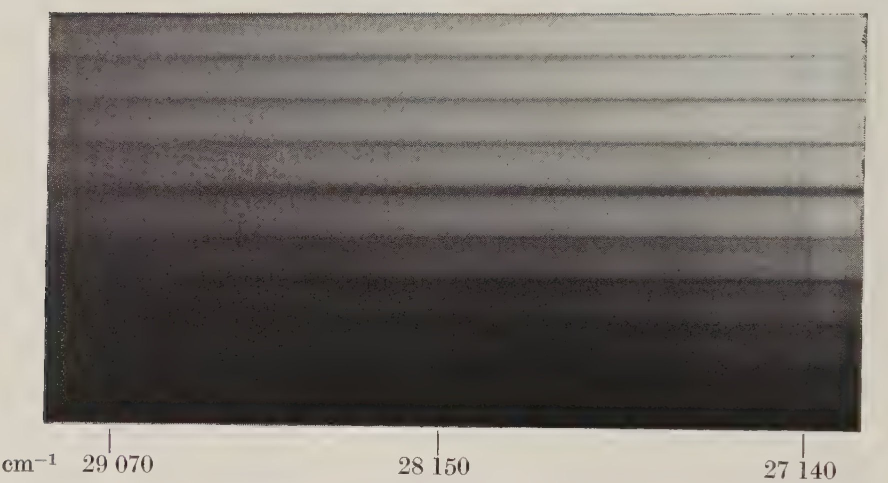

Absorption lines of $MnCl_2.4H_2O$ at 20°K (27 000–29 000 cm⁻¹ region).

Fig. 17

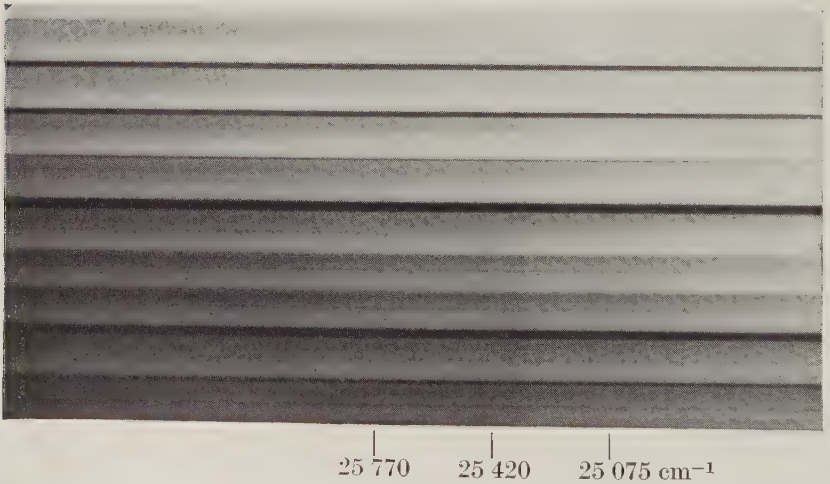

Lines of $MnSFi_6.6H_2O$ at 20°K.

Fig. 5

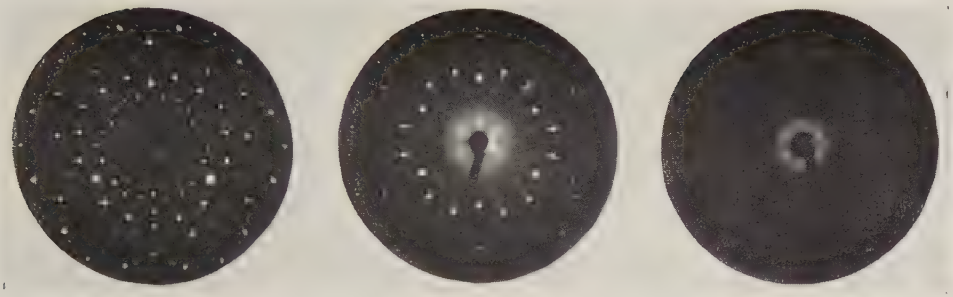

(*a*) (*b*) (*c*)

Laue transmission photographs, quartz single crystals oriented with incident x-ray beam parallel to *c*-axis. (*a*) Before irradiation, (*b*) after 7×10^{19} neutrons/cm^2, (*c*) after $1{\cdot}2 \times 10^{20}$ neutrons/cm^2.

Fig. 8

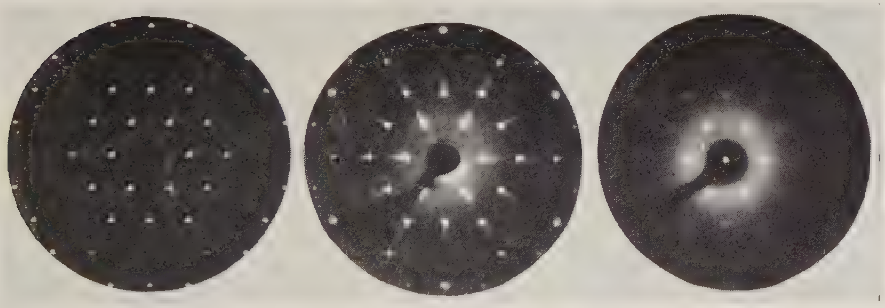

(*a*) (*b*) (*c*)

Precession photographs, zero level (hk0) projection, quartz single crystal. (*a*) Before irradiation, (*b*) after 7×10^{19} neutrons/cm^2, (*c*) after $1{\cdot}2 \times 10^{20}$ neutrons/cm^2.

Fig. 10

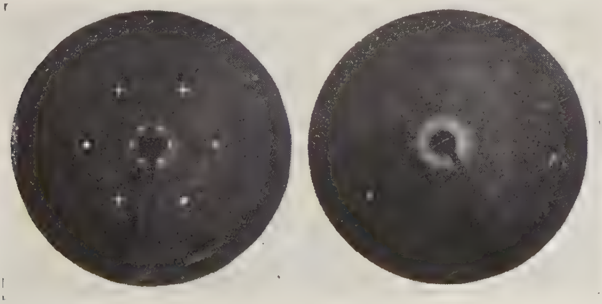

(*a*) (*b*)

X-ray transmission scattering patterns from neutron irradiated quartz single crystals. Monochromatic $\mathrm{Mo}_{K\alpha}$ radiation. (*a*) After 7×10^{19} neutrons/cm^2, (*b*) after $1{\cdot}2 \times 10^{20}$ neutrons/cm^2.

Fig. 3

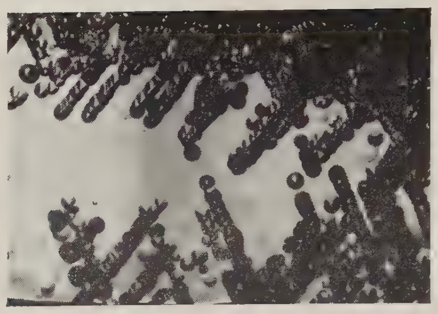

Dislocations in a bar of InSb bent through a small angle. $(\bar{1}\bar{1}\bar{1})$ face. ×47.

Fig. 4

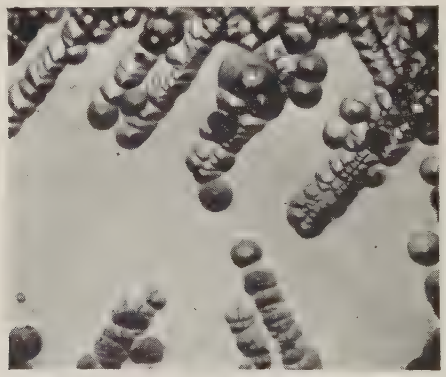

An enlargement of part of fig. 3 showing slip on neighbouring glide planes. ×93.

Fig. 5

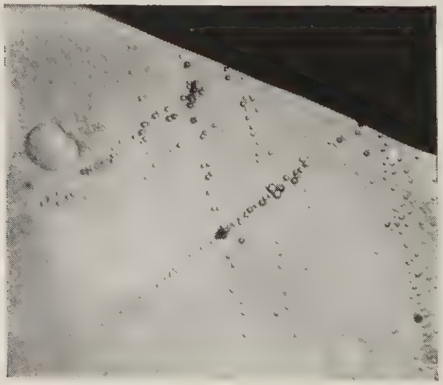

Dislocations in intersecting glide planes. $(\bar{1}\bar{1}\bar{1})$ face of InSb. ×180.

Fig. 1

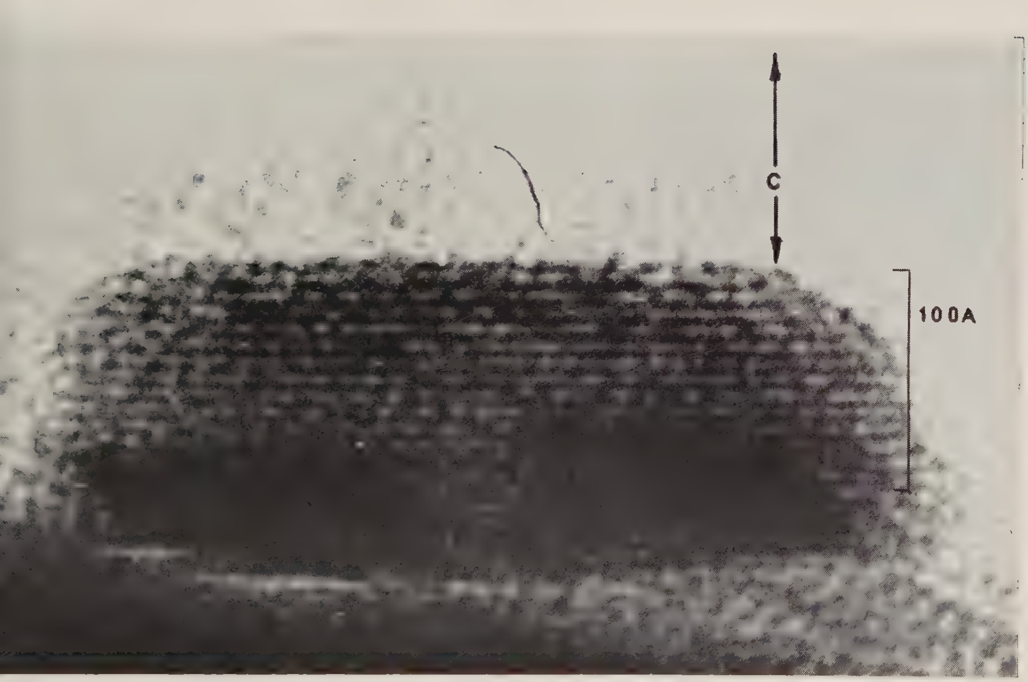

Electron micrograph of molybdenum trioxide crystal showing (020) planes resolved. ($d_{(020)}=6{\cdot}93$ Å.) Magnification ×3 000 000.

SUBJECT INDEX

PAGE
Activation energy of high temperature creep in metals 584
Air showers, intensive 797, 804, 891, 900
Alpha particle, photodisintegration 1211
Anhysteretic magnetization, permanent alloys 719
Annealing of deformed nickel 15
Atomic heats of titanium, zirconium and hafnium 1246
Axial ratio of zinc and of eta and epsilon brasses 716

Band structure of transition metals 1364
Barium titanite ceramics, decay effects 1100
β-decay, parity non-conservation 1050
β-particles, longitudinal polarization 1105
Book notices 141, 575, 1057
Book reviews 141, 288, 425, 573, 830, 939, 1055, 1176, 1286, 1396
Boron 10, 4·77 Mev level 1085

Carbon steel, metallography under compression 548
Cerium–lanthanum alloys, specific heat and susceptibility at low temperatures 811
Climb phenomena in synthetic fluorite crystals 561
Cobalt alloys, magnetization 659
Cold-work, existence of microcracks 1
Cold-worked copper at low temperatures, internal friction 1427
Colour centre formation in quartz 864
Conductivity, thermal and electrical, chromium low temperatures 577
Copper and silver alloys, liquid–solid equilibrium 1177
Cosmic radiation :
    intensive air showers 797, 804, 891, 900
    interactions of heavy nuclei 293
    primary, charge distribution 1059
    spectrum of α particles, low energy end 157
Crossing symmetry 831, 839
Crystal growth from aqueous solution 317, 635

Diffusion of zinc in zinc oxide 708
Dislocations in crystals :
    centre of a 1197
    decoration in alkali halides, new method 704
    density change in crystal 1053
    etching in silver halides 1047
    formation and properties of helical 355
    helicoidal lines in fluorite 94
    helical and spiral etch pits 1264
    locking, and fracture in α-iron 649
    photoelastic study 772
    surface distribution in metals 977

PAGE
Electric polarizability of atoms and molecules 591
Electromagnetic cascades in nuclear emulsions, energy . . . 1389
Electron-correlation 245
Electron and positron single scattering in argon 196
Electron diffraction from crystals with stacking faults . . . 1121, 1303
Electronic conductivity of silver halide crystals 1276
Electronic structure of palladium–uranium alloys 491
Electronic subtraction of background with kicksorter . . . 113
Electrostatic fields round localized defects in metals 1226
Etching of diamonds 859
Etch pits, rectilinear on diamonds 1003
Etch pits, spiral, in germanium and silicon 1285
Evaporated films, texture 455

Fatigue damage 437
Fermi surface, determination proposal 1147
Ferromagnetism of gas of hard sphere fermions 404
Flow stress in polycrystalline aluminium 1011
Fluorine 19, excitation by inelastic neutron scattering . . . 628
Fluorine 19 levels, interpretation 311

Growth of thin metal films, initial stages 750
γ-rays, circular polarization, parity failure 710
(γ, p) and (γ, n) cross sections, effect of isotopic spin impurity . . 5
γ-ray, delayed angular correlations in tantalum 181 1325
γ-ray cascade in sulphur 34 angular correlation 1255
γ-rays circular polarization 710
γ-rays from ^{14}N, 8·06 MEV level 499
Germanium 71, L/K-capture 427

Half-lives determination, graphical method 998
Hall effect and magneto-resistance in indium–antimonide . . . 1393
Hardening and embrittlement of steel, irradiation with neutrons . . 1271
Helium, liquid, specific heat 143
Hydromagnetic stability problems 33

Impurity–vacancy interaction in a metal 985
Indium antimonide, mechanical properties 1475
Indium–magnesium and indium–lithium alloys 1354
Infra-red absorption spectrum, α-quartz, effects of radiation . . . 941
Intensity fluctuations in stationary optical fields 351
Inter-diffusion of two charged particles, ion exchange . . . 599
Irradiation damage, magnesium oxide 607
Isotopic spin impurities 286
Isotopic spin selection rules 57, 61, 63, 83

K capture in carbon 11 1089

Laminar flow in curved channels, stability 305
Lanthanum, natural radioactivity 49
Lattice conduction, effect of free electrons. 292, 422, 1396
Lattice constants in crystal statistics 733
Liquid immiscibility in metal systems 259

PAGE
Lithuim 6, life-time of 3·56 MEV state 1468
Lithuim 8, emission from heavy element disintegrations . . . 149
Lithuim fluoride, neutron irradiated, X-ray study 1018
London–Van der Waals force, influence of retardation . . . 571
Lunar atmosphere, radio observations 1040
Lutecium 176, search for electron capture 699

Madelung constants for cubic ionic lattices 284
Magnetization of cobalt–manganese and cobalt–chromium alloys . 659
Magnetization, remanent, single domain ferromagnetic particles . . 1333
Magnetic behaviour of α ferric oxide, effect of titanium and aluminium . 505
Magnetic properties of Mn, Al, Zn, C and Mn, Ga, Zn, C alloys . . 554
Magnetic saturation of Neodymium alloys at low temperatures . . 726
Magnetic susceptibility of α and β brass 389
Magnetic transition in hematite 827
Magnetohydrodynamic shock waves in solar corona 1287
Magneto-resistance in metals 97
Mesons :
    heavy K, cascade decay 936
    meson–nucleon scattering 176, 467
    μ, fusion induced by 910
    μ, polarization 1143
    π^-, 4·2 GEV in G5 emulsions 37
    π-mesonic X-rays, measurements 957
    π, production by proton–proton collisions 215
    π, slow, absorption in emulsions 777
Metals, pure, isomorphous phases 384
Multipole order of lattice cells of ionic crystals 568

Neodymium ethylsulphate thermal and magnetic properties at low temperatures 521
Neodymium 147, nuclear alignment 534
Neutron groups from $^{10}B(d, n)^{11}C$ 138
Neutron irradiated quartz, structural behaviour 1445
Neutron (cold) scattering in aluminium 694
Neutrons, intense, cold beams, production 917
Nitrogen 14, 8·06 and 8·70 MEV states 1006
Nuclear forces and structure of lithium isotopes 1219
Nuclear photo-effect in light nuclei 780
Nuclei, reactions in complex 473

Optical absorption lines of hydrated manganous salts at low temperature 1397

Pair production, angular distribution in emulsions 133
Parity conservation breakdown 684, 710, 1050, 1105
Periodic structures below 10 Å, electron microscopic observation . . 1482
Photographic latent image, nature and formation 1149
Propane bubble chamber 820
Proton emission on neutron bombardment 785
Proton–proton elastic scattering at 925 MEV 204
Protons, quasi-elastic collisions, 925 MEV 231

Quenching vacancies 379, 570, 1387

PAGE
Radium D, weak gamma lines 713
Rochelle salt, theory 1027

Scattering of polarized positrons by polarized electrons . . . 1472
Scattering of positive ions by neutral atoms 761
Scattering, small angle, from deformed metals 589
Shock waves, reflection and transmission 182, 189
Single crystals in polymers, folded chain 1171
Slip bands in fatigued copper 131
Slip in polycrystalline copper 1103
Solution of inert gas atoms in metals 1345
Specific heat and high frequency viscosities, organic liquids . . . 441
Specific heat of solids at high temperatures 1415
Stacking faults in face-centred cubic metals and alloys . . . 669
Strip-scanning, effects of incomplete resolution, application to radio astronomy 119
Surface free energy and specific heat of a metal 702

Thermal conductivity of metals at low temperatures 541
Thermal expansion of solids 639
Thermal expansion of solids at high temperatures 1421
Thermal instability of rotating fluid sphere heated within . . 845, 1282
Thermoelectric power of ionic conducting crystals 1462

Vanadium, natural radioactivity 697
Vector potential distributions in axially symmetrical system . . 576
Velocity of sound in metals at high temperatures 1113

Work hardening and softening of face-centred cubic metal crystals . 323
Work hardening, mechanism in face-centred cubic metals . . 105, 1237

Ytterbium ethyl sulphate, thermal and magnetic properties between 20°K and 1°K 928
Ytterbium 175, nuclear alignment 1079

INDEX OF AUTHORS (WITH TITLES)

PAGE
Alfred, L. C. R., and March, N. H.: Impurity–vacancy interaction in a metal . . . 985
Allen, J.: The mechanical properties of indium antimonide . . . 1475
Allsopp, H. L.: Decay effects in barium titanate ceramics . . . 1100
Alston, Margaret H., Collinge, B., Evans, W. H., Newport, R. W., and Williams, P. R.: A propane bubble chamber . . . 820
Alston, Margaret H., Evans, W. H., Morgan, T. D. N., Newport, R. W., Williams, P. R., and Kirk, A.: Polarization of μ-mesons observed in a propane bubble chamber . . . 1143
Amelinckx, S., Bontinck, W., and Dekeyser, W.: Helical dislocations and spiral etch-pits . . . 1264
Amelinckx, S., Bontinck, W., Dekeyser, W., and Seitz, F.: Formation and properties of helical dislocations . . . 355
Amelinckx, S., with Bontinck, W.: Observation of helicoidal dislocation lines in fluorite crystals . . . 94
Atkinson, H. H., and Lowde, R. D.: Small angle scattering from deformed metals . . . 589
Aub, M. R., Power, E. A., and Zienau, S.: The influence of retardation on the London–Van der Waals force . . . 571
Azuma, R. E., and Lewis, G. M.: Delayed γ-ray angular correlations in tantalum 181 . . . 1325

Ball C. J.: Surface distributions of dislocations in metals: II . . . 977
Ball, C. J.: The flow stress of polycrystalline aluminium . . . 1011
Barber, D. J., Harvey, K. B., and Mitchell, J. W.: A new method for decorating dislocations in crystals of alkali halides . . . 704
Barker, F. C.: Isotopic spin impurities . . . 286
Barker, F. C.: The nuclear photoeffect in light nuclei . . . 780
Barker, F. C., and Mann, A. K.: The effect of isotopic spin impurity on (γ, p) and (γ, n) cross sections . . . 5
Barnard, A. C. L., and Haywood, B. C.: The weak lines in the radium D gamma spectrum . . . 713
Bassett, G. A., and Menter J. W.: Electron microscopic observation of periodic structures below 10 Å . . . 1482
Beattie, I. R., and Davies, D. R.: The inter-diffusion of two charged particles (with particular reference to ion-exchange in zeolites) . 599
Bell, J. F. W.: The velocity of sound in metals at high temperatures . 1113
Bishop, G. R., Grace, M. A., Johnson, C. E., Lemmer, H. R., and Perez y Jorba, J.: Nuclear alignment of ^{147}Nd . . . 534
Bloom, S. D., Toppel, B. J., and Wilkinson, D. H.: Isotopic spin selection rules, IX: The 9·58 MeV state of ^{16}O . . . 57
Bloom, S. D., with Toppel, B. J., and Wilkinson, D. H.: Isotopic spin selection rules, X: The 7·18 MeV state of ^{20}Ne . . . 61
Bloom, S. D., with Wilkinson, D. H.: Isotopic spin selection rules, XI: The 8·06 and 6·23 MeV states of ^{14}N . . . 63
Bontinck, W.: Climb phenomena in synthetic fluorite crystals . . . 561
Bontinck, W., and Amelinckx, S.: Observation of helicoidal dislocation lines in fluorite crystals . . . 94
Bontinck, W., with Amelinckx, S., Dekeyser, W., and Seitz, F.: On the formation and properties of helical dislocations . . . 355
Bontinck, W., with Amelinckx, S., and Dekeyser, W.: Helical dislocations and spiral etch-pits . . . 1264

PAGE

Bowness, C., and Cusack, N.: A comparison of electron and positron single scattering in argon 196
Bradley, E. F., with West, D.: Proportional counter measurements of π-mesonic X-rays 957
Bradshaw, F. J., and Pearson, S.: Quenching vacancies in aluminium 570
Bradshaw, F. J., and Pearson, S.: Quenching vacancies in gold 379
Bradshaw, F. J., with Pearson, S.: Quenching vacancies in dilute binary platinum solid solutions 1387
Bransden, B. H., Douglas, A. C., and Robertson, H. H.: Photodisintegration of the alpha particle 1211
Broude, C., Green, L. L., Singh, J. J., and Willmott, J. C.: On the 8·06 and 8·70 MeV states in ^{14}N 1006
Broude, C., Green, L. L., Singh, J. J., and Willmott, J. C.: The γ-rays from the 8·06 MeV level in ^{14}N 499
Brown, G., and Hughes, I. S.: Absorption of slow negative π-mesons, by the elements in nuclear emulsions 777
Brown, G., and Muirhead, H.: An analysis of the reactions induced in complex nuclei by nucleons with energies between 10 and 20 MeV 473
Brown, G., Morrison, G. C., Muirhead, H., and Morton, W. T.: A study of protons emitted from aluminium, iron and rhodium on bombardment with neutrons of 13·2 MeV 785
Burns, Jennifer, with Hume-Rothery, William: Liquid$\rightleftharpoons$solid equilibrium in copper and silver alloys; with an appendix on the equilibrium diagram of the system copper–arsenic 1177
Butterworth, I., Egelstaff, P. A., London, H., and Webb, F. J.: The production of intense cold neutron beams 917

Campbell, J. D., Duby, J., and Puttick, K. E.: Metallography of a medium carbon steel subjected to slow and impact compression 548
Catterall, J. A.: The electronic structure of palladium–uranium alloys 491
Cavanagh, P. E., Turner, J. F., Coleman, C. F., Gard, G. A., and Ridley, B. W.: On the longitudinal polarization of β-particles 1105
Chadwick, G. B., Durrani, S. A., Eisberg, L. M., Jones, P. B., Wignall, J. W. G., and Wilkinson, D. H.: The breakdown of parity conservation in the π–μ–e decay and a test of the two component neutrino theory 684
Chandrasekhar, S.: The thermal instability of a rotating fluid sphere heated within 845
Chandrasekhar, S.: The thermal instability of a rotating fluid sphere heated within: II 1282
Chia-Shun Yih and Sangster, W. M.: Stability of laminar flow in curved channels 305
Childs, B. G., and Penfold, J.: The magnetic susceptibility of α and β brass 389
Churchman, A. T., Mogford, I., and Cottrell, A. H.: The hardening and embrittlement of steel by irradiation with neutrons 1271
Clarke, F. P.: Irradiation damage in single crystals of magnesium oxide 607
Clarke, J. O., and Major, J. V.: Interaction lengths and diffraction scattering of 4·2 GeV π^--Mesons in G5 emulsion 37
Coleman, C. F., with Cavanagh, P. E., Turner, J. F., Gard, G. A., and Ridley, B. W.: On the longitudinal polarization of β-particles 1105
Collinge, B., with Alston, Margaret H., Evans, W. H., Newport, R. W., and Williams, P. R.: A propane bubble chamber 820
Cooke, A. H., McKim, F. R., Meyer, H., and Wolf, W. P.: The thermal and magnetic properties of ytterbium ethyl sulphate between 20°K and 1°K 928

PAGE

Cottrell, A. H., with Churchman, A. T., and Mogford, I.: The hardening and embrittlement of steel by irradiation with neutrons . . . 1271
Cottrell, A. H., with Rimmer, D. E.: The solution of inert gas atoms in metal . . . 1345
Crangle, J.: The magnetization of cobalt–manganese and cobalt–chromium alloys . . . 659
Cranshaw, T. E., and Galbraith, W.: Observations on extensive air showers, I: Apparatus . . . 797
Cranshaw, T. E., and Galbraith, W.: Observations on extensive air showers, II: Time variations in the energy region of 10^{17} ev . . . 804
Cranshaw, T. E., Galbraith, W., and Porter, N. A.: Observations on extensive air showers, III: The distribution of charged particles . . . 891
Cranshaw, T. E., with Porter, N. A., and Galbraith, W.: Observations on extensive air showers, IV: The lateral distribution of penetrating particles . . . 900
Cusack, N., with Bowness, C.: A comparison of electron and positron single scattering in argon . . . 196

Davies, D. R., with Beattie, I. R.: The inter-diffusion of two charged particles (with particular reference to ion-exchange in zeolites) . . . 599
Dekeyser, W., with Amelinckx, S., and Bontinck, W.: Helical dislocations and spiral etch-pits . . . 1264
Dekeyser, W., with Amelinckx, S., Bontinck, W., and Seitz, F.: On the formation and properties of helical dislocations . . . 355
Devonshire, A. F.: Theory of Rochelle salt . . . 1027
Diehl, J., with Seeger, A., Mader, S., and Rebstock, H.: Work-hardening and work-softening of face-centred cubic metal crystals . . . 323
Domb, C., and Sykes, M. F.: The calculation of lattice constants in crystal statistics . . . 733
Douglas, A. C., with Bransden, B. H., and Robertson, H. H.: Photodisintegration of the alpha particle . . . 1211
Drever, R. W. P., and Moljk, A.: The L K-capture ratio of germanium 71 . . . 427
Duby, J., with Campbell, J. D., and Puttick, K. E.: Metallography of a medium carbon steel subjected to slow and impact compression . . . 548
Duke, P. J., Lock, W. O., March, P. V., Gibson, W. M., McEwen, J. G., Hughes, I. S., and Muirhead, H.: The elastic scattering of protons by protons at 925 Mev . . . 204
Duke, P. J., with McEwen, J. G., and Gibson, W. M.: Quasi-elastic collisions of 925 Mev protons . . . 231
Durrani, S. A., with Chadwick, G. B., Eisberg, L. M., Jones, P. B., Wignall, J. W. G., and Wilkinson, D. H.: The breakdown of parity conservation in the π–μ–e decay and a test of the two component neutrino theory . . . 684

Eastabrook, J. N.: Specific heat of solids at high temperatures . . . 1415
Eastabrook, J. N.: Thermal expansion of solids at high temperatures . . . 1421
Edwards, S. F., and Matthews, P. T.: A simple treatment of meson–nucleon scattering . . . 176
Edwards, S. F., and Matthews, P. T.: Crossing symmetry and relativistic equation for two fermions . . . 831
Edwards, S. F., and Matthews, P. T.: Relativistic theory of meson nucleon scattering . . . 467
Edwards, S. F., and Matthews, P. T.: Remarks on crossing symmetry . . . 839

PAGE

Egelstaff, P. A., with Butterworth, I., London, H., and Webb, F. J.: The production of intense cold neutron beams 917
Ehrman, Joachim B.: Ferromagnetism of a gas of hard sphere fermions . 404
Eisberg, L. M., with Chadwick, G. B., Durrani, S. A., Jones, P. B., Wignall, J. W. G., and Wilkinson, D. H.: The breakdown of parity conservation in π–μ–e decay and a test of the two component neutrino theory 684
Ellis, S. G.: On spiral etch pits in germanium and silicon . . . 1285
Elsmore, B.: Radio observations of the lunar atmosphere . . . 1040
Evans, W. H., with Alston, Margaret H., Collinge, B., Newport, R. W., and Williams, P. R.: A propane bubble chamber . . . 820
Evans, W. H., with Alston, Margaret, H., Morgan, T. D. N., Newport, R. W., Williams, P. R., and Kirk, A.: Polarization of μ-mesons observed in a propane bubble chamber 1143

Feltham, P., and Meakin, J. D.: On the mechanism of work hardening in face-centred cubic metals, with special reference to polycrystalline copper 105
Feltham, P., and Meakin, J. D.: On the mechanism of work hardening in face-centred cubic metals with special reference to polycrystalline copper: II 1237
Feltham, Paul: On the activation energy of high temperature creep in metals 584
Fischer, Gaston and MacDonald, D. K. C.: Hall effect and magneto-resistance in indium–antimonide 1393
Fisher, P. S., and Shute, G. G.: The angular correlation of the gamma cascade in sulphur 34 1255
Fletcher, G. C.: The thermal expansion of solids 639
Forsyth, P. J. E.: Some observations on the nature of fatigue damage . 437
Fowler, P. H., Hillier, R. R., and Waddington, C. J.: Interactions of the heavy nuclei of the cosmic radiation 293
Fowler, P. H., Waddington, C. J., Freier, P. S., Naugle, J., and Ney, E. P.: The low energy end of the cosmic ray spectrum of alpha-particles 157
Freeman, Joan, M.: The excitation of a 2·79 MeV level in ^{19}F by inelastic neutron scattering 628
Freier, P. S., with Fowler, P. H., Waddington, C. J., Naugle, J., and Ney, E. P.: The low energy end of the cosmic ray spectrum of alpha-particles 157
Fumi, F. G., and Tosi, M. P.: Multipole order of lattice cells of ionic crystals 568
Fumi, F. G., and Tosi, M. P.: On the Naor relations between Madelung constants for cubic ionic lattices 284

Galbraith, W., with Cranshaw, T. E.: Observations on extensive air showers, I: Apparatus 797
Galbraith, W., with Cranshaw, T. E.: Observations on extensive air showers, II: Time variations in the energy region of 10^{17} ev . 804
Galbraith, W., with Cranshaw, T. E., and Porter, N. A.: Observations on extensive air showers, III: The distribution of charged particles . 891
Galbraith, W., with Porter, N. A., and Cranshaw, T. E.: Observations on extensive air showers, IV: The lateral distribution of penetrating particles 900

PAGE

Gard, G. A., with Cavanagh, P. E., Turner, J. F., Coleman, C. F., and Ridley, B. W. : On the longitudinal polarization of β-particles . 1105

Gibson, W. M., with Duke, P. J., Lock, W. O., March, P. V., McEwen, J. G., Hughes, I. S., and Muirhead, H. : The elastic scattering of protons by protons at 925 Mev . 204

Gibson, W. M., with McEwen, J. G., and Duke, P. J. : Quasi-elastic collisions of 925 Mev protons . 231

Glover, R. N., and Watt, D. E. : A search for electron capture in ^{176}Lu . 699

Glover, R. N., and Watt, D. E. : A search for natural radioactivity in vanadium . 697

Glover, R. N., and Watt, D. E. : The natural radioactivity of lanthanum 49

Goldsack, S. J., Lock, W. O., and Munir, B. A. : ^{8}Li emission from heavy element disintegrations produced by 5·7 Bev protons . 149

Grace, M. A., Johnson, C. E., Scurlock, R. G., and Sowter, C. V. : A demonstration of parity non-conservation in β-decay . 1050

Grace, M. A., with Bishop, G. R., Johnson, C. E., Lemmer, H. R., and Perez y Jorba, J. : Nuclear alignment of ^{147}Nd . 534

Grace, M. A., Johnson, C. E., Scurlock, R. G., and Taylor, R. T. : Nuclear alignment of ytterbium 175 . 1079

Graham, J., and Raynor, G. V. : Indium-rich indium–magnesium and indium–lithium alloys . 1354

Graue, A., and Trumpy, B. : An investigation of neutron groups from the reaction ^{10}B(d, n)^{11}C at 7·0 Mev deuteron energy . 138

Green, L. L., with Broude, C., Singh, J. J., and Willmott, J. C. : On the 8·06 and 8·70 Mev states in ^{14}N . 1006

Green, L. L., with Broude, C., Singh, J. J., and Willmott, J. C. : The γ-rays from the 8·06 Mev level in ^{14}N . 499

Haig, F. D., with Michell, D. : Investigation of the annealing of deformed nickel powder by x-ray and stored energy measurements . 15

Haigh, G. : Observations on the magnetic transition in hematite at $-15°$c . 877

Haigh, G. : The effect of added titanium and aluminium on the magnetic behaviour of α ferric oxide . 505

Harper, A. F. A., Kemp, W. R. G., Klemens, P. G., Tainsh, R. J., and White, G. K. : The thermal and electrical conductivity of chromium at low temperatures . 577

Harvey, K. B., with Barber, D. J., and Mitchell, J. W. : A new method for decorating dislocations in crystals of alkali halides . 704

Haywood, B. C., with Barnard, A. C. L. : The weak lines in the radium D gamma spectrum . 713

Heslop, J., and Petch, N. J. : Dislocation locking and fracture in α-iron . 649

Hill, R. W., and Lounasmaa, O. V. : The specific heat of liquid helium . 143

Hillier, R. R., with Fowler, P. H., and Waddington, C. J. : Interactions of the heavy nuclei of the cosmic radiation . 293

Hirsch, P. B., with Whelan, M. J. : Electron diffraction from crystals containing stacking faults : I . 1121

Hirsch, P. B., with Whelan, M. J. : Electron diffraction from crystals containing stacking faults : II . 1303

Howard, R. E., and Lidiard, A. B. : Thermoelectric power of ionic conducting crystals . 1462

Howe, L., and Myers, H. P. : Magnetic properties of alloys having the compositions $Mn_{60}Al_xZn_{20-x}C_{20}$ and $Mn_{60}Ga_xZn_{20-x}C_{20}$. 554

Hughes, I. S., March, P. V., Muirhead, H., and Lock, W. O. : The production of π-mesons in proton–proton collisions at 925 Mev . 215

PAGE
Hughes, I. S., with Brown, G.: The absorption of slow negative π-mesons by the elements in nuclear emulsions 777
Hughes, I. S., with Duke, P. J., Lock, W. O., March, P. V., Gibson, W. M., McEwen, J. G., and Muirhead, H.: The elastic scattering of protons by protons at 925 MeV 204
Hume-Rothery, William and Burns, Jennifer, : Liquid$\rightleftharpoons$solid equilibrium in copper and silver alloys, with an appendix on the equilibrium diagram of the system copper–arsenic 1177

Johnson, C. E., with Bishop, G. R., Grace, M. A., Lemmer, H. R., and Perez y Jorba, J.: Nuclear alignment of ^{147}Nd 534
Johnson, C. E., with Grace, M. A., Scurlock, R. G., and Sowter, C. V.: A demonstration of parity non-conservation in β-decay . . . 1050
Johnson, C. E., with Grace, M. A., Scurlock, R. G., and Taylor, R. T.: Nuclear alignment of ytterbium 175 1079
Jones, D. A., and Mitchell, J. W.: The etching of dislocations in crystals of silver halides 1047
Jones, P. B., with Chadwick, G. B., Durrani, S. A., Eisberg, L. M., Wignall, J. W. G., and Wilkinson, D. H.: The breakdown of parity conservation in the π–μ–e decay and a test of the two component neutrino theory 684

Kehoe, R. B.: On the texture of evaporated films 455
Keller, A.: A note on single crystals in polymers: Evidence for a folded chain configuration 1171
Kemp, W. R. G., with Harper, A. F. A., Klemens, P. G., Tainsh, R. J., and White, G. K.: Thermal and electrical conductivity of chromium at low temperatures 577
Kemsley, D. S.: Observations on the distribution of slip in polycrystalline copper 1103
Kemsley, D. S.: The nature of persistent slip bands in fatigued copper . 131
Kenawi, M., with Omar, M.: The etching of diamonds by low pressure oxygen 859
Kirk, A., with Alston Margaret H., Evans, W. H., Morgan, T. D. N., Newport, R. W., and Williams, P. R.: Polarization of μ-mesons observed in a propane bubble chamber 1143
Klemens, P. G., with Harper, A. F. A., Kemp, W. R. G., Tainsh, R. J., and White, G. K.: Thermal and electrical conductivity of chromium at low temperatures 577
Kothari, L. S., and Singwi, K. S.: Cold neutron scattering in aluminium. 694
Krisement, O.: Some remarks about electron-correlation . . . 245
Kuščer, I., Mihailovič, M. V., and Park, E. C.: A graphical method for the determination of half-lives 998

Lee, P. M., and March, N. H.: Electrostatic fields round localized defects in metals 1226
Lemmer, H. R., with Bishop, G. R., Grace, M. A., Johnson, C. E., and Perez y Jorba, J.: Nuclear alignment of ^{147}Nd 534
Lewis, G. M., with Azuma, R. E.: Delayed γ-ray angular correlations in tantalum 181 1325
Lewis, G. M., with Scobie, J.: K-capture in carbon 11 1089
Lidiard, A. B., with Howard, R. E.: Thermoelectric power of ionic conducting crystals 1462

PAGE

Lock, J. M.: Magnetic saturation in alloys of neodymium at low temperatures 726
Lock, J. M., with Roberts, Lois M.: The specific heats and magnetic susceptibilities of alloys of cerium with lanthanum at low temperatures 811
Lock, W. O., with Duke, P. J., March, P. V., Gibson, W. M., McEwen, J. G., Hughes, I. S., and Muirhead, H.: The elastic scattering of protons by protons at 925 MEV 204
Lock, W. O., with Goldsack, S. J., and Munir, B. A.: ^{8}Li emission from heavy element disintegrations produced by 5·7 BEV protons . . 149
Lock, W. O., with Hughes, I. S., March, P. V., and Muirhead, H.: The production of π-mesons in proton-proton collisions at 925 MEV . 215
Lomer, W. M.: Density change of a crystal containing dislocations . 1053
London, H., with Butterworth, I., Egelstaff, P. A., and Webb, F. J.: The production of intense cold neutron beams 917
Lounasmaa, O. V., with Hill, R. W.: The specific heat of liquid helium . 143
Lowde, R. D., with Atkinson, H. H.: Small angle scattering from deformed metals 589

McCutcheon, C. W.: Electronic subtraction of background with a Hutchinson–Scarrott kicksorter 113
MacDonald, D. K. C.: Magneto-resistance in metals 97
MacDonald, D. K. C., with Fischer, Gaston: Hall effect and magneto-resistance in indium–antimonide 1393
McEwen, J. G., with Duke, P. J., Lock, W. O., March, P. V., Gibson, W. M., Hughes, I. S., and Muirhead, H.: The elastic scattering of protons by protons at 925 MEV 204
McEwen, J. G., Gibson, W. M., and Duke, P. J.: Quasi-elastic collisions of 925 MEV protons 231
McKim, F. R., with Cooke, A. H., Meyer, H., and Wolf, W. P.: The thermal and magnetic properties of ytterbium ethyl sulphate between 20°K and 1°K 928
Mader, S., with Seeger, A., Diehl, J., and Rebstock, H.: Work-hardening and work-softening of face-centred cubic metal crystals . . 323
Major, J. V., with Clarke, J. O.: Interaction lengths and diffraction scattering of 4·2 GEV π^--mesons in G5 emulsion, . . . 37
Mann, A. K., with Barker, F. C.: The effect of isotopic spin impurity on (γ, p) and (γ, n) cross sections 5
March, N. H., with Alfred, L. C. R.: Impurity–vacancy interaction in a metal 985
March, N. H., with Lee, P. M.: Electrostatic fields round localized defects in metals 1226
March, P. V., with Duke, P. J., Lock, W. O., Gibson, W. M., McEwen, J. G., Hughes, I. S., and Muirhead, H.: The elastic scattering of protons by protons at 925 MEV 204
March, P. V., with Hughes, I. S., Muirhead, H., and Lock, W. O.: The production of π-mesons in proton-proton collisions at 925 MEV . 215
Matthews, P. T., with Edwards, S. F.: A simple treatment of meson–nuclean scattering 176
Matthews, P. T., with Edwards, S. F.: Crossing symmetry and the relativistic equation for two fermions 831
Matthews, P. T., with Edwards, S. F.: Relativistic theory of meson-nucleon scattering 467

PAGE

Matthews, P. T., with Edwards, S. F.: Remarks on crossing symmetry 839

Meakin, J. D., with Feltham, P.: On the mechanism of work-hardening in face-centred cubic metals, with special reference to polycrystalline copper 105

Meakin, J. D., with Feltham, P.: On the mechanism of work hardening in face-centred cubic metals with special reference to polycrystalline copper: II 1237

Menter, J. W., with Bassett, G. A.: Electron microscopic observation of periodic structures below 10 Å. 1482

Meyer, H., with Cooke, A. H., McKim, F. R., and Wolf, W. P.: The thermal and magnetic properties of ytterbium ethyl sulphate between 20°K and 1°K 928

Meyer, Horst.: Thermal and magnetic properties of neodymium ethylsulphate at low temperatures 521

Michell, D., and Haig, F. D.: Investigation of the annealing of deformed nickel powder by X-ray and stored energy measurements . . 15

Mihailovič, M. V., with Kuščer, I., and Park, E. C.: A graphical method for the determination of half-lives 998

Mitchell, E. W. J., and Rigden, J. D.: The effects of radiation on the near infra-red absorption spectrum of α-quartz 941

Mitchell, J. W.: On the electronic conductivity of crystals of silver halides 1276

Mitchell, J. W., and Mott, N. F.: The nature and formation of the photographic latent image. 1149

Mitchell, J. W., with Barber, D. J., and Harvey, K. B.: A new method for decorating dislocations in crystals of alkali halides . . . 704

Mitchell, J. W., with Jones, D. A.: The etching of dislocations in crystals of silver halides 1047

Mogford, I., with Churchman, A. T., and Cottrell, A. H.: The hardening and embrittlement of steel by irradiation with neutrons . . 1271

Moljk, A., with Drever, R. W. P.: The L/K-capture of germanium 71 . 427

Morgan, T. D. N., with Alston, Margaret H., Evans, W. H., Newport, R. W., Williams, P. R., and Kirk, A.: Polarization of μ-mesons observed in a propane bubble chamber 1143

Morrison, G. C., with Brown, G., Muirhead, H., and Morton, W. T.: Study of protons emitted from aluminium, iron and rhodium on bombardment with neutrons of 13·2 MeV 785

Morton, W. T., with Brown, G., Morrison, G. C., and Muirhead, H.: Study of protons emitted from aluminium, iron and rhodium on bombardment with neutrons of 13·2 MeV 785

Mott, B. W.: Liquid immiscibility in metal systems 259

Mott, N. F., and Stevens, K. W. H.: The band structure of the transition metals 1364

Mott, N. F., with Mitchell, J. W.: The nature and formation of the photographic latent image 1149

Muirhead, H., with Brown, G.: An analysis of the reactions induced in complex nuclei by nucleons, with energies between 10 and 20 MeV . 473

Muirhead, H., with Brown, G., Morrison, G. C., and Morton, W. T.: A study of protons emitted from aluminium, iron and rhodium on bombardment with neutrons of 13·2 MeV 785

Muirhead, H., with Duke, P. J., Lock, W. O., March, P. V., Gibson, W. M., McEwen, J. G., and Hughes, I. S.: The elastic scattering of protons by protons at 925 MeV 204

Muirhead, H., with Hughes, I. S., March, P. V., and Lock, W. O.: The production of π-mesons in proton–proton collisions at 925 MeV . 215

PAGE

Munir, B. A., with Goldsack, S. J., and Lock, W. O.: ^{8}Li emission from heavy element disintegrations produced by 5·7 Bev protons 149
Myers, H. P., with Howe, L.: Magnetic properties of alloys having the compositions $Mn_{60}\,Al_x\,Zn_{20-x}\,C_{20}$ and $Mn_{60}\,Ga_x\,Zn_{20-x}\,C_{20}$ 554

Nabarro, F. R. N.: The axial ratio of zinc, and of the eta and epsilon brasses 716
Naugle, J., with Fowler, P. H., Waddington, C. J., Freier, P. S., and Ney, E. P.: The low energy end of the cosmic ray spectrum of alpha-particles 157
Newman, R. C.: The initial stages of growth of thin metal films on a silver single-crystal substrate 750
Newport, R. W., with Alston, Margaret, H., Collinge, B., Evans, W. H., and Williams, P. R.: A propane bubble chamber 820
Newport, R. W., with Alston, Margaret, H., Evans, W. H., Morgan T. D. N., Williams, P. R., and Kirk, A.: Polarization of μ-mesons observed in a propane bubble chamber 1143
Ney, E. P., with Fowler, P. H., Waddington, C. J., Freier, P. S., and Naugle, J.: The low energy end of the cosmic ray spectrum of alpha-particles 157
Niblett, D. H., and Wilks, J.: Internal friction of cold worked copper at low temperatures 1427
Nye, J. F., Spence, R. D., and Sprackling, M. T.: Photoelastic study of dislocation arrangements in crystals 772

Omar, M., and Kenawi, M.: The etching of diamonds by low pressure oxygen 859

Pack, D. C.: The reflection and transmission of shock waves, I: The reflection of a detonation wave at a boundary 182
Pack, D. C.: The reflection and transmission of shock waves, II: The effect of shock waves on an elastic target of finite thickness 189
Paige, E. G. S.: The kinetics of colour centre formation in quartz 864
Pappalardo, R.: Optical absorption lines of hydrated manganous salts at low temperatures 1397
Park, E. C., with Kuščer, I., and Mihailovič, M. V.: A graphical method for the determination of half-lives 998
Patel, A. R., with Tolansky, S.: Rectilinear etch pits on diamond 1003
Paul, E. B.: The interpretation of the levels of ^{19}F on the rotational model 311
Pearson, S., and Bradshaw, F. J.: Quenching vacancies in dilute binary platinum solid solutions 1387
Pearson, S., with Bradshaw, F. J.: Quenching vacancies in aluminium 570
Pearson, S., with Bradshaw, F. J.: Quenching vacancies in gold 379
Penfold, J., with Childs, B. G.: The magnetic susceptibility of α and β brass 389
Perez y Jorba, J., with Bishop, G. R., Grace, M. A., Johnson, C. E., and Lemmer, H. R.: Nuclear alignment of ^{147}Nd 534
Petch, N. J., with Heslop, J.: Dislocation locking and fracture in π-iron 649
Pinkau, K.: Energy determination of electromagnetic cascades in nuclear emulsions 1389
Pippard, A. B.: A proposal for determinining the fermi surface by magneto-acoustic resonance 1147
Pople, J. A., and Schofield, P.: Electric polarizability of atoms and molecules 591

PAGE

Porter, N. A., Cranshaw, T. E., and Galbraith, W. : Extensive air showers, IV : The lateral distribution of penetrating particles . 900
Porter, N. A., with Cranshaw, T. E., and Galbraith, W. : Observations on extensive air showers, III · The distribution of charged particles . 891
Power, E. A., with Aub, M. R., and Zienau, S. : The influence of retardation on the London–Van der Waals force 571
Puttick, K. E., with Campbell, J. D., and Duby, J. : Metallography of a medium carbon steel subjected to slow and impact compression . 548

Raynor, G. V., with Graham, H. : Indium-rich indium–magnesium and indium–lithium alloys 1354
Rebstock, H., with Seeger, A., Diehl, J., and Mader, S. : Work-hardening and work-softening of face-centred cubic metal crystals . . . 323
Richardson, E. G., and Tait, R. I. : Ratios of specific heat and high-frequency viscosities in organic liquids under pressure, derived from ultrasonic propagation 441
Ridley, B. W., with Cavanagh, P. E., Turner, J. F., Coleman, C. F., and Gard, G. A. : Longitudinal polarization of β-particles . . . 1105
Rigden, J. D., with Mitchell, E. W. J. : The effects of radiation on the near infra-red absorption spectrum of α-quartz 941
Rimmer, D. E., and Cottrell, A. H. : The solution of inert gas atoms in metal 1345
Roalsvig, J. P. : Angle distribution by pair production in photographic emulsions 133
Roberts, J. P., and Wheeler, C. : Diffusion of zinc in zinc oxide . . 708
Roberts, Lois M., and Lock, J. M. : The specific heats and magnetic susceptibilities of alloys of cerium with lanthanum at low temperatures 811
Robertson, H. H., with Bransden, B. H., and Douglas, A. C. : Photo-disintegration of the alpha particle 1211
Rose, H. J., and Warburton, E. K. : Lifetime of the 3·56 MEV state of lithium 6 1468
Rosenberg, H. M. : The thermal conductivity of metals at low temperatures. Deviations from ideal behaviour 541

Sangster, W. M., with Chia-Shun Yih : Stability of laminar flow in curved channels 305
Schofield, P., with Pople, J. A. : Electric polarizability of atoms and molecules 591
Schopper, H. : Circular polarization of γ-rays : Further proof for parity failure in β decay 710
Scobie, J., and Lewis, G. M. : K-capture in carbon 11 1089
Scott, J. M. C. : Scattering of polarized positrons by polarized electrons 1472
Scurlock, R. G., with Grace, M. A., Johnson, C. E., and Sowter, C. V. : A demonstration of parity non-conservation in β-decay . . . 1050
Scurlock, R. G., with Grace, M. A., Johnson, C. E., and Taylor, R. T. : Nuclear alignment of ytterbium 175 1079
Seeger, A., Diehl, J., Mader, S., and Rebstock, H. : Work-hardening and work-softening of face-centred cubic metal crystals . . 323
Seitz, F., with Amelinckx, S., Bontinck, W., and Dekeyser, W. : On the formation and properties of helical dislocations 355
Sen Gupta, S. N., and Sinha, M. S. : Cascade decay of a heavy K-meson 936
Shute, G. G., with Fisher, P. S. : The angular correlation of the gamma cascade in sulphur 34 1255

PAGE

Sida, D. W. : The scattering of positive ions by neutral atoms . . 761

Singh, J. J., with Broude, C., Green, L. L., and Willmott, J. C. : On the 8·06 and 8·70 MeV states in ^{14}N 1006

Singh, J. J., with Broude, C., Green, L. L., and Willmott, J. C. : The γ-rays from the 8·06 MeV level in ^{14}N 499

Singwi, K. S., with Kothari, L. S. : Cold neutron scattering in aluminium 694

Sinha, M. S., with Sen Gupta, S. N. : Cascade decay of a heavy K-meson 936

Skyrme, T. H. R. : Fusion induced by mu-mesons 910

Smallman, R. E., and Westmacott, K. H. : Stacking faults in face-centred cubic metals and alloys 669

Smallman, R. E., and Willis, B. T. M. : An x-ray study of neutron irradiated lithium fluoride 1018

Smerd, S. F., and Wild, J. P. : The effects of incomplete resolution on surface distributions derived from strip-scanning observations, with particular reference to an application in radio astronomy . . 119

Soper, J. M. : Nuclear forces and the structure of the lithium isotopes . 1219

Sowter, C. V., with Grace, M. A., Johnson, C. E., and Scurlock, R. G. : A demonstration of parity non-conservation in β-decay . . . 1050

Spence, R. D., with Nye, J. F., and Sprackling, M. T. : Photoelastic study of dislocation arrangements in crystals 772

Sprackling, M. T., with Nye, J. F., and Spence, R. D. : Photoelastic study of dislocation arrangements in crystals 772

Stevens, K. W. H., with Mott, N. F. : The band structure of the transition metals 1364

Stratton, R. : On the surface free energy and specific heat of a metal . 702

Stratton, R. : The effect of free electrons on lattice conduction at high temperatures 422

Stroh, A. N. : The existence of micocracks after cold-work . . . 1

Sykes, M. F., with Domb, C. : Calculation of lattice constants, in crystal statistics 733

Tainsh, R. J., with Harper, A. F. A., Kemp, W. R. G., Klemens, P. G., and White, G. K. : Thermal and electrical conductivity of chromium 577 at low temperatures 577

Tait, R. I., with Richardson, E. G. : Ratios of specific heat and high-frequency viscosities in organic liquids under pressure, derived from ultrasonic propagation 441

Taylor, R. J. : A note on hydromagnetic stability problems . . . 33

Taylor, R. T., with Grace, M. A., Johnson, C. E., and Scurlock, R. G. : Nuclear alignment of ytterbium 175 1079

Tolansky, S., and Patel, A. R. : Rectilinear etch pits on diamond . . 1003

Tonge, D. G., with Wohlfarth, E. P. : The remanent magnetization of single domain ferromagnetic particles 1333

Toppel, B. J., Bloom, S. D., and Wilkinson, D. H. : Isotopic spin selection rules, X : The 7·18 MeV state of ^{20}Ne 61

Toppel, B. J., with Bloom, S. D., and Wilkinson, D. H. : Isotopic spin selection rules, IX : The 9·58 MeV state of ^{16}O 57

Tosi, M. P., with Fumi, F. G. : Multipole order of lattice cells of ionic crystals 568

Tosi, M. P., with Fumi, F. G. : On the Naor relations between Madelung constants for cubic ionic lattices 284

Trumpy, B., with Graue, A. : An investigation of neutron groups from the reaction ^{10}B(d, n)^{11}C at 7·0 MeV deuteron energy . . . 138

PAGE

Turner, J. F., with Cavanagh, P. E., Coleman, C. F., Gard, G. A., and Ridley, B. W.: On the longitudinal polarization of β-particles 1105

Varley, J. H. O.: The existence of a metastable phase isomorphous with the stable phase of a pure metal 384

Waddington, C. J.: The charge distribution of multiply charged nuclei in the primary cosmic radiation, I: The light and medium nuclei 1059
Waddington, C. J., with Fowler, P. H., and Hillier, R. R.: Interactions of the heavy nuclei of the cosmic radiation 293
Waddington, C. J., with Fowler, P. H., Freier, P. S., Naugle, J., and Ney, E. P.: The low energy end of the cosmic ray spectrum of alpha-particles 157
Warburton, E. K., with Rose, H. J.: Lifetime of the 3·56 MEV state of lithium 6 1468
Warhanek, H.: The 4·77 MEV level in boron 10 1085
Watt, D. E., with Glover, R. N.: A search for electron capture in ^{176}Lu 699
Watt, D. E., with Glover, R. N.: A search for natural radioactivity in vanadium 697
Watt, D. E., with Glover, R. N.: The natural radioactivity of lanthanum 49
Webb, F. J., with Butterworth, I., Egelstaff, P. A., and London, H.: Production of intense cold neutron beams 917
West, D., and Bradley, E. F.: Proportional counter measurements of π-mesonic X-rays 957
Westfold, K. C.: Magnetohydrodynamic shock waves in the solar corona, with applications to bursts of radio-frequency radiation 1287
Westmacott, K. H., with Smallman, R. E.: Stacking faults in face-centred cubic metal and alloys 669
Wheeler, C., with Roberts, J. P.: Diffusion of zinc in zinc oxide 708
Whelan, M. J., and Hirsch, P. B.: Electron diffraction from crystals containing stacking faults: I 1121
Whelan, M. J., and Hirsch, P. B.: Electron diffraction from crystals containing stacking faults: II 1303
White, G. K., with Harper, A. F. A., Kemp, W. R. G., Klemens, P. G., and Tainsh, R. J.: The thermal and electrical conductivity of chromium at low temperatures 577
Wignall, J. W. G., with Chadwick, G. B., Durrani, S. A., Eisberg, L. M., Jones, P. B., and Wilkinson, D. H.: Breakdown of parity conservation in the π–μ–e decay and a test of the two component neutrino theory 684
Wild, J. P., with Smerd, S. F.: The effects of incomplete resolution on surface distributions derived from strip-scanning observations, with particular reference to an application in radio astronomy 119
Wilkinson, D. H.: Isotopic selection rules, XII: The mirror reactions ^{6}Li(d, n)^{7}Be and ^{6}Li(d, p)^{7}Li 83
Wilkinson, D. H., and Bloom, S. D.: Isotopic spin selection rules, XI: The 8·06 and 7·23 MEV state of ^{14}N 63
Wilkinson, D. H., with Bloom, S. D., and Toppel, B. J.: Isotopic spin selection rules, IX: The 9·58 MEV state of ^{16}O 57
Wilkinson, D. H., with Chadwick, G. B., Durrani, S. A., Eisberg, L. M., Jones, P. B., and Wignall, J. W. G.: The breakdown of parity conservation in the π–μ–e decay and a test of the two component neutrino theory 684

PAGE

Wilkinson, D. H., with Toppel, B. J., and Bloom, S. D. : Isotopic spin selection rules, X : The 7·18 Mev state of ^{20}Ne 61

Wilks, J., with Niblett, D. H. : Internal friction of cold worked copper at low temperatures 1427

Williams, Anne, P : A study of the growth of crystals from solution when subjected to local deformation 635

Williams, Anne, P : The growth of lead nitrate crystals from aqueous solution 317

Williams, P. R., with Alston, Margaret H., Collinge, B., Evans, W. H. and Newport, R. W. : A propane bubble chamber . . . 820

Williams, P. R., with Alston, Margaret H., Evans, W. H., Morgan, T. D. N., Newport, R. W., and Kirk, A. : Polarization of μ-mesons observed in a propane bubble chamber 1143

Willis, B. T. M., with Smallman, R. E. : An x-ray study of neutron irradiated lithium fluoride 1018

Willmott, J. C., with Broude, C., Green, L. L., and Singh, J. J. : The γ-rays from the 8·06 Mev level in ^{14}N 499

Willmott, J. C., with Broude, C., Green, L. L., and Singh, J. J. : On the 8·06 and 8·70 Mev states in ^{14}N 1006

Wittels, M. C. : Structural behaviour of neutron irradiated quartz . . 1445

Wohlfarth, E. P. : Anhysteretic magnetization of permanent magnet alloys 719

Wohlfarth, E. P., and Tonge, D. G. : The remanent magnetization of single domain ferromagnetic particles 1333

Wolcott, N. M. : Atomic heats of titanium, zirconium and hafnium . 1246

Wolf, E. : Intensity fluctuations in stationary optical fields . . . 351

Wolf, W. P., with Cooke, A. H., McKim, F. R., and Meyer, H. : Thermal and magnetic properties of ytterbium ethyl sulphate between 20°K and 1°K 928

Yoffe, Elizabeth H. : The centre of a dislocation : I 1197

Zienau, S., with Aub, M. R., and Power, E. A. : Influence of retardation on the London–Van der Waals force 571

Ziman, J. M. : Effect of free electrons on lattice conduction. . . . 292

END OF THE SECOND VOLUME

Printed by Taylor & Francis, Ltd.
Red Lion Court, Fleet Street, London, E.C.4

U. of Haw.